

# **Final Report**

## **Assessing Near-Field Exposures from Distributed Residential Wood Smoke Combustion Sources**

Principal Investigators:

**Tracy Thatcher**  
Cal Poly San Luis Obispo

**Thomas Kirchstetter**  
Lawrence Berkeley National Laboratory

Prepared for:

California Air Resources Board  
and  
California Environmental Protection Agency

Prepared by:

Tracy Thatcher, Stella Tan, Christopher Malejan, and Courtney Ward  
Civil and Environmental Engineering  
California Polytechnic State University

Thomas Kirchstetter  
Environmental Energy Technologies Division  
Lawrence Berkeley National Laboratory

**September 2011**

Contract # 07-308

## Disclaimer

The statements and conclusions in this Report are those of the contractor and not necessarily those of the California Air Resources Board. The mention of commercial products, their source, or their use in connection with material reported herein is not to be construed as actual or implied endorsement of such products.

## Acknowledgments

The authors would like to thank Dane Westerdahl, Steve Hui, Michael Gabor, and Peggy Jenkins at the California Air Resources Board for their helpful guidance during this project. We would also like to thank Karen Brooks and Joel Craig at the San Luis Obispo County Air Pollution Control District for their support and assistance and the Ventura County Air Pollution Control District for their assistance with PM<sub>2.5</sub> sampling.

This project would not have been possible without the cooperation and patience of the many Cambria residents who allowed us to come into their homes and yards to place sampling equipment. We would also like to thank the Cambria Fire Department and the Cambria Cal Fire Station for allowing us to place equipment at their facilities.

This report was submitted in fulfillment of Contract 07-308 *Assessing Near-Field Exposures from Distributed Residential Wood Smoke Combustion Sources* By California Polytechnic University San Luis Obispo and Lawrence Berkeley National Laboratory and under the sponsorship of the California Air Resources Board. Work was completed as of September 2011.

# Assessing Near-Field Exposures from Distributed Residential Wood Smoke Combustion Sources

## Contents

|       |   |      |
|-------|---|------|
| 1     | Abstract.....   | xii  |
| 2     | Executive Summary.....  | xiii |
| 3     | Statement of Significance.....                                      | 1    |
| 4     | Project Objectives.....   | 3    |
| 5     | Experimental Overview.....  | 4    |
| 5.1   | Location Selection.....   | 4    |
| 5.2   | Study Area Description.....   | 7    |
| 6     | Determination of Wood Smoke Concentrations.....                     | 9    |
| 6.1   | Wood Smoke Composition.....   | 9    |
| 6.2   | Methods.....  | 10   |
| 6.2.1 | Thermal-Optical Analysis (TOA) Methods.....                         | 10   |
| 6.2.2 | Light Attenuation Method.....                                       | 11   |
| 6.3   | Comparisons Between Analytical Methods.....                         | 12   |
| 6.3.1 | Carbon Comparisons.....   | 13   |
| 6.3.2 | Levoglucosan Analysis.....  | 15   |
| 6.3.3 | Spectral dependence of light absorption.....                        | 17   |
| 6.4   | Comparison of Methods with PM <sub>2.5</sub> .....                  | 20   |
| 7     | Variability of Outdoor Wood Smoke Concentrations.....               | 23   |
| 7.1   | Methods.....  | 23   |
| 7.2   | Summary of Intensive Operational Periods.....                       | 27   |
| 7.3   | Variability of Real Time Measurements.....                          | 28   |
| 7.4   | Variability of Filter BC Measurements.....                          | 33   |
| 7.5   | Variability of 12-hr Integrated Ångström Absorption Exponent.....   | 40   |
| 7.6   | Spatial Variability of Meteorological Stations.....                 | 43   |
| 8     | Quality Assurance and Quality Control.....                          | 47   |
| 8.1   | Quality Assurance.....  | 47   |
| 8.2   | Quality Control.....  | 48   |
| 9     | Statistical Modeling.....   | 51   |
| 9.1   | Background.....   | 53   |
| 9.2   | Regression Analysis of Aethalometer Black Carbon.....               | 56   |
| 9.2.1 | Predictors for Aethalometer Average Black Carbon Concentration..... | 58   |

|       |   |     |
|-------|---|-----|
| 9.2.2 | Predictors for Aethalometer Black Carbon Deviation .....          | 63  |
| 9.3   | Regression Analysis of Integrated Black Carbon Measurements ..... | 65  |
| 9.3.1 | PEM BC Average Concentration and BC Deviation .....               | 65  |
| 9.3.2 | Directional Effects on PEM BC .....                               | 69  |
| 10    | Physical Modeling .....   | 77  |
| 10.1  | Background.....   | 77  |
| 10.2  | Dispersion Modeling Results.....                                  | 80  |
| 11    | Transfer of Wood Smoke Indoors.....                               | 89  |
| 11.1  | Methods .....   | 89  |
| 11.2  | Indoor/Outdoor Ratios .....                                       | 91  |
| 12    | Intake Fraction .....   | 98  |
| 12.1  | Methods .....   | 98  |
| 12.2  | Near-field Effects on Intake Fraction .....                       | 101 |
| 13    | Summary and Conclusions .....                                     | 102 |
| 14    | Recommendations.....  | 105 |
| 15    | References.....   | 106 |
| 16    | Glossary of Terms.....  | 112 |

# List of Figures

|             |   |    |
|-------------|---|----|
| Figure 5.1  | Map of Cambria California neighborhoods.....  | 5  |
| Figure 5.2  | Black carbon concentrations over a ten day period in Cambria, CA. Data was collected during the location selection phase of the project to assure that wood smoke concentrations were detectable within the selected neighborhood. The hours from approximately 9pm to 3am are shaded to help identify the period which is expected to have the highest wood burning emissions.....       | 7  |
| Figure 5.3  | Approximate tree coverage within the study area (Cambria, CA) showing the variation of land usage within the 1km <sup>2</sup> sampling domain.....  | 8  |
| Figure 5.4  | Study area, outlined by black box, with approximate sampling locations for February 28, 2010 .....  | 9  |
| Figure 6.1  | Method comparison IOP showing four PEMS, two aethalometers, and a mini-vol sampler co-located in a resident's backyard. ....  | 12 |
| Figure 6.2  | Comparison of Total Carbon determined from NIOSH 5040 and LBNL TOA methods for 12 hour integrated filter samples collected at 4 different locations within Cambria, CA on 2 different days (samples 1 through 4 were collected on 3/7/09 and samples 5 through 8 were collected on 3/13/09) .....   | 13 |
| Figure 6.3  | Comparison of black and elemental carbon concentrations for 12 hour integrated filter samples collected at 4 different locations within Cambria, CA on 2 different days (samples 1 through 4 were collected on 3/7/09 and samples 5 through 8 were collected on 3/13/09) .....  | 14 |
| Figure 6.4  | Levoglucosan versus organic carbon fraction, with and without removal of the gaseous carbon artifact, for 12 hour integrated filter samples collected at 4 different locations within Cambria, CA on 2 different days.....  | 15 |
| Figure 6.5  | The fraction of total carbon represented by levoglucosan, with and without removal of the gaseous carbon artifact, for 12 hour integrated filter samples collected at 4 different locations within Cambria, CA on 2 different days .....  | 16 |
| Figure 6.6  | Comparison of BC and EC concentrations to levoglucosan for 12 hour integrated filter samples collected at 4 different locations within Cambria, CA on 2 different days .....  | 17 |
| Figure 6.7  | The light attenuation of sample 1 collected in Cambria, CA on 3/7/09 (short dashes), and the portion of the attenuation attributed to black carbon (long dashes).....   | 18 |
| Figure 6.8  | Light attenuation of a sample collected in Cambria, CA on 3/7/09 (short dashes line) showing the amount of attenuation due to black carbon based on the extrapolation from the sample attenuation at 880nm and assuming an AAE of black carbon of 1.1. The solid line is the best-fit power law regression for Sample 3.....  | 20 |
| Figure 6.9  | PM <sub>2.5</sub> concentrations for 12 hour integrated filter samples collected using mini vol samplers at 4 different locations within Cambria, CA on 2 different days (samples 1, 3, and 4 were collected on 3/7/09 and samples 6 through 8 were collected on 3/13/09) Two pairs of samples, 3 &7 and 4 &8, were collected at the same locations, respectively, on different days..... | 21 |
| Figure 6.10 | Results for levoglucosan, EC, and BC as a percentage of the PM <sub>2.5</sub> concentration at 12 hour integrated filter concentrations for each sample.  |    |

|             |  |    |
|-------------|--|----|
|             | Samples 1, 3 and 4 were collected on 7 March 2009. Samples 6, 7, and 8 were collected on 13 March 2009. Two pairs of samples, 3 & 7 and 4 & 8, were collected at the same locations, respectively, on different days. ....   | 22 |
| Figure 6.11 | Concentrations for BC, EC, levoglucosan, and PM <sub>2.5</sub> averaged over all of the 12 hour integrated filter sampling periods for which PM <sub>2.5</sub> samples were obtained (samples 1, 3, and 4 on 3/7/09 and samples 6, 7, and 8 on 3/13/09). The wide bars represent PM <sub>2.5</sub> .....   | 22 |
| Figure 7.1  | Personal Environmental Monitor (PEM) shown deployed on top of the protective housing with the sampling pump and sound proofing material inside. ....   | 25 |
| Figure 7.2  | Sampler arrangement for IOP 7b showing locations of 12 hour integrated filter samplers (PEMs) and aethalometers within the Cambria, CA study area. ....  | 27 |
| Figure 7.3  | Sample infrared camera image showing the chimney base at 48.8F with a peak temperature of approximately 130F at the spark arrestor on top of the chimney .....   | 28 |
| Figure 7.4  | 30 minute average aethalometer black carbon concentrations at 4 locations within the study area, as shown in Figure 7.5, during IOP 7b (collected from 5pm 3/11/10 to 5am 3/12/10).....  | 31 |
| Figure 7.5  | Aethalometer sampling locations used during the Intensive Operational Periods (IOPs). Note: Aethalometers were not deployed at all locations during every IOP. ....  | 32 |
| Figure 7.6  | Box plot comparing aethalometer black carbon (BC) concentrations between sites, as shown in Figure 7.5, over all IOPs. Note: Aethalometers were not deployed at all locations during every IOP .....   | 33 |
| Figure 7.7  | Labels for all PEM sample locations used during the study. Only a subset of these locations was used for each Intensive Operational Period (IOP). Location symbols are coded to assist with grouping of results. ....  | 34 |
| Figure 7.8  | Box plots showing black carbon concentrations for 12 hour PEM filter samples by Intensive Operational Period (IOP) .....   | 36 |
| Figure 7.9  | Black carbon concentrations for 12 hour PEM 2.5 filters samples by location and Intensive Operational Period (IOP). Sampling locations names are shown in Figure 7.7 <i>Note that the concentration for E1 IOP5b exceeds the graph limits and equals 2790 ng/m<sup>3</sup></i> .....   | 37 |
| Figure 7.10 | Average 12 hour PEM filter black carbon concentration averaged by sampling location for all IOPs. Section symbols match markers on Figure 7.7.....   | 38 |
| Figure 7.11 | 12 hour PEM filter and 12 hour average aethalometer black carbon PEM 2.5 concentrations (ng/m <sup>3</sup> ) for IOP 3b collected from 6pm 1/30/10 to 6 am 1/31/10. Results have been shaded by concentration, using the schematic in the upper left, to aid in visualization. Arrows represent average wind speeds and directions for two local meteorological stations. Flame icon denotes location of a detected burning source ..... | 39 |
| Figure 7.12 | 12 hour PEM filter and 12 hour average aethalometer black carbon PEM 2.5 concentrations (ng/m <sup>3</sup> ) for IOP 1a collected from 6pm 1/31/09 to 6 am 2/1/09. Results have been shaded by concentration, using the schematic in the upper left, to aid in visualization. Arrows represent average wind speeds and directions for two local meteorological stations. Flame icon denotes location of a detected burning source .....  | 40 |

|             |  |    |
|-------------|--|----|
| Figure 7.13 | Distribution of Absorption Ångström Exponents (AAE) of particulate matter samples collected in 2009 and 2010. AAE values are based on statistical regression of light transmission measurements of samples over the 350-700 nm spectrum.....                               | 41 |
| Figure 7.14 | Relationship between Absorption Ångström Exponents (AAE) and BC concentrations of particulate matter samples collected in 2010. The oval surrounds the nine samples with the lowest AAE values .....   | 42 |
| Figure 7.15 | Time series of Absorption Ångström Exponents (AAE) of particulate matter samples collected at several locations in 2010. The oval highlights samples with the lowest AAE values, all of which were collected on 15-March, 2010.....  | 43 |
| Figure 7.16 | Map of meteorological stations in Cambria, CA area relative to the study area, as shown by the box in the northern portion of the map.....   | 45 |
| Figure 7.17 | Meteorological parameter (wind speed, relative humidity, and temperature) averages and standard deviations during each Intensive Operational Period (IOP) for the stations shown in Figure 7.16.....   | 46 |
| Figure 8.1  | Comparison of Absorption Angstrom Exponent from duplicate analyses performed on a subset of filter samples for QA/QC purposes.....   | 48 |
| Figure 8.2  | Black carbon concentrations prior to adjustment of the specific attenuation cross-section values for a calibration run on January 19, 2010 .....   | 50 |
| Figure 8.3  | Black carbon concentrations after adjustment of the specific attenuation cross-section values for a calibration run on January 19, 2010 (shown prior to adjustment in Figure 8.2) .....  | 50 |
| Figure 9.1  | ACF analysis results for the time lag of the 30 minute average aethalometer black carbon concentration using data from the CSDF meteorological station. Autocorrelations that exceed the dotted horizontal lines are considered significant.....                           | 57 |
| Figure 9.2  | Comparison between residual charts for un-normalized ( $BC_{ave}$ ) and normalized ( $BC_{ave}^{-0.7}$ ) black carbon concentration shows that the transformation yields a normal distribution of residuals .....  | 58 |
| Figure 9.3  | Parameter plots from the multiple linear regression model for normalized 30 minute average aethalometer black carbon concentrations when modeled using meteorological data from the EBAM station .....   | 61 |
| Figure 9.4  | Parameter plots from the multiple linear regression model for normalized 30 minute average aethalometer black carbon concentrations when modeled using meteorological data from the EBAM and LH-CSDF combined stations.....  | 62 |
| Figure 9.5  | Parameter plots from the multiple linear regression model for normalized 30 minute average aethalometer black carbon concentration deviation ( $BC_{dev}^{0.5}$ ) when modeled using meteorological data from the LH-CSDF station.....                                     | 64 |
| Figure 9.6  | Parameter plots from the multiple linear regression model for normalized 12 hour filter (PEM) black carbon concentrations ( $BC_{ave}^{0.4}$ ) averaged by Intensive Operational Period (IOP) when modeled using meteorological data from the Marine Terrace station ..... | 67 |
| Figure 9.7  | Parameter plot from the multiple linear regression model for normalized 12 hour filter (PEM) black carbon concentrations ( $\ln(BC_{ave})$ ) averaged by Intensive Operational Period (IOP) when modeled using meteorological data from the LH CSDF station.....           | 68 |

|              |  |    |
|--------------|--|----|
| Figure 9.8   | Parameter plots from the multiple linear regression model for normalized 12 hour filter (PEM) black carbon concentrations ( $\ln(BC_{ave})$ ) averaged by Intensive Operational Period (IOP) when modeled using combined meteorological data from the LH CSDF and Marine Terrace (MT) stations ..... | 68 |
| Figure 9.9   | Parameter plot from the multiple linear regression model for normalized 12 hour filter (PEM) black carbon concentration deviation ( $\ln(BC_{dev})$ ) by Intensive Operational Period (IOP) as a function of number of wood burning sources.....   | 69 |
| Figure 9.10  | Study area divisions used for directional regression models.....   | 71 |
| Figure 9.11  | Residual plot for the directional linear regression model for normalized 12 hour filter (PEM) black carbon concentration ( $\ln(BC)$ ) .....   | 72 |
| Figure 9.12  | Normalized 12 hour filter (PEM) black carbon concentration ( $\ln(BC)$ ) versus number of burning sources in the division, as shown in Figure 8.10, sorted by location and level of vegetation and structures surrounding PEM for IOPs 2b through 10b .....  | 74 |
| Figure 9.13  | Normalized 12 hour filter (PEM) black carbon concentration ( $\ln(BC)$ ) versus number of upwind burning sources in location sorted by division, as shown in Figure 8.10, and level of vegetation and structures surrounding PEM for IOPs 4b through 10b .....                                       | 75 |
| Figure 9.14. | Box plot showing normalized 12 hour filter (PEM) black carbon concentration ( $\ln(BC)$ ) by division, as shown in Figure 8.10, and degree of PEM obstruction for IOPs 2b through 10b .....  | 76 |
| Figure 10.1  | Schematic of structure representations in BEEST for dispersion modeling .....  | 79 |
| Figure 10.2  | Box plots showing the ratio modeled black carbon to measured black carbon for ISC Prime and ISCST3 for all 12 hour integrated filter samples over all intensive operational periods (IOPs).....  | 81 |
| Figure 10.3  | ISC-PRIME modeled versus measured BC concentration for all samples over all IOPs. The dotted line represents a one-to-one ratio between measured and modeled BC concentrations. The solid line is an applied trendline with equation and $R^2$ value shown.....                                      | 82 |
| Figure 10.4  | ISCST3 modeled versus measured BC concentration for all samples over all IOPs. <i>The dotted line represents a one-to-one ratio between observed and modeled BC concentrations. The solid line is an applied trendline with equation and <math>R^2</math> value shown.</i> .....                     | 82 |
| Figure 10.5  | Corrected modeled BC versus observed BC concentration for the ISC-PRIME and ISCST3 models after adjustment of average modeled values to match the average measured values. <i>The dotted line represents a one-to-one ratio between observed and modeled BC concentrations.</i> .....                | 84 |
| Figure 10.6  | ISC-Prime and ISCST3 dispersion model contour maps for IOP 6b. Modeled values have been adjusted so that the average modeled concentration equals the average measured concentration. Measured values are represented by circles shaded to match the concentration scale of the model. ....          | 85 |
| Figure 10.7  | ISC-Prime and ISCST3 dispersion model contour maps for IOP 4b. Modeled values have been adjusted so that the average modeled concentration equals the average measured concentration. Measured values are represented by circles shaded to match the concentration scale of the model. ....          | 86 |

|             |   |     |
|-------------|---|-----|
| Figure 10.8 | ISC-PRIME contour plots for IOPs 4a and 4b. Modeled values have been adjusted so that the average modeled concentration equals the average measured concentration. Measured values are represented by circles shaded to match the concentration scale of the model. ....                            | 87  |
| Figure 10.9 | ISCST3 contour plot for IOP 9b and ISC-PRIME contour plot for IOP 10b. Modeled values have been adjusted so that the average modeled concentration equals the average measured concentration. Measured values are represented by circles shaded to match the concentration scale of the model. .... | 88  |
| Figure 11.1 | Important processes which can influence the concentrations of particles in the indoor environment.....  | 90  |
| Figure 11.2 | Calculated indoor concentration response to a theoretical spike in outdoor concentration for a conservative pollutant with an air exchange rate of 0.5/hr (based on a mass balance model).....  | 92  |
| Figure 11.3 | Indoor/outdoor ratios that would be obtained from the data in Figure 10.2 for 8 hour integrated filters started at different times.....   | 92  |
| Figure 11.4 | Indoor and outdoor aethalometer black carbon concentrations (10 minute averages) for home E in Cambria, CA.....   | 94  |
| Figure 11.5 | Modeled versus measured indoor black carbon aethalometer concentrations for Home E on March 16-17, 2009.....  | 96  |
| Figure 11.6 | Model fit for the burning event on March 16-17, 2009 shown in Figure 10.5.....  | 96  |
| Figure 12.1 | Study area divisions used for intake fraction calculations .....  | 100 |

# List of Tables

|            |   |     |
|------------|---|-----|
| Table 6.1  | Absorption Ångström Exponent for each sample determined from a best-fit power law regression over two spectral regions and corresponding sample EC/TC ratio for 12 hour integrated filter samples collected at 4 different locations within Cambria, CA on 2 different days (samples 1 through 4 were collected on 3/7/09 and samples 5 through 8 were collected on 3/13/09)..... | 19  |
| Table 7.1  | Summary of instruments deployment and sampling times of Intensive Operational Periods (IOPs) for the field study conducted in Cambria, CA.....  | 29  |
| Table 7.2  | Aethalometer black carbon (BC) concentrations averages and variability for 12 hour sampling periods over thirteen Intensive Operational Periods (IOPs) conducted in Cambria, CA during the winters of 2009 and 2010. ....   | 30  |
| Table 7.3  | Black carbon (BC) concentrations averaged by sampling location for all IOPs using 30 minute averaged aethalometer data. Note: Aethalometers were not deployed at all locations for every IOP.....   | 31  |
| Table 7.4  | Black carbon concentrations for 12 hour PEM filter samples averaged by Intensive Operational Period (IOP) .....   | 35  |
| Table 9.1  | Meteorological data available at each station .....   | 55  |
| Table 9.2  | Resulting coefficients and fit from multiple regression models for normalized 30 minute average aethalometer black carbon concentration $(BC_{ave})^{-0.7}$ using the EBAM station and a combination of the EBAM< and CSDF stations.....  | 60  |
| Table 9.3  | Resulting coefficients and fit from the multiple regression model for normalized 30 minute average aethalometer black carbon concentration deviation $(BC_{dev})^{0.5}$ using the LH-CSDF station.....  | 63  |
| Table 9.4  | Linear regression parameters for normalized 12 hour filter (PEM) black carbon concentrations averaged by Intensive Operational Period (IOP) for 3 different meteorological data sets .....  | 66  |
| Table 9.5  | Linear regression parameters for normalized 12 hour filter (PEM) black carbon deviation $(\ln(BC_{dev}))$ by Intensive Operational Period (IOP) as a function of number of burning sources.....   | 69  |
| Table 9.6  | Multiple linear regression model parameters for normalized 12 hour filter (PEM) black carbon concentration $(\ln(BC))$ for the directional model using the divisions in Figure 8.10 .....   | 72  |
| Table 10.1 | Required Meteorological Inputs for ISCST3 and AERMOD.....   | 78  |
| Table 11.1 | Indoor/outdoor ratios for 12 hour integrated black carbon concentrations by residence and intensive operation period (IOP).....   | 93  |
| Table 12.1 | Fractional area and number of houses in each division shown in Figure 11.1 .....  | 100 |
| Table 12.2 | Intake fraction ratio by IOP based on concentrations and housing densities by division as shown in Table 11.1.....  | 101 |

## 1 Abstract

In many communities, residential wood burning produces a significant fraction of wintertime PM<sub>2.5</sub>. This study investigated the impact of near-field burning sources on exposures. Wood smoke samples, meteorological data, and burning source location were analyzed for 15 nights within a 1 km<sup>2</sup> area in Cambria, CA. Black carbon, a significant component of soot, served as an indicator compound for wood smoke. Large concentration variations were observed each night both at a single location and between locations. The standard deviation of 12 hour integrated concentrations measured at all sites ranged from 20% to 150% of the average on any given night. Sites with the highest overall concentrations (averaged over all nights) were 2 to 10 times higher than the lowest concentration sites. Neither multiple linear regression nor dispersion models yielded a strong representation of measured concentrations. Thirteen indoor/outdoor measurement pairs from 4 different residences showed an average indoor/outdoor concentration ratio of  $0.88 \pm 0.41$ . Based on measured concentrations, the intake fraction calculated using near-field concentrations was 25% higher than that calculated using the average concentration for the region. This study demonstrates that near-field effects can lead to higher exposures for some individuals than would be predicted using regional monitors.

## **2 Executive Summary**

### **Background**

In many California communities, particles from residential wood burning represent a significant fraction of fine ambient particulate matter (PM<sub>2.5</sub>) during the winter. Since significant health effects have been linked to PM<sub>2.5</sub> exposure in general, and wood smoke specifically, understanding these exposures is an important step in protecting the health of Californians. While many pollutants originate sources outside of residential areas, like industrial facilities and freeways, wood smoke originates from sources within our neighborhoods. The proximity of these sources to receptors (people in their homes) leads to the potential for a significant variation in exposure between residents of the same neighborhood. Regional air monitoring networks, which are designed to assess average concentrations over a large area without interference from nearby sources, are inadequate to determine the effects of local sources in the near-field. This study assessed the variation of wood smoke concentrations within a residential neighborhood and evaluated the impact that this variation has on our understanding of wood smoke exposures.

### **Methods**

Wood smoke samples, meteorological data, and locations of burning sources within a 1 km<sup>2</sup> area in Cambria, CA, were analyzed for 15 nights during the winters of 2008-09 and 2009-10. Cambria was chosen for the study because wood burning is prevalent in the area and the winter season meteorology leads to higher ambient concentrations (low winds speeds, inversions, and limited precipitation/fog). For this coastal community of approximately 6,500 people with no major highways or industries, wood smoke was the only major source of black carbon, a significant component of soot, the indicator compound for wood smoke in this study. The absorption Ångström exponent, a metric of how the light absorption of particulate matter varies with wavelength and an indicator of wood smoke, was determined by measuring spectral light transmission through collected samples. For each 12 hour sampling period, from 8 to 16 outdoor filter samplers and 1 to 4 aethalometers (measuring time resolved black carbon concentrations) were deployed at sample locations distributed throughout the study area. On some nights, samplers and/or aethalometers were also placed indoors to investigate wood smoke transport into residences. Burning sources were located using an infrared camera to identify chimneys with elevated temperatures. On two additional nights, multiple samples were collected at 4 sites to compare different analytical methods for quantifying wood smoke concentrations.

### **Results**

Black carbon measurements within the 1 km<sup>2</sup> study area showed substantial variability over a multitude of metrics. Over a single 12 hour sampling period, peak black carbon concentrations measured with an aethalometer were 2 to 100 times higher than the average concentration and up to 2500 times larger than the minimum recorded concentrations. Large variations in black carbon concentration were observed at each location and between locations. For 12 hour integrated filter samples, the standard deviation of concentrations for a single sampling period ranged between 20% and 150% of the average concentration. Although the relative concentration between sites was not always consistent, general trends indicated that the regions with higher home density in the southwestern portion of the study area generally had higher concentrations. Higher concentration sites showed average concentrations 2 to 10 times higher than those observed at the sites with the lowest average concentrations. Black and elemental carbon concentrations estimated using four techniques (aethalometer, two methods of thermal-optical analysis, light transmission) showed significant differences, illustrating the degree of measurement uncertainty, but followed similar trends. Since our study focused on a

comparison between concentrations, as opposed to absolute concentrations, these differences should not impact our conclusions. Particulate matter absorption Ångström exponents were most commonly equal to 2 and 95% of the time (barring one sampling day) exhibited high values typically associated with wood smoke rather than motor vehicle exhaust. Multiple linear regression analyses of the data sets did not yield strong correlations between concentrations and measured parameters such as wind speed, wind direction, or number of burning sources. In addition, dispersion modeling did not yield a consistently accurate description of the concentration profile with the region. The failure of these tools to describe the concentrations found may be due to the stochastic nature of turbulent flow in the near-field and the complexity of ground level air flow in a residential area where obstruction by trees, streets, and homes influences the direction and speed of air motion. The impact of near-field effects on exposure was estimated using the ratio of the intake fraction calculated based on local concentrations in sub-regions of the study area to the intake fraction calculated using the average concentration for the entire area. Using this metric, a ratio of 2 would mean that including near-field effects doubled the intake fraction. For the 15 sampling periods in this study, the intake ratio ranged between 0.95 and 1.8, with all but 2 of the values being greater than 1, meaning that including local effects generally increased the intake fraction. Outdoor concentrations can be somewhat mitigated in the indoor environment by losses to the surfaces. To evaluate the magnitude of this effect, thirteen indoor/outdoor measurement pairs at 4 different residences showed an average indoor/outdoor concentration ratio of  $0.88 \pm 0.41$ . In addition, a time dependent mass balance model was used in conjunction with aethalometer measurements taken over 16 nights at a single residence to estimate an average air exchange rate of  $0.26/\text{hr} \pm 0.08$ , a deposition loss rate of  $0.08/\text{hr} \pm 0.03$ , and a penetration factor of  $0.97 \pm 0.02$ . Using these average values in a steady state model predicts an average indoor/outdoor concentration ratio of 0.74 for the residence studied and using the air exchange rate from the LBNL infiltration model yields a ratio of 0.84. This study has several implications for regulatory programs. First, since some locations were shown to generally have higher concentrations than the average for the region, the study demonstrates that near-field effects can lead to higher exposures for some individuals than would be predicted using regional monitors. In addition, regional data may lead to an under-prediction of the intake fraction for sources distributed within neighborhoods, particularly when sources are located in relative proportion to population density. Finally, although indoor concentrations are reduced relative to adjacent outdoor concentrations, wood smoke particles generated in the near-field are relatively persistent in the indoor environment when compared to many other ambient pollutants.

### **Conclusions**

In response to the four original main objectives for this project, this study showed that concentration variability associated with wood burning in a residential neighborhood could have substantial impacts on exposures for individuals, causing much higher exposure for some individuals that would be predicted using regional concentration values. The near-source contribution could not be accurately estimated using multiple linear regression models or dispersion models based on local meteorological, geographic, and source data. However, simple indoor-outdoor models did provide an adequate representation of indoor exposures when wood smoke specific parameters were used. In this study, failure to account for near-field concentration variability resulted in an under-prediction of intake fraction. Future studies are needed to quantify these effects under different conditions/locations and to improve near-field concentration predictions.

### 3 Statement of Significance

Most efforts to characterize and control ambient air pollution have focused on sources that degrade air quality over large portions of an air basin, creating a relatively similar concentration within regions of the air basin. Consistent with this objective, most ambient air quality monitoring stations are deliberately sited to avoid influences of local emission sources. This creates a gap in our understanding of exposures near outdoor pollutant sources. Although zoning regulations tend to group industrial sources away from residential areas, generation can occur within residential neighborhoods. Since the objective of air quality regulation is to protect the public from risks associated with pollutant exposures, it is crucial to understand not only regional trends, but also local effects. Residential wood smoke is an especially relevant pollutant, with potentially significant variation between ambient concentrations and individual exposures. Wood smoke is especially important owing to its significant contribution to fine particulate matter (PM<sub>2.5</sub>) emissions within California, and is widely recognized as a major contributor to wintertime PM<sub>2.5</sub> concentrations in many residential areas of the state. Assessments by California Air Resources Board attribute over 100 tons per day of PM<sub>2.5</sub> emissions to residential wood combustion, nearly twice the emissions estimated for all on road vehicles. In addition, these wood smoke emissions are not distributed equally in time, occurring mainly during the winter months when the weather is cold. Residential wood combustion is typically considered an ‘area’ source, since the wide distribution of small sources can be well characterized as an area source when concentrations are viewed at a regional scale. However, when viewed on the scale of individuals within a neighborhood, these sources may have significantly variable impacts based on the location of the person relative to each source. Being able to better quantify the importance of the near-field exposure component to overall exposures is critical for understanding the relative exposure to wood smoke emissions. When attempting to determine the health risks associated with wood smoke emissions, the following two questions arise. (1) Is monitoring station data a reasonable proxy for the average wood-smoke concentrations to which people are exposed? (2) How much does the exposure vary for individuals within the same community based on their location within the source field? The answers to these questions depend on the characteristics and variability of the near-field concentrations within an “area source” of residential wood burning.

While some studies have evaluated the variability of PM variability in urban environments that primarily originates from diesel or gasoline exhaust and/or industrial sources, no studies have evaluated the impact of wood burning sources on near-field PM variability. Studies demonstrating small scale variability generally involve mobile sampling methods and tend not to use simultaneous sampling strategies. For example, Robinson et al. (2007) found large differences in PM<sub>2.5</sub> concentration averages over a distance of only 41 meters (35 µg/m<sup>3</sup> and 90 µg/m<sup>3</sup>) when sampling with a mobile nephelometer, a device measuring light scattering by particles which can then be related to PM<sub>2.5</sub> concentrations. Higher concentrations were found in areas where wood burning was prevalent. While mobile sampling can demonstrate differences in concentrations over short distances, changes to concentrations over time remain unaccounted for.

Studies evaluating wood smoke contributions to PM concentrations in small areas have only measured pollutant variability at one location and have had to differentiate between PM contributors. One study evaluated both coal and wood burning contributions to winter PM<sub>10</sub> and black smoke in the Czech Republic within a small rural village (Branis et al., 2000) and found

that concentrations varied by more than a factor of 10. A strong correlation between black smoke and  $PM_{10}$  concentrations indicated that the main source of  $PM_{10}$  was likely household combustion processes.

In contrast to the scarcity of near-field PM variability studies, there are a larger number of reports investigating spatial variability in PM from vehicular or unspecified sources. Many of these studies evaluated PM variability within urban scales, defined as 4 through 100 km in diameter, length, or width, and neighborhood scales, defined as 500 m to 4 km in diameter, length, or width (*40 CFR part 58*). While some researchers have found low variability within urban scales (Gorin et al., 2006; Goswami et al., 2002), other studies have found significant variability on the smaller neighborhood scale.

PM concentrations have been found to vary considerably over short distances, especially in the presence of abundant pollutant emissions. Gulliver and Briggs (2004) found large standard deviations when measuring  $PM_{10}$ ,  $PM_{2.5}$ , and  $PM_1$  concentrations at 1 second resolution over two routes comprising high traffic and low traffic areas while walking and driving. Both the walking and driving routes yielded standard deviations in concentration that were approximately equal to the average concentrations. Due to the nature of the study designs, these standard deviations combine both spatial and temporal variability in concentration. Higher variability in PM has been shown to occur in the presence of numerous gasoline and diesel vehicles, while variability declines when only background PM levels are observed (Weijers et al., 2005).

A study conducted in four French metropolitan areas of contrasting urban settings and air quality also found fixed monitoring locations to under-represent individual exposure to  $PM_{2.5}$  (Nerriere et al., 2005). Three areas within each city were selected to represent locations with high traffic emission exposure, abundant influence by local industry, and urban background levels. Volunteers within each area carried personal monitoring devices, a Harvard ChemPass along with a portable pump, and comparisons were made between the individuals and fixed monitoring stations in each area over a period of between 24 and 48 hours. Significant wintertime average differences were found between personal and fixed station  $PM_{2.5}$  concentrations, with all winter average concentrations reading lower at fixed stations. It is important to note that measured  $PM_{2.5}$  may have been contributed by indoor activities and sources, in addition to outdoor sources, although volunteers were all non-smokers who had declared no exposure to environmental tobacco smoke. Several other studies have also attributed the difficulty of representing personal pollutant exposure with fixed-monitoring stations to the abundance of indoor pollutant sources (Wilson et al., 2000; Zeger et al., 2000; Turpin et al., 2007).

Although the phenomenon of higher near-field exposures has been documented for some sources, wood smoke from residential heating is a pollutant source that differs significantly from those studied previously. With wood smoke, the receptors of interest (people in their homes) are interspersed within a field of small stationary sources. Wood burning for home heating occurs mostly at night and in the winter, periods when atmospheric mixing can be suppressed by low inversions and stagnant conditions. The variability in heat output and therefore plume rise from the individual sources adds a further layer of complication. Both Gorin et al. (2006) and Glasius, et al. (2006) found an increase in wood smoke concentration in samples taken in residential areas. However, neither study provided the spatial resolution needed to determine the variation of concentrations within those residential areas.

In residential areas, the primary exposure to people is expected to occur indoors. Not only do Californians spend eighty-seven percent of their time indoors (Jenkins et al., 1992), but during peak periods of wood smoke generation, evenings and nights, people are more likely to be inside their homes. However, most of the research on particle transport into the indoor environment has classified particles by size, with some research on classification by chemical composition. By sampling in a region where ambient particles are dominantly from residential combustion, this study adds important information to our understanding of transport of wood smoke particles into homes and, ultimately, to our understanding of human health impacts.

One important measure of the impact of a particular source or source type is the intake fraction (iF). Intake fraction methodology is used to quantify the relationship between pollutants that are emitted and their intake by populations (Bennett, et al. 2002). The intake fraction for a particular source depends on a variety of factors such as emission location relative to receptors, meteorology and transport, loss mechanisms, and population distributions. Typically, intake fraction is calculated across a city or region using regional monitoring data. This study assesses the impact of near-field effects on intake fraction calculations.

Overall, major gaps remain in our understanding of near-field exposure impacts across the array of potentially important sources. This study provides a unique data set for assessing near-field wood smoke concentration variability within a neighborhood and the potential impact these variations have on our understanding of human exposures to wood smoke particles.

## **4 Project Objectives**

The goal of this research was to contribute to the understanding of near-source variability for primary air pollutants generated within a residential area. The study focused on wood smoke particulate matter generated within a residential area in a region where residential wood burning is the primary source of particles. The research addressed four primary questions:

- What is the concentration variability associated with wood burning within a residential neighborhood?
- Can near-source contributions be properly estimated based on information on burning patterns, meteorology, and regional monitoring site data?
- Does indoor exposure to outdoor wood smoke sources correlate with expected values based on simple indoor-outdoor models?
- How does the near-source contribution affect intake fraction calculations for wood smoke exposures?

The results of this project improve our understanding of the contribution of wood smoke variability to overall PM<sub>2.5</sub> exposure, and can be used to aid in the development of PM<sub>2.5</sub> source reduction prioritization, increase our understanding of the importance of variability of acute exposures, and improve the effectiveness of source control programs for reducing PM<sub>2.5</sub> exposures. To the extent that wood smoke behavior can be generalized to other locally distributed emission sources (such as distributed power generation) this work will aid in decision making regarding siting of sources, improve impact calculations, and be a valuable resource for determining the potential for environmental justice concerns.

## 5 Experimental Overview

The purpose of the field study was to gather information to understand better the near-source variability of wood smoke within a residential area. To this end, different types of sampling were performed to accomplish different study objectives. The field study consisted of three major components: method comparison tests, outdoor Intensive Operational Periods (IOPs), and indoor/outdoor sampling.

Method comparison tests were performed to understand more quantitatively the relationship between commonly used analysis methods. During the method comparison tests, multiple filter samplers and an aethalometer were co-located at 4 different sites within the study area. The filters were then analyzed by different methods and the results compared. The methodologies and results of these comparison tests are detailed in Section 6.

The main portion of the study, the Intensive Operation Periods (IOPs), investigated the variability of outdoor concentrations. For each IOP, filter samplers and aethalometers were placed within the study area, with the filter samplers programmed to draw air for 12 hours during the evening and morning hours when burning is most prevalent. Twenty four hour samples were not used since aerosols generated during the daytime hours are typically low in wood smoke particles and higher in aerosols from other sources. The inclusion of these daytime aerosols would have made it more difficult to assess the near-field component due to wood smoke combustion within the study area. In addition, the study area was surveyed using an infrared camera to determine which homes were actively using their chimneys. The methods and results from the IOPs are detailed in Section 7. Sections 8 and 9 explore these results using statistical and dispersion models, respectively.

Indoor/outdoor sampling was also performed to improve our understanding of the relationship between the outdoor concentrations measured during the main portion of this study and the indoor concentrations to which people are typically exposed. Pairs of integrated filter samples were placed indoors and directly outside of three different residences in the study region during some IOPs. In addition, indoor/outdoor aethalometer pairs were placed during supplementary periods to provide time resolved data. Both the integrated filter results and aethalometer data were used to investigate indoor concentrations due to residential wood burning. Details of the methods and results of the indoor/outdoor sampling are given in Section 11.

### 5.1 Location Selection

An important aspect of the field plan was selecting a study area that provided the best opportunity to fulfill the objectives of this project. The region needed to have residential wood burning as the primary or most significant contributor to wintertime  $PM_{2.5}$  and meteorology conducive to the study objectives. The ideal meteorological features were (1) wintertime inversions and relatively low wind speeds that would lead to higher and more easily measureable concentrations, and (2) limited fog and precipitation to prevent wood smoke particles from being scavenged from the atmosphere. Secondary features of interest for the study area included limited interference from other sources of combustion particles, a safe environment for deploying instruments and working at night, cooperative local individuals for siting instruments in yards and inside homes, limited migration of pollutants into the study area, and a local air district enthusiastic about cooperating with the research.

In the original proposal, the Fresno, CA area was considered a likely area for the field study. During the initial selection investigation, surveys were performed in several Fresno and

Clovis neighborhoods, using an infrared camera to detect chimney activity and a portable condensation nucleus counter to detect elevated particle concentrations. Filter samples were also placed at two different homes to collect overnight samples. However, these surveys revealed many non-ideal features of this region. For instance, evening traffic made it difficult to conduct the surveys and the prevalence of fog significantly reduced the number of available sampling days. One of the most significant disadvantages was that since Fresno represents a large region with significant wood smoke emissions, any 1 km<sup>2</sup> study area chosen would experience significant transport of wood smoke emissions into the study area. However, since these emissions were from sources located at varying distances from the study area boundary, characterizing the entry of particles into the study area would be very difficult. Although winter-time PM levels can be very high in Fresno, the magnitude of the PM concentration is not critical for the purposes of this study since the focus is on the variability of the contribution from near-field sources as opposed to overall concentrations. During the selection process, several other California locations were also considered. Based on the results from the selection process, Cambria, California (Figure 5.1) was chosen because it most effectively meet both the primary and secondary requirements for the study. Situated along the California coast, Cambria is 30 miles northwest of San Luis Obispo in San Luis Obispo (SLO) County, between San Francisco and Los Angeles. The town spans about 3 km<sup>2</sup>, is populated by approximately 6,500 people, and lists tourism, light industry, and agriculture as its main industrial activities (Cambria Chamber of Commerce, 2010).

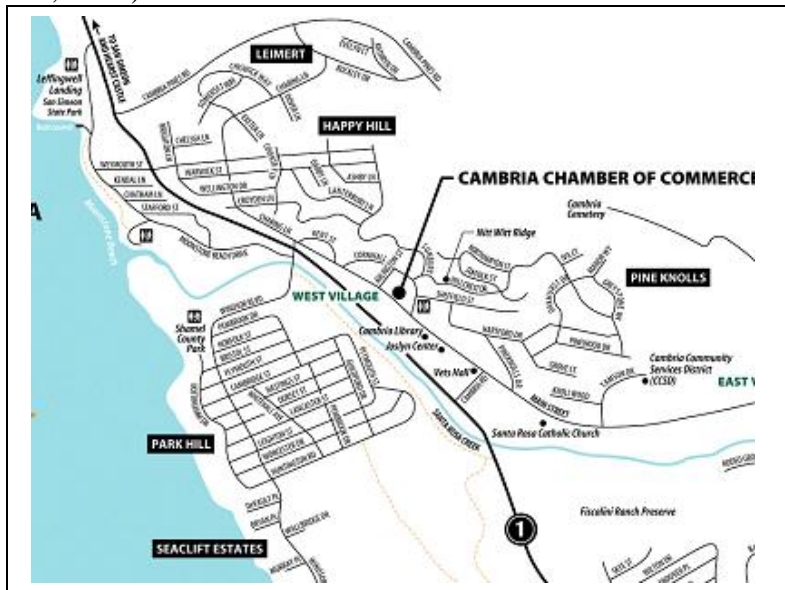


**Figure 5.1 Map of Cambria California neighborhoods**

One of the most significant advantages of Cambria over other locations was the nearly complete lack of potentially interfering sources. Cambria is located on the central coast of California (35.554030, -121.087394) with elevations ranging from sea level to 250 feet. It is bordered to the west by the Pacific Ocean and to the east by the Santa Lucia Range. Cambria has nearly no conflicting PM<sub>2.5</sub> sources such as industry or vehicular traffic. There are no major freeways in the area and little or no traffic during the evenings and nighttime. The largest road, Highway 1, is one lane each way and serves only local truck traffic. There are no major PM<sub>2.5</sub> producing local industries. The nearest major cities are Monterey (population 410,000)

approximately 80 miles north-west, San Luis Obispo (population 270,000) approximately 30 miles south-east, and Paso Robles (population 28,000) approximately 20 miles east. Due to the distance, topography, prevailing meteorology, and relatively good air quality in these nearby regions, transport of pollutants does not significantly impact air quality in Cambria.

Although Cambria does not have other significant pollutant sources, residential wood burning is common. Because of the age of the neighborhoods and the characteristics of the homes, a large percentage of the homes in Cambria have fireplaces and/or woodstoves. In addition, the close proximity to available wood results in many homes using wood for all or a significant portion of their heating needs. Cambria lies in a rural portion of San Luis Obispo County. Over the entire county, residential wood combustion was estimated to constitute 26 percent of the total winter  $PM_{2.5}$  in 2005 (CA ARB, 2006). However, other major  $PM_{2.5}$  sources within the county, such as managed burning and disposal, paved/unpaved road dust, and farming operations, are not significant in the area surrounding Cambria so wood burning was expected to form a larger fraction of  $PM_{2.5}$  emissions in Cambria. Additionally, road dust and farming operations that suspend dust would not contribute to carbonaceous PM, which is the measurement focus of this study.

As part of the assessment of the Cambria location, an aethalometer was placed within the study area for a 10 day period in December, 2008. Aethalometers use the optical absorbing properties of the fraction of carbon containing particles known as black carbon to determine concentrations based on optical attenuation through a particle-laden filter. Since black carbon is a by-product of combustion, the aethalometer measurements shown in Figure 5.2 were used to determine whether residential wood combustion was a potentially significant source within the proposed study area. The data shows that during the evenings, shaded in the figure, there is generally a sharp increase in black carbon concentration that lasts until at least midnight. This pattern is consistent with residential wood burning since most residential fireplaces are lit as the temperature drops in the late afternoon/evening and are then allowed to burn out overnight. The lack of morning/evening peaks indicates that commuter driving is not a significant source in this area. This lack of significant car and truck traffic was also confirmed by observation of the area during the evening and nighttime.

Cambria also has generally favorable weather conditions for the study. The area typically experiences relatively cool winter temperatures (historical average highs around 62 °F and lows around 42 °F) and frequent wintertime inversions. Rainfall is fairly low with about 3.5" per month in the winter and an average of 31 rain days per winter. Although low fog is a common summertime phenomena, there is seldom ground level fog during the winter.

The Cambria location yielded many opportunities for relatively easy access to study locations and excellent support from the local APCD (San Luis Obispo County Air Pollution Control District). Not only is Cambria a small town where it was safe to work at night and uncomplicated to disseminate information regarding the study, the APCD had logged a history of complaints regarding wood smoke levels from several residents in the area, and therefore had a ready list of potentially cooperative home owners. A subset of these concerned residents provided access for the indoor study, placement locations for outdoor samplers, and locations with power for aethalometers.

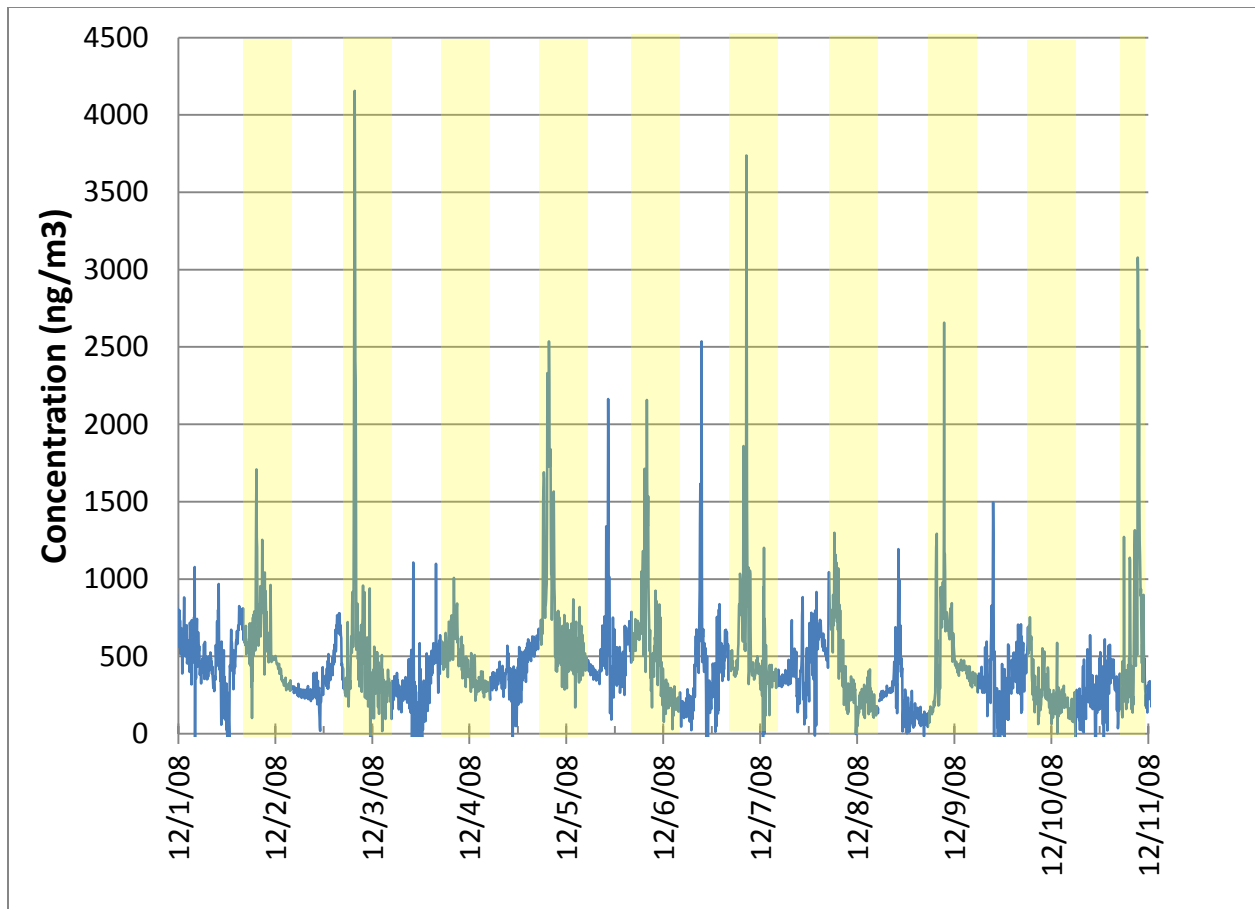


**Figure 5.2 Black carbon concentrations over a ten day period in Cambria, CA. Data was collected during the location selection phase of the project to assure that wood smoke concentrations were detectable within the selected neighborhood. The hours from approximately 9pm to 3am are shaded to help identify the period which is expected to have the highest wood burning emissions**

## **5.2 Study Area Description**

The study area within Cambria was approximately 1 km<sup>2</sup> and located in northern Cambria in portions of neighborhoods known as “Leimert” and “Happy Hill” (south of Leimert), encompassing about 400 homes. This section of Cambria was chosen because it is representative of typical Cambria neighborhoods, with a prevalence of chimneys, chimney use, and homes ranging from 1 to 50 years old. Chimney use was confirmed using thermal imaging prior to the start of the study. Additionally, to assure that BC concentrations were measurable, the study area was scanned over several evenings under different meteorological conditions using a mobile portable aethalometer driven through the neighborhood. The chosen study area, shown in Figure 5.3, is comprised of residential homes within an area with substantial tree coverage in the northern portion and more open area in the southern portion. The 2000 US census indicated a median population age of 50.9, and 46 percent of structures (including homes) built before 1980 and 32 percent built between 1980 and 1989 (US Census Bureau, 2000).

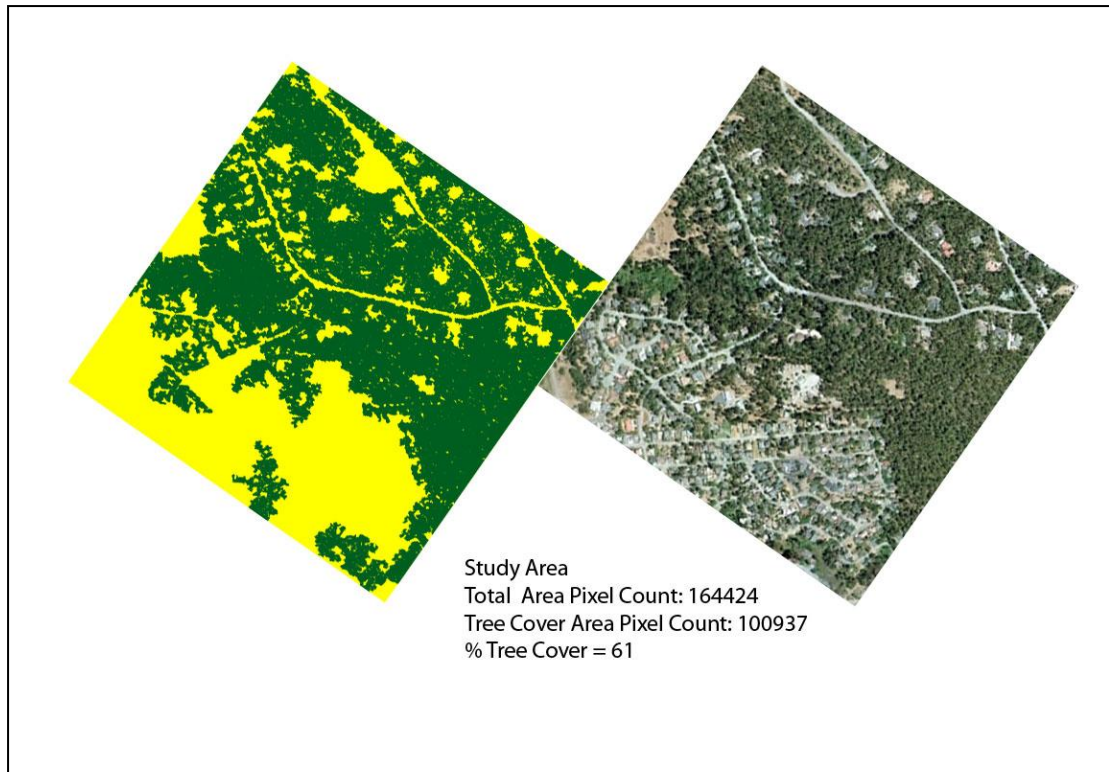


**Figure 5.3 Approximate tree coverage within the study area (Cambria, CA) showing the variation of land usage within the 1km<sup>2</sup> sampling domain.**

In areas of higher housing density (mostly the Happy Hills neighborhood), homes are spaced closely together, often with the backs of two houses facing one another, and almost every house contains trees on two sides of the residence. In the area of lower housing density (mostly the Leimert neighborhood), homes are often spaced greater than 50 feet apart with trees surrounding the homes on all sides. Cambria’s downtown is located just south of the study area, comprised of mostly one long street running south-east from the study site. The downtown area located closest to the study site consists of restaurants, novelty shops, art galleries, hotels, a couple of gas stations, and other small retail businesses.

Once this area was confirmed to be suitable, daytime visits were made to locate sampling locations. Contact was made with local law enforcement to inform them of our activities. The Cambria contacts made through the APCD helped to spread the word about the research project, facilitating access to more homes. **Error! Reference source not found.** the study area location on a Cambria map and the locations of the sampling devices for the sampling period starting on February 28, 2010. To the extent possible, the same sampling locations were used throughout the study. However, some changes in locations occurred between sampling seasons and slight variations occurred due to access changes and equipment availability.

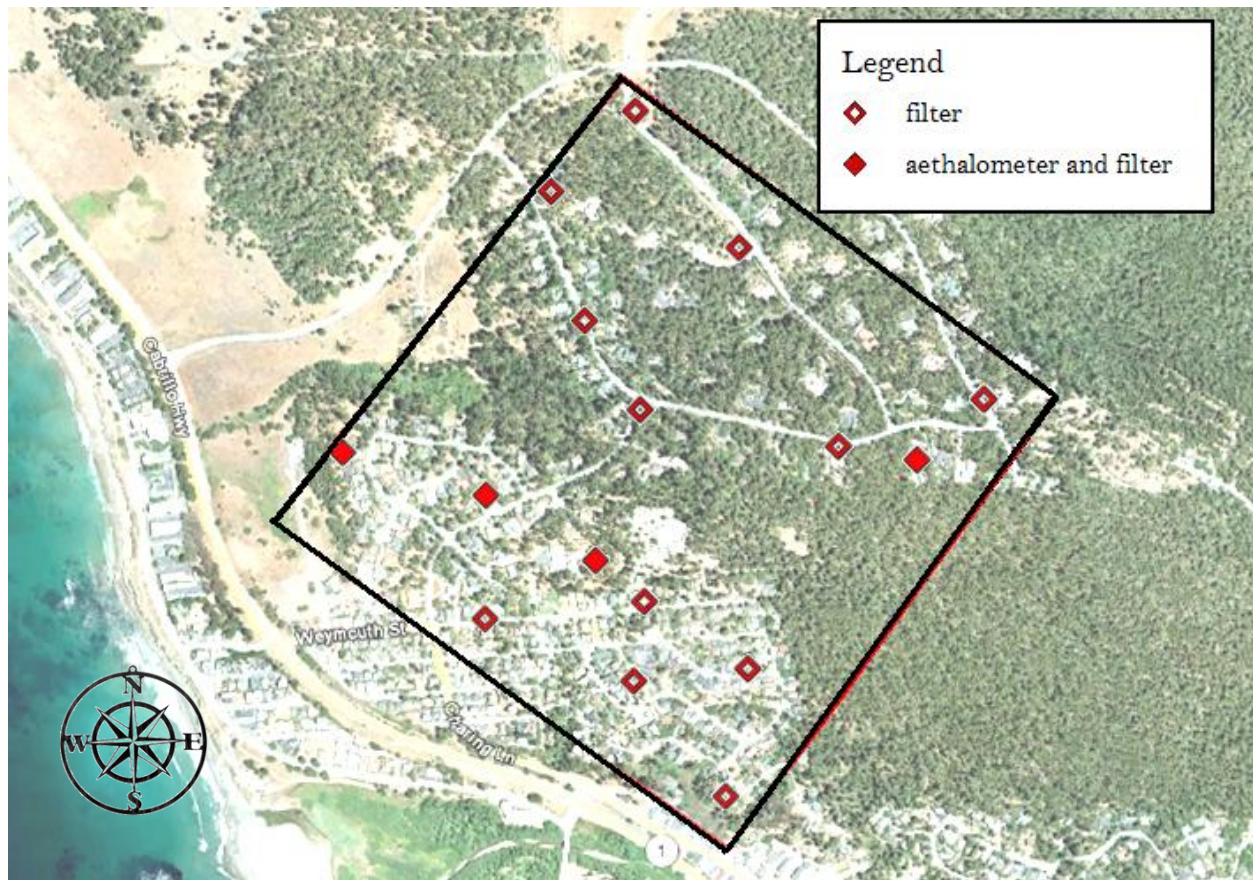


**Figure 5.4 Study area, outlined by black box, with approximate sampling locations for February 28, 2010**

## **6 Determination of Wood Smoke Concentrations**

### **6.1 Wood Smoke Composition**

Particulate matter from wood smoke primarily consists of carbonaceous, sub-micron particles commonly split into two major fractions, elemental carbon (EC) and organic carbon (OC). Minor wood smoke constituents include ions and metals (Fine et al., 2002; Fine et al., 2004a). Black carbon (BC) and brown carbon are other classifications sometimes used to describe the carbonaceous portion of wood smoke. BC refers to the portion of particulate matter that appears black in sunlight, and it is thought to be composed mostly of elemental carbon. Brown carbon refers to OC that absorbs light with lower mass efficiency and greater spectral selectivity than BC (Kirchstetter et al., 2004; Andreae & Gelencser, 2006). The methods used to measure these carbon constituents are discussed below.

The composition of wood smoke is heavily influenced by burning conditions. For example, Rau (1989) found that the fraction of EC in total carbon (TC, equal to the sum of EC and OC) ranged between 52 and 73% for higher combustion temperatures and between 5 and 13% for lower combustion temperatures. Kocbach et al. (2005) reported similar findings. McMeeking et al. (2009) reported that EC emissions were associated with flaming-phase combustion, and that the particulate EC/TC ratio was ~0 during the smoldering phase and 0.5

during the flaming phase of a fire of ponderosa pine. Additionally, the light-absorbing efficiency of the OC in wood smoke depends on combustion temperature, where higher combustion temperatures lead to OC with higher mass absorption efficiency (Chen and Bond, 2010).

*Pinus radiata* or Monterey Pine, which is a native California tree, inhabits much of Cambria and other central coast locations such as Santa Cruz and Monterey. Thus, it can be assumed that the wood burned in fireplaces in Cambria in this study would mostly consist of Monterey Pine. While it has been shown that wood smoke composition is influenced by wood type, e.g., Fine et al. (2004b) reported that the EC fraction of particles varied between 1 and 33% depending on the species burned, we would expect more variation due to burning conditions.

Of the organic species emitted from the combustion of wood smoke, levoglucosan is significantly more abundant than others. Levoglucosan has been found in large quantities in combustion emissions from all wood types studied (Simoneit et al., 1999) and has been found to constitute 7% of total organic carbon (Yan et al., 2007). In Fresno CA, where PM concentrations regularly exceed California standards during the winter months, levoglucosan concentrations have been as high as  $4 \mu\text{g}/\text{m}^3$  (Simoneit et al., 1999). Levoglucosan is stable in the atmosphere and specific to only cellulose pyrolysis (Fraser & Lakshmanan, 2000; Locker, 1988) and is, therefore, considered a chemical marker for biomass combustion. However, levoglucosan is not a quantitative tracer for wood smoke since it is not emitted at the same rate from all wood types and its emission is affected by burning temperature.

## **6.2 Methods**

### **6.2.1 Thermal-Optical Analysis (TOA) Methods**

EC and OC are measured by thermal-optical analysis (TOA) methods. In TOA, particulate matter previously collected on a quartz fiber filter is heated at a prescribed rate in a controlled atmosphere. There are two widely used TOA methods to determine EC/OC: the Interagency Monitoring of Protected Visual Environments (IMPROVE) method (Chow et al., 1993) and the National Institute of Occupational Safety and Health 5040 method (NIOSH, 2003; Birch and Cary, 1996). In both cases, the temperature of the particulate matter sample is stepwise increased, with each increase evolving more refractory carbon compounds. A plot of the rate of carbon evolution with time (or temperature) is known as a carbon thermogram and is integrated over the duration of each temperature step to determine the mass of carbon that was in the sample.

The temperature protocols of the two TOA methods differ. IMPROVE measures organic carbon in a 100% helium environment by integrating OC1 (120°C), OC2 (250°C), OC3 (450°C), and OC4 (550°C) and further measures elemental carbon in a 2% oxygen 98% helium environment by integrating EC1 (550°C), EC2 (700°C) and EC3 (850°C). NIOSH measures organic carbon in a 100% helium environment by integrating OC1 (250°C), OC2 (500°C), OC3 (650°C), and OC4 (850°C) and further measures elemental carbon in a 2% oxygen 98% helium environment by integrating EC1 (650°C), EC2 (750°C) and EC3 (850°C). It has been shown that EC/OC determination depends on the TOA temperature protocol and comparisons of the two methods often yield substantially different estimates of EC, especially for OC dominated samples such as wood smoke (Watson et al., 2005). Both of these TOA methods, therefore, provide different operational definitions for EC and OC. The differences in the temperature profiles between these methods lead to different values for each fraction, however the methods are also similar in many aspects. There is no indication in the literature that one method is better

able to quantify EC and OC from wood smoke. For this study, the proposal called for the use of the NIOSH method for EC/OC determination.

Another TOA method performed at Lawrence Berkeley National Laboratory (LBNL TOA), and described most recently by Hadley et al. (2008), is appreciably different from the IMPROVE and NIOSH methods. The LBNL method heats the sample at 40°C/min from 50 to 750°C in an oxygen atmosphere rather than first in helium and second in a mixture of oxygen and helium. A notable difference is that in the LBNL method, white light transmitted through the sample is measured with a spectrometer. In the more common TOA methods described above, red light transmitted through the sample is monitored and used to aid in the distinction between EC and OC. As in the methods described above, in the LBNL TOA method the carbon thermogram is integrated to determine the mass of carbon in the analyzed sample. In contrast to the above methods, the spectral transmission measurements permit the use of absorption selectivity to aid in distinguishing between carbon types. The LBNL method reports OC and BC rather than OC and EC because of the reliance on optical properties and the absence of a He-only heating phase, which is intended to isolate EC.

In this study, NIOSH 5040 was used to determine EC and OC and LBNL TOA was used to determine BC and OC.

### 6.2.2 *Light Attenuation Method*

We used a light transmission method to characterize the spectral light absorption by aerosol samples collected on quartz fiber filters. Transmission was measured using a custom built optical spectrometer that allowed placement of filter samples between the light source and detector. The light source was a lamp with an emission spectrum extending from the near ultraviolet to the near infrared and the spectrometer was equipped with a fixed diffraction grating and a linear CCD-array detector. Light attenuation (ATN) was calculated from measured sample light transmission (T):  $ATN = 100\ln(1/T)$ . In this study, T was defined as  $(I_s/I_{s,o}) \times (I_{r,o}/I_r)$ , where  $I_s$  and  $I_{s,o}$  are the measured intensities of light transmitted through a quartz filter sample prior to and after removal of carbonaceous material by heating to 800 °C in oxygen,  $I_r$  and  $I_{r,o}$  are the intensities of light transmitted through a reference quartz filter measured at the same time as  $I_s$  and  $I_{s,o}$ , respectively. Measurements of  $I_s$  and  $I_{s,o}$  were made using the same quartz filter.

The amount of light absorbed by particulate matter generally increases with decreasing wavelength, and a power law relationship is often used to express the spectral selectivity:  $ATN = K \cdot \lambda^{-AAE}$ , where ATN is the spectrally dependent light attenuation measured, K is a constant,  $\lambda$  is the wavelength of light transmitted through particulate matter samples, and AAE is the absorption Ångström exponent. The value of the AAE is indicative of the source of the particulate matter. For example, the AAE of motor vehicle exhaust is ~1, whereas biomass burning smoke exhibits stronger absorption selectivity with AAE ~2 (Kirchstetter et al., 2004; Sandradewi et al., 2008a; Sandradewi et al., 2008b). For example, it has been shown that smoldering combustion of pine needles produces soluble particles (i.e., not BC) that exhibit a strong absorption spectral dependence (Patterson and McMahon 1984). The increased spectral selectivity is directly related to the presence of light-absorbing organic carbon in the sample. By extracting from a biomass smoke sample a large portion of the OC, Kirchstetter et al. (2004) found that AAE decreased from 2.2 to 1.3. In contrast, removal of OC from motor vehicle particulate matter had a negligible effect on the AAE.

We computed black carbon concentrations based on the analysis of quartz filter samples by dividing the measured ATN at 880 nm by 16.6 m<sup>2</sup>/g, which is consistent with the attenuation coefficient and calculation of black carbon concentrations in the aethalometer.

### 6.3 Comparisons Between Analytical Methods

On March 7<sup>th</sup> and March 15<sup>th</sup>, 2009, methods comparisons field tests were executed. The goal was to compare methods for determining wood smoke EC and OC. To compare different methods, four filter samples and one or two aethalometers were co-located at four different sites in Cambria, California. Filter samples were collected using SKC Inc. Model 200 Personal Environmental Monitors (PEMs) with PM<sub>2.5</sub> size selection. The Model 200 PEM is designed to operate at a 10 L/min flow rate. Leland Legacy flow-controlled pumps (SKC Inc.) were used to achieve the desired flow rate. In addition, either a battery operated mini-vol sampler (loaned from the California Air Resources Board) or an FRM PM<sub>2.5</sub> sampler was also placed at each location to obtain PM<sub>2.5</sub> filter samples. Figure 6.1 Method comparison IOP showing four PEMs, two aethalometers, and a mini-vol sampler co-located in a resident's backyard shows a method comparison IOP set-up at one site.



**Figure 6.1 Method comparison IOP showing four PEMs, two aethalometers, and a mini-vol sampler co-located in a resident's backyard.**

For each co-location site, two of the PEM quartz filters were sent to Sunset Laboratories (Tigard, OR) for EC/OC analysis by the NIOSH 5040 method. One of these quartz filters collected particulate matter whereas the other was placed in the PEM underneath a Pall Fiberfilm (Teflon-coated glass fiber) filter and was used to measure a sampling artifact that affects the determination of particulate OC. Quartz fiber filters adsorb gaseous organic compounds in addition to collect particulate OC. Therefore, when these filters are analyzed by TOA, the quantified OC overstates the particulate OC. This overestimation is known as the positive OC sampling artifact (Kirchstetter et al., 2001). Since the Teflon filter does not significantly adsorb organic gases but does remove particles, the quartz filter behind the Teflon will only adsorb organic gases. Therefore, the OC on the backup filter provides an estimate of the OC sampling

artifact associated with the quartz filter exposed to both particles and gases. Subtracting the OC mass on the backup filter from the OC mass on the exposed quartz filter provides a correction for this OC sampling artifact. The third PEM filter from each site was analyzed at LBNL using the light attenuation and TOA method describe above. Wisconsin State Laboratory of Hygiene analyzed the fourth PEM filter for levoglucosan.

### 6.3.1 Carbon Comparisons

The bar chart below (Figure 6.2 Comparison of Total Carbon determined from NIOSH 5040 and LBNL TOA method) shows the comparison between total carbon (TC) concentrations from the two TOA methods. Here, TC is the sum of the EC and OC (without artifact removal) in each sample. The eight samples were taken over the course of two weekends at 4 different sites; samples 1-4 for one weekend and 5-8 for the following weekend. Samples 1 and 5 were collected at one site; 2 and 6, 3 and 7, and 4 and 8 were all collected at the other 3 sites, respectively. All of the samples, except 4 and 8, were collected within 1 square mile of each other, while samples 4 and 8 were collected approximately 2 miles to the south.

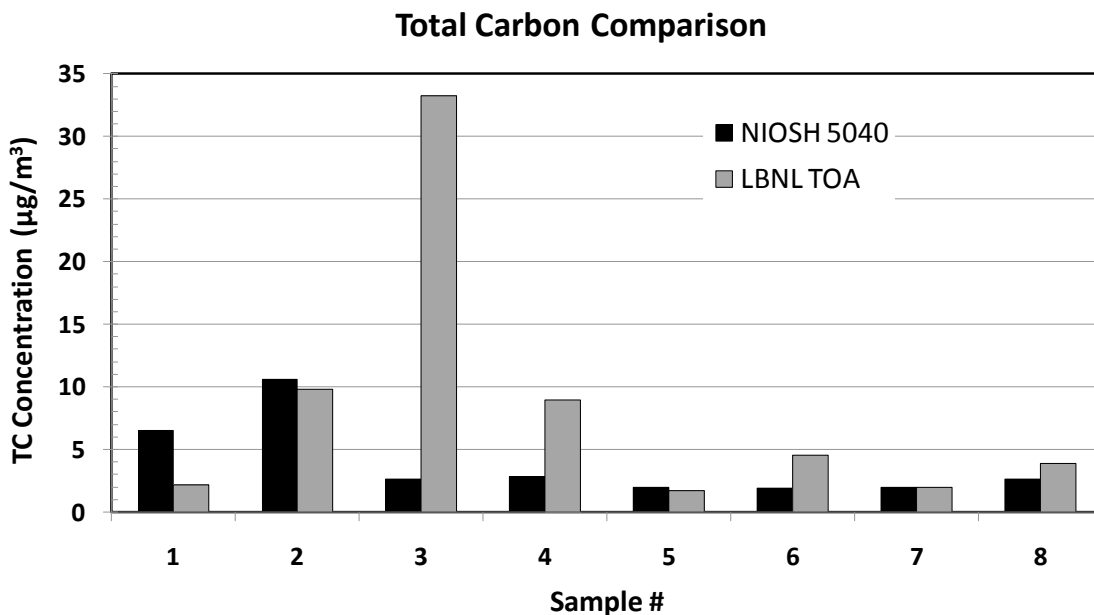


**Figure 6.2 Comparison of Total Carbon determined from NIOSH 5040 and LBNL TOA methods for 12 hour integrated filter samples collected at 4 different locations within Cambria, CA on 2 different days (samples 1 through 4 were collected on 3/7/09 and samples 5 through 8 were collected on 3/13/09)**

The two methods produce comparable values in some cases but not in others, such as with sample 3. It is likely that these differences exist due to handling differences in the filters after collection which could have led to sorption or desorption of organic gases, since TOA measurements of samples had not originally been planned. However in sample 3, the most likely cause is organic carbon contamination of the LBNL sample. Discounting sample number 3, the average LBNL TOA/NIOSH 5040 ratio was  $1.4 \pm 0.9$  using a 95% confidence interval.

The elemental (NIOSH 5040) and black carbon (LBNL TOA, ATN, and aethalometer) concentrations are shown in Figure 6.3. On average, the LBNL TOA/NIOSH 5040 ratio was  $2.11 \pm 0.67$ . This discrepancy illustrates the significant uncertainty associated with quantifying

black carbon concentrations, summarized by Watson et al. (2005). For example, black carbon has been found to be 3.3 times elemental carbon ( $r^2 = 0.84$ ) in one location and 2.7 ( $r^2 = 0.6$ ) in another (Jeong et al., 2004); and during a forest fire event, black carbon was only 30 to 35% of EC. Even when comparing EC determined using the NIOSH 5040 and IMRPOVE TOA methods, the discrepancy can be large, with the IMRPOVE method typically reporting double the concentration of NIOSH 5040 (Chow et al., 2001).

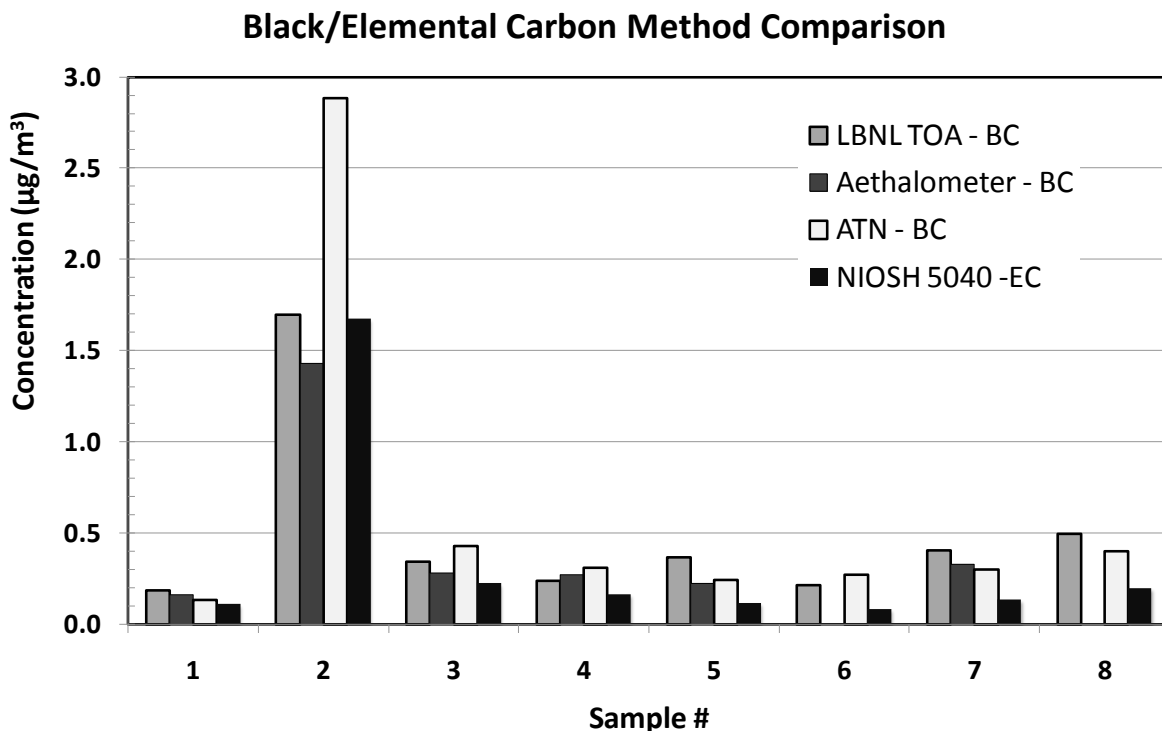


**Figure 6.3 Comparison of black and elemental carbon concentrations for 12 hour integrated filter samples collected at 4 different locations within Cambria, CA on 2 different days (samples 1 through 4 were collected on 3/7/09 and samples 5 through 8 were collected on 3/13/09)**

For samples with a high organic fraction, as in wood smoke, black carbon concentrations have been reported 50 times greater than actual concentrations due to misidentification of organic carbon as black carbon (Novakov & Corrigan, 1995). The organic fraction of wood smoke contains about 6-20% of refractory organic carbon compounds that have combustion temperatures close to black carbon, which may result in misidentification. Moreover, the study found that in the presence of potassium and sodium, both of which are found in wood smoke, combustion temperatures of some organics and black carbon are indistinguishable. Figure 6.3 also compares the BC concentrations measured using three techniques: LBNL TOA, aethalometer, and LBNL light attenuation. The aethalometer was not present during the collection of samples 6 and 8. These three measurements of BC agreed more closely than did the BC and EC measurements discussed above. The LBNL TOA-BC/Aethalometer-BC ratio was  $1.21 \pm 0.25$  and the LBNL TOA-BC/LBNL ATN-BC ratio was  $1.05 \pm 0.30$ .

### 6.3.2 Levoglucosan Analysis

Levoglucosan has been identified as a tracer for wood smoke because of its specificity to biomass combustion. Levoglucosan is an abundant compound in the organic carbon fraction of wood smoke and can be detected even at low OC concentrations. If levoglucosan emissions were a consistent fraction of total wood smoke PM or total wood smoke OC, then its role as a biomass tracer would be validated. Figure 6.4 compares levoglucosan concentrations to organic carbon from NIOSH 5040 with and without subtracting the OC sampling artifact.

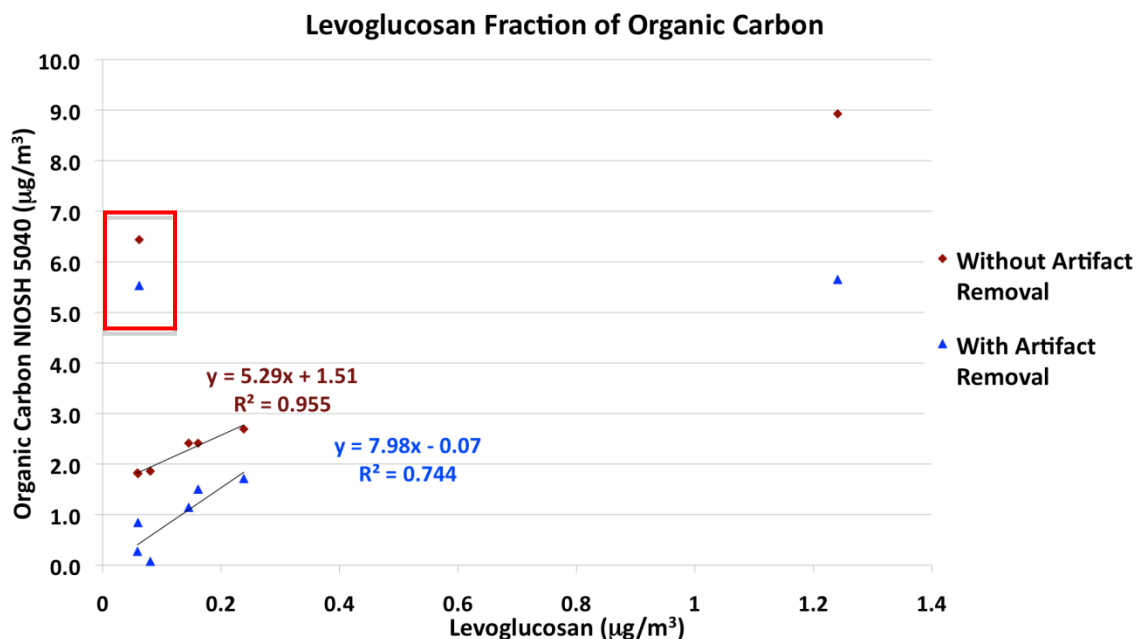


**Figure 6.4 Levoglucosan versus organic carbon fraction, with and without removal of the gaseous carbon artifact, for 12 hour integrated filter samples collected at 4 different locations within Cambria, CA on 2 different days**

*The outlying points in the box and the points with the highest concentrations were not included in the linear regression*

A fairly linear relationship exists between levoglucosan and organic carbon for most of the samples, regardless of whether the organic artifact was removed or not. The points in the box were removed from the regression line because of their influence as outliers. The other extreme points to the far right of the graph were also removed because of their heavy leverage on the regression model. Without artifact removal, levoglucosan represents  $5.9 \pm 3.7\%$  of the total organic carbon present, while with artifact removal, levoglucosan represents  $28 \pm 32\%$  organic carbon using a 95% confidence interval. Yan et al. (2007) reported levoglucosan concentrations around 7% of total organic carbon from a prescribed wildfire episode, which is similar to the results found in this study. The variation after the OC artifact was removed was much greater, as shown by the much larger confidence interval. From this data, it would appear that levoglucosan was a better predictor of organic carbon without artifact removal. Unfortunately, there is a large gap in data between the extreme events and the lower range of concentrations, where the extreme event can heavily influence the slope of the regression. In general, in the analysis for both organic and total carbon the predictor variable does not change much when extreme values are included. For instance, the regression line for OC without artifact removal becomes  $5.24x + 2.2$  when all points are included. However, although the slope is only slightly affected, the fit of the

line falls to an  $R^2$  of 0.63. In this study, the NIOSH method was chosen instead of the IMPROVE method. Comparisons using the IMPROVE analytical method would be expected to show different slopes, due to the differences in the temperature profiles used.

Figure 6.5 shows the relationship between total carbon and levoglucosan. The graph looks nearly identical to Figure 6.4 because of the comparatively low elemental to organic carbon ratios and the relatively stable fractions of elemental carbon to total carbon in each sample. Although this leads to a very similar looking graph, the slopes are a little bit larger in Figure 6.5, indicating a smaller overall fraction of levoglucosan to total carbon. Without artifact removal, levoglucosan represents  $5.4 \pm 3.1\%$  of total carbon, while with artifact removal, levoglucosan represents  $16 \pm 10\%$  of total carbon using a 95% confidence interval. While the percentages in the samples without artifact removal did not significantly change from organic carbon to total carbon, there was a significant reduction from organic carbon to total carbon percentage of levoglucosan with artifact removal. This was due to a few samples with elemental carbon concentrations nearing that of organic carbon after artifact removal. The highest concentrations of OC and TC in Figure 6.4 and Figure 6.5, respectively, correspond to Sample 2. Sample 2 exhibited high levels of TC, OC, BC (by four different methods), and levoglucosan. The absorption angstrom exponent was lowest and the EC/TC was highest for this sample (Table 6.1). Based on the AAE and the EC/TC ratio, Sample 2 is more representative of black carbon dominated aerosols, such as emitted from a diesel vehicle, rather than biomass aerosols. However the presence of high levels of levoglucosan suggests the presence of wood smoke. The reason that Sample 2 is so different from the other samples is unclear, although there may be significant influence from a nearby source. The sample was collected on the same day as Samples 1, 3, and 4 and was collected at the same location as sample 5, but on a different day.

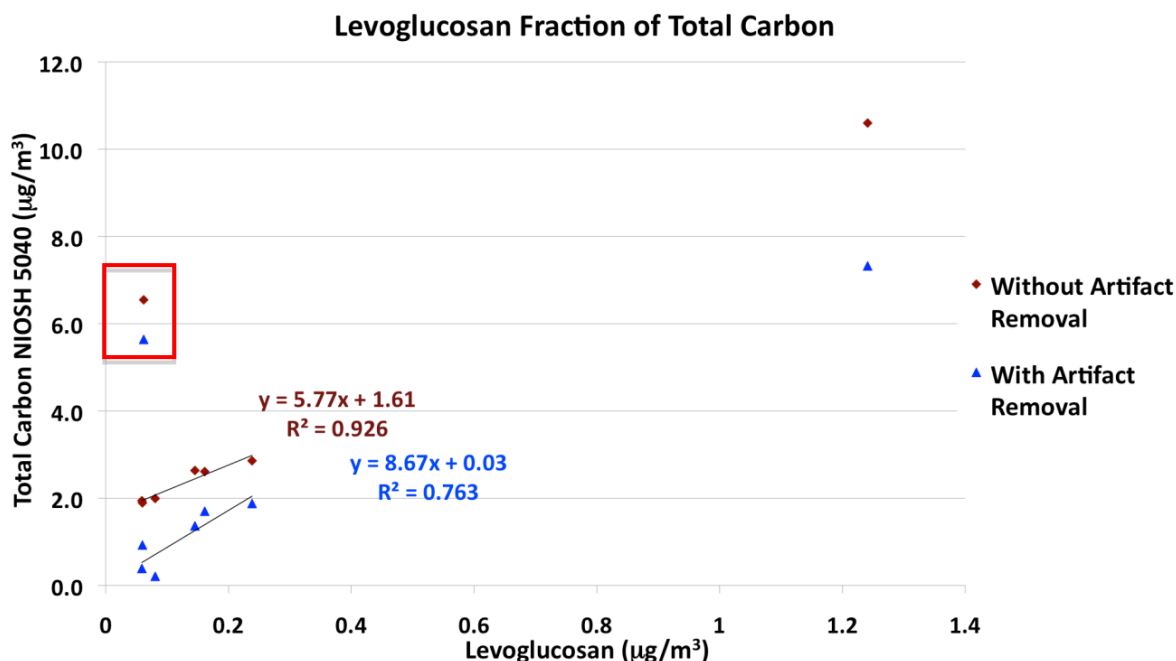


**Figure 6.5** The fraction of total carbon represented by levoglucosan, with and without removal of the gaseous carbon artifact, for 12 hour integrated filter samples collected at 4 different locations within Cambria, CA on 2 different days

The outlying points in the box and the points with the highest concentrations were not included in the linear regression.

The trend between levoglucosan and elemental/black carbon concentrations appears to be generally good with high  $R^2$  values, as shown in Figure 6.6. However, the trend lines are highly influenced by the one measurement with significantly higher concentrations (Sample 2). If Sample 2 is removed from the comparison in Figure 6.5 the  $R^2$  values for all trend lines drop to less than 0.5. This poorer fit may be due to variations in the composition of the wood smoke concentrations for the other samples. If there were multiple samples at higher concentrations then this variability might be evident in higher concentration samples too. The correlation between levoglucosan and the organic fraction may be expected to be better than the correlation between levoglucosan and the non-organic carbon fraction. Since levoglucosan is part of the organic fraction of wood smoke, burning conditions that lead to an increase in levoglucosan may also increase the emission rate of other organic particles in the smoke, leading to an overall increase in OC. However, conditions that favor organic particle formation will not favor BC and EC formation.

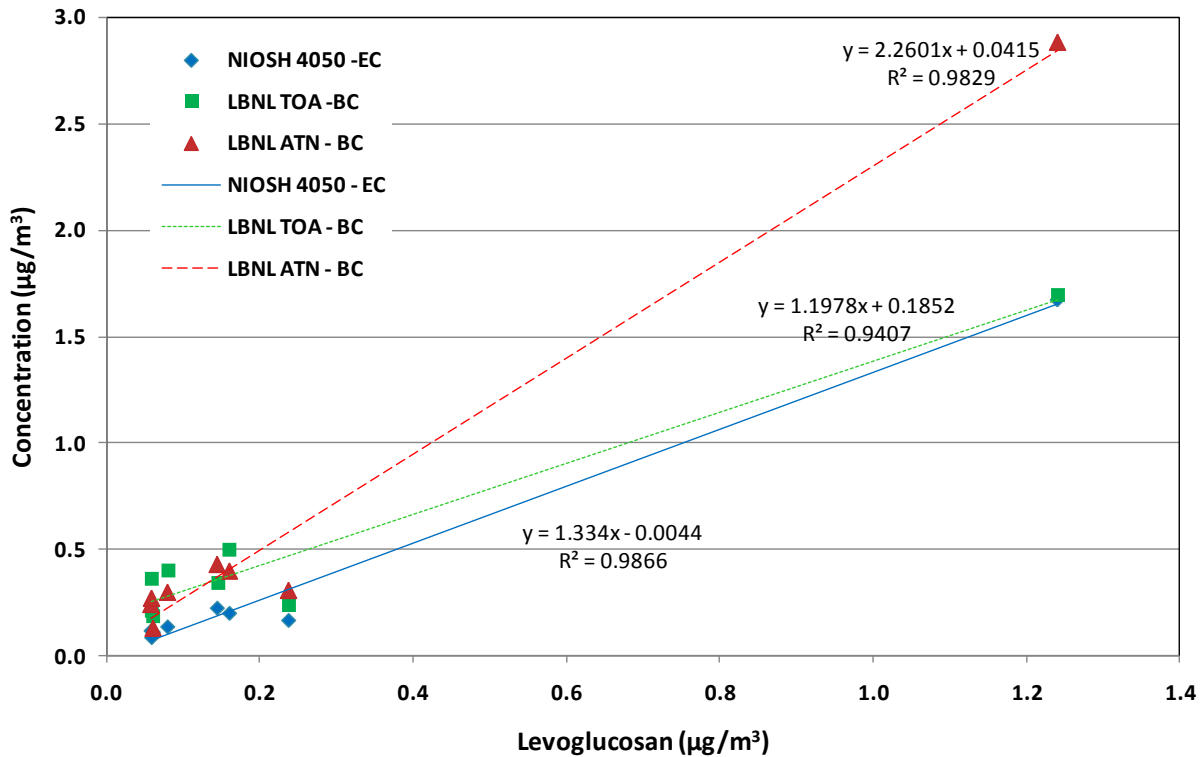


Figure 6.6 Comparison of BC and EC concentrations to levoglucosan for 12 hour integrated filter samples collected at 4 different locations within Cambria, CA on 2 different days

### 6.3.3 Spectral dependence of light absorption

Biomass smoke contains light-absorbing organic carbon in addition to light-absorbing black carbon. Unlike black carbon, which absorbs light broadly over the solar spectrum, the organic carbon in biomass smoke absorbs light much more strongly in the blue and near ultraviolet spectral region. Consequently the light absorption of biomass smoke exhibits a strong spectral dependence (Kirchstetter et al., 2004).

In this study, an overwhelming majority of the samples displayed a strong spectral dependence on light absorption, as exemplified in Figure 6.7. The short dashed line represents the light attenuation of Sample 1 over the range of 350 to 600 nm, which increases with decreasing wavelength. The high AAE value for this sample (2.5) indicates the presence of light absorbing organic carbon typical of biomass smoke. The long dashed line is included in Figure 6.7 to show how much of the total sample attenuation is due to black carbon. This line is extrapolated from the sample's attenuation at 880 nm using the power law and assuming an AAE of 1.1, a typical value for black carbon (Kirchstetter et al., 2004; Schnaiter et al., 2003). Therefore, the sample attenuation above the long dashed line is due to organic carbon as opposed to black carbon.

For biomass smoke, an AAE of around 2 is generally observed. The exponents for each sample from the methods comparison are listed in Table 6.1. The spectral selectivity of all but one sample, Sample 2, resembled wood smoke rather than traffic-derived aerosols, which typically exhibit AAE values of about 1. The low AAE value of Sample 2 is consistent with the high EC/TC ratio for the sample. The EC/TC ratio of Sample 2 was double the next highest EC/TC ratio. The high ratio along with the spectral data suggests that Sample 2 was influenced by motor vehicle exhaust.

The spectral variation in attenuation was generally greater than predicted by the power law fit to the data when a wide wavelength region was considered. Restricting the fit to wavelengths less than 600 nm resulted in an improved fit for most samples.

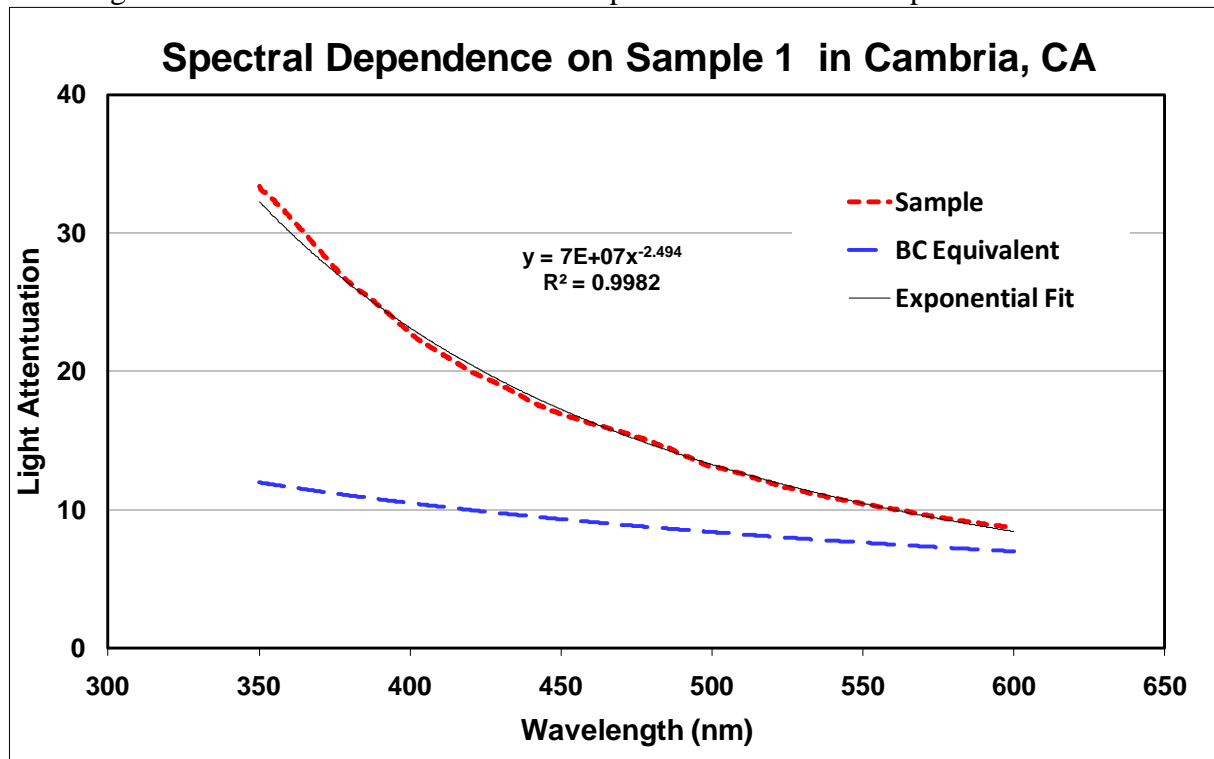


**Figure 6.7** The light attenuation of sample 1 collected in Cambria, CA on 3/7/09 (short dashes), and the portion of the attenuation attributed to black carbon (long dashes)  
*Curves determined by extrapolating from the sample attenuation at 880nm and assuming an AAE of black carbon of 1.1. The solid line is the best-fit power law regression for Sample 1*

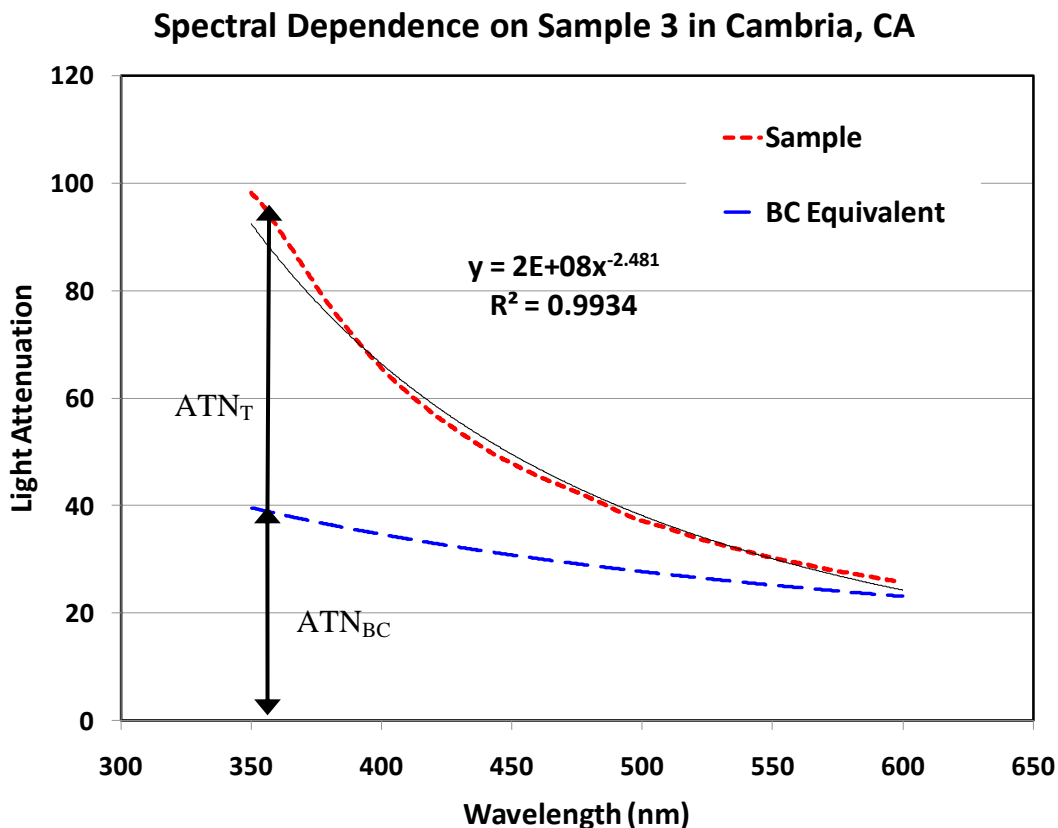
At wavelengths greater than 600nm, there was little to no difference in attenuation between the sample and that expected for black carbon. However, at wavelengths less than 600 nm, the sample attenuation diverges rapidly from that expected for black carbon. This implies that black carbon is the dominant light absorbing species at wavelengths greater than 600nm. At wavelengths less than 600 nm, however, the organic carbon in the sample absorbs a significant amount of light. One group of organic compounds that are present in biomass burning aerosols and absorb light at short wavelengths are humic-like substances (HULIS), which have been found in isolated form to have AAE values near 6 and 7 (Hoffer et al., 2006).

In Figure 6.8, the absorbance due to organic carbon is illustrated by the total attenuation in the sample less the attenuation in the BC equivalent line, or  $ATNOC = ATNT - ATNBC$ . This figure illustrates what was observed for other samples, with exception of sample 2, that at wavelengths below about 450 nm, the amount of light OC absorbs is comparable to or greater than the amount of light BC absorbs. The reason is that these wood smoke samples contained much more OC than BC.

Based on the AAE and the EC/TC ratio, sample 2 is more representative of black carbon dominated aerosols, such as emitted from a diesel vehicle, rather than biomass aerosols. Hence, the attenuation difference between the black carbon equivalent line and sample line was small compared to the amount of OC present in the sample.

**Table 6.1 Absorption Ångström Exponent for each sample determined from a best-fit power law regression over two spectral regions and corresponding sample EC/TC ratio for 12 hour integrated filter samples collected at 4 different locations within Cambria, CA on 2 different days (samples 1 through 4 were collected on 3/7/09 and samples 5 through 8 were collected on 3/13/09)**

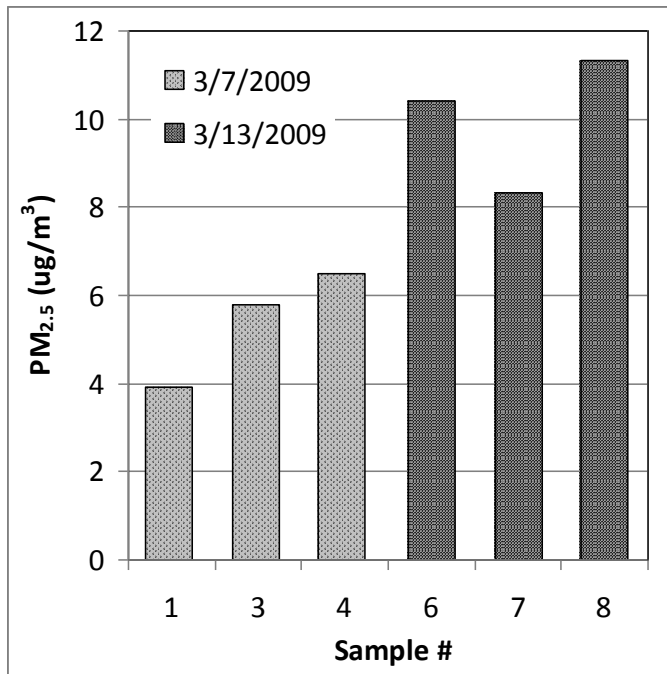
| Sample # | Ångström Exponent<br>Best Fit 350-1000 nm | Ångström<br>Best Fit 350-<br>600nm | NIOSH 4050<br>EC/TC Ratio<br>(artifact corrected) |
|----------|---|------------------------------------|---|
| 1        | 2.0                                       | 2.5                                | 0.02  |
| 2        | 1.1                                       | 1.3                                | 0.23  |
| 3        | 1.7                                       | 2.5                                | 0.16  |
| 4        | 1.9                                       | 2.6                                | 0.09  |
| 5        | 1.7                                       | 2.3                                | 0.30  |
| 6        | 1.5                                       | 2.1                                | 0.09  |
| 7        | 1.7                                       | 2.3                                | 0.64  |
| 8        | 1.8                                       | 2.4                                | 0.12  |



**Figure 6.8** Light attenuation of a sample collected in Cambria, CA on 3/7/09 (short dashes line) showing the amount of attenuation due to black carbon based on the extrapolation from the sample attenuation at 880nm and assuming an AAE of black carbon of 1.1. The solid line is the best-fit power law regression for Sample 3

#### **6.4 Comparison of Methods with $PM_{2.5}$**

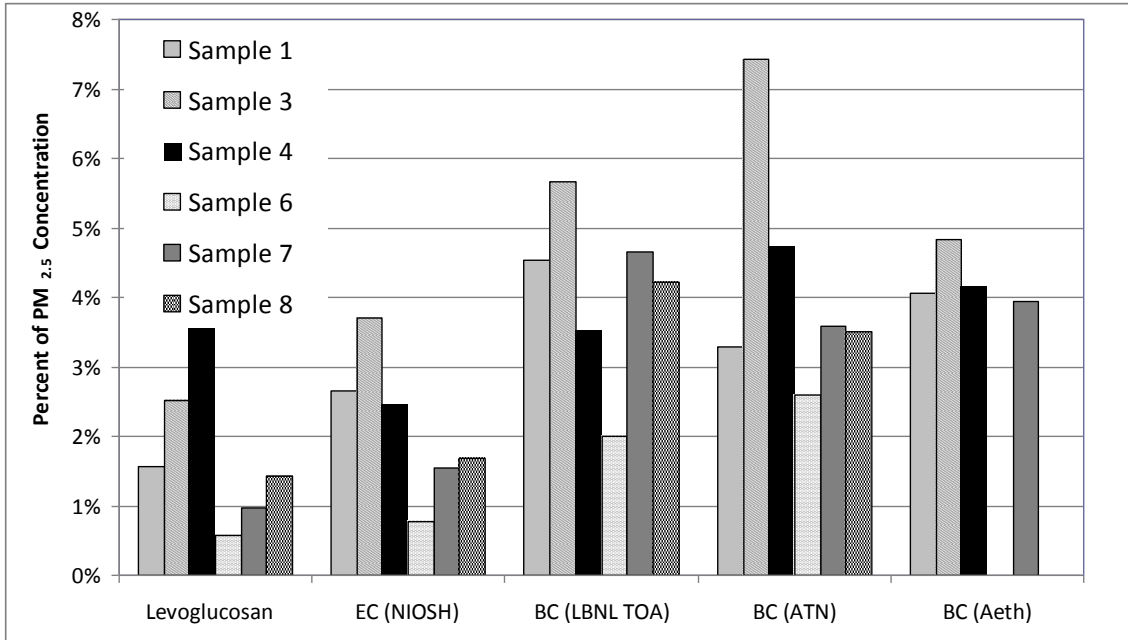
Although measurement of PM mass was beyond the original scope of work, the study took advantage of an opportunity which arose to perform limited  $PM_{2.5}$  filter measurements during the method comparison runs. A battery operated mini-vol sampler or FRM sampler was placed at each method comparison site, however 2 of the 8 runs yielded unusable data due to equipment problems. Results from the six  $PM_{2.5}$  samples are shown in Figure 6.9 by date sampled. Samples 3 and 7 were taken in the same location on different days, as were samples 4 and 8. Concentrations were higher at all sampling locations on the second day than on the first and concentration variation was similar on the two days, but as a fraction of the sample average concentration, the concentration variation was lower on the second day.



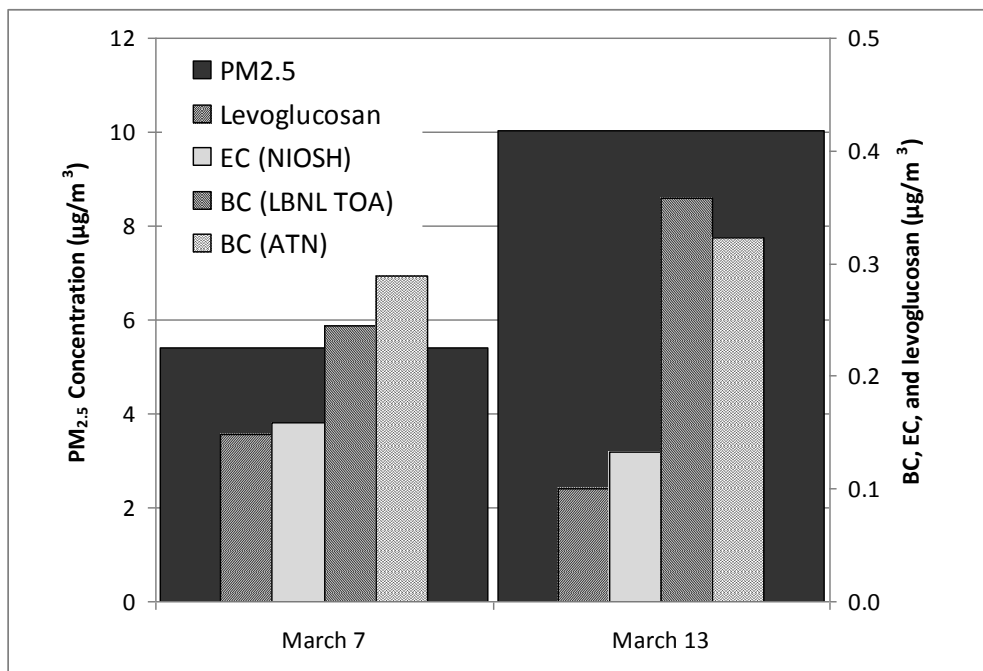
**Figure 6.9** PM<sub>2.5</sub> concentrations for 12 hour integrated filter samples collected using mini vol samplers at 4 different locations within Cambria, CA on 2 different days (samples 1, 3, and 4 were collected on 3/7/09 and samples 6 through 8 were collected on 3/13/09) Two pairs of samples, 3 & 7 and 4 & 8, were collected at the same locations, respectively, on different days.

Figure 6.10 compares the concentrations for levoglucosan, EC (NIOSH), BC (LBNL TOA), BC (ATN), and BC integrated from aethalometer measurements with corresponding PM<sub>2.5</sub> concentrations. A notable feature of the graph is that all measurement methods show considerable variability in the percentage of PM<sub>2.5</sub> represented. This is particularly important in this application since almost all of the ambient PM<sub>2.5</sub> in this region is expected to be wood smoke. Therefore, if wood smoke concentrations were to be estimated from one of these methods there would be significant uncertainty in the outcome. For example, levoglucosan ranges from 0.6% to 3.7% of the sample, so 1 µg/m<sup>3</sup> of levoglucosan could result from a PM<sub>2.5</sub> wood smoke concentration between 30 and 170 µg/m<sup>3</sup>. Although the NIOSH method was used instead of the IMPROVE method to determine EC concentrations, it is expected that the results would be similar if IMPROVE had been used since the variability appears to be due more to changes in the wood smoke composition than inaccuracies of the analytical method chosen.

In addition to general variability, there is a trend for all methods to represent a smaller fraction of total PM<sub>2.5</sub> on the second sampling day (samples 6, 7, and 8). This is particularly true for sample 6, which for all methods had the lowest percentage of any sample (aethalometer BC data is not available to compare with PM sample 6). However, the PM<sub>2.5</sub> concentration was similar at each location (samples 6, 7, and 8) on the same day. The difference between the two days is illustrated in Figure 6.11 with PM<sub>2.5</sub> represented by the wide black bars in the background with the other concentrations superimposed on top of them. Although PM<sub>2.5</sub> concentrations were higher on the second day, levoglucosan and EC concentrations were lower. BC concentrations were higher on day two than day one, but still did rise in proportion with PM<sub>2.5</sub> concentrations.



**Figure 6.10** Results for levoglucosan, EC, and BC as a percentage of the PM<sub>2.5</sub> concentration at 12 hour integrated filter concentrations for each sample. Samples 1, 3 and 4 were collected on 7 March 2009. Samples 6, 7, and 8 were collected on 13 March 2009. Two pairs of samples, 3 & 7 and 4 & 8, were collected at the same locations, respectively, on different days.



**Figure 6.11** Concentrations for BC, EC, levoglucosan, and PM<sub>2.5</sub> averaged over all of the 12 hour integrated filter sampling periods for which PM<sub>2.5</sub> samples were obtained (samples 1, 3, and 4 on 3/7/09 and samples 6, 7, and 8 on 3/13/09). The wide bars represent PM<sub>2.5</sub>

## 7 Variability of Outdoor Wood Smoke Concentrations

The main portion of the study was devoted to investigating the variability of black carbon (BC) concentration within the study area. The field study consisted of 15 intensive operation periods (IOP) over the course of two winter seasons (2009 and 2010). An IOP refers to a 12 hour sampling period where BC was collected throughout the study area using a combination of aethalometers and integrated filter measurements. Due to the project objective of determining the near-field contribution of wood smoke sources, a twelve hour sampling period was preferable to a twenty four hour sample since wood burning occurred primarily between 5 or 6 pm and 5 or 6 am. IOP nights were chosen based on favorable meteorological forecasts. Ideal IOP weather included a combination of low temperatures (to encourage wood burning), moderate to low wind speeds (to reduce dispersion), inversions (to reduce vertical dispersion), and dry weather (to eliminate precipitation scavenging and prevent filter moisture). The original proposal specified 10 IOPs over a single winter season, however contracting delays and a State of California Stop-Work-Order made it impossible to conduct 10 IOPs during the first sampling season, requiring sampling during a second winter season. The project was able to conduct five additional IOPs during the second sampling season due to the favorable conditions at the Cambria, CA study area. Indoor measurements were only collected during the first sampling season. For the second sampling season, the filter samplers that had been deployed indoors were reallocated to the outdoor sampling array to improve spatial coverage.

### 7.1 Methods

Each intensive operation periods (IOP) required instrument and equipment preparation and placement, wood burning source identification, and equipment and instrument pickup. Black carbon (BC) measurements were performed using both integrated filter samples and real time aethalometer measurements. In addition, local meteorological data was supplemented with instruments placed within the study area for some IOPs.

Filter samples were collected using SKC Inc. Model 200 Personal Environmental Monitors (PEMs) with PM<sub>2.5</sub> size selection. A mask containing a 2 cm opening was used to decrease the deposit area and thus increase measurement sensitivity. The Model 200 PEM is designed to operate at a 10 L/min flow rate. Leland Legacy flow-controlled pumps (SKC Inc.) were used to achieve the desired flow rate. The pumps were calibrated using a Model DC-HC-1 Bios DryCal DC-2 calibrator. To protect the pumps and decrease noise disturbance in the neighborhood, the pumps were placed inside of a plastic container surrounded by pieces of foam during sampling. PEM were placed either on top of or near the housing depending on the sampling location, as shown in Figure 7.1. For each IOP, all SKC pumps were programmed to run for 12 hours either between 6 p.m. and 6 a.m. or 5 p.m. and 5 a.m., depending on when sunset occurred. The twelve hour sampling period was chosen to coincide with the hours where wood burning is most prevalent and exclude daytime hours where burning is not prevalent and other aerosol sources are more dominant. After collection, samples were analyzed using light attenuation methods.

The original proposal anticipated a study area with a significant number of interfering sources for both black carbon and organic carbon. Consequently, in the initial analytical plan it was anticipated that analysis of the absorption spectrum would be required to determine the fraction of the overall particle loading that could be attributed to wood smoke emissions. However, the study area selected had no significant interfering sources. As shown in Sections 6.3 and 6.4, spectral analysis indicated that wood smoke was the dominant particle source and that

black carbon concentration performed as well as any of the other surrogate measurements of wood smoke particle concentration. As a result, the analysis of the variability of wood smoke concentrations within the study area has been performed using black carbon (BC) concentrations to represent the amount of wood smoke at the sampling locations.

BC measurements were performed using Magee Scientific aethalometers at 1- or 2-minute time resolution. Of the four different aethalometers used in this study, one was multi-wavelength, measuring light attenuation at 370, 470, 520, 590, 660, 880, and 950 nm and three were dual wavelength, measuring light attenuation at 370 and 880 nm. Aethalometers were co-located with a PEM and placed outside of the homes of volunteers in locations where they would not be disturbed and where an outdoor power source was available. The original sampling plan specified one mobile aethalometer driven around within the study area. However, due to the large temporal fluctuations in concentration, data from the mobile aethalometer was not useful and its deployment was discontinued during the site selection screening process.

It is important to note that due to the algorithm used in the aethalometer, extremely low BC concentrations can be read as negative values. This has been attributed to desorption of organic vapors from the filter surface as relatively clean air passes through the aethalometer. This desorption results in a decrease of UV absorbing material, which is then interpreted as a negative value in the aethalometer algorithm (Hansen, 2005). To correct for negative BC readings, the lowest detection limit (LDL) was used to replace each negative value. In accordance with the aethalometer manual, the LDL was calculated assuming 1 ng noise per 20 liters air flow (Hansen, 2005).

For this study, the aethalometers were calibrated by adjusting their internal calibration values,  $\sigma_{SG}$ , to more precisely represent one another. Aethalometers were simultaneously run side-by-side over a period of 24 hours once early in the winter sampling period and then a second time after sampling was completed. The multi-wavelength aethalometer was not tested after sampling completion because the aethalometer filter tape was unexpectedly used up and changing the tape may have changed calibrated  $\sigma_{SG}$  values. Determined  $\sigma_{SG}$  values for winter 2010 demonstrated a percent difference from between 17 and 31 percent in comparison to values for winter 2009. The difference in instrument response between 2009 and 2010 may have been due to drift in the calibration of the internal flow meters or other factors such as relative humidity.

For each side-by-side aethalometer run, the  $\sigma_{SG}$  values for each aethalometer was reduced or increased over one time interval of measured BC concentrations to achieve the average BC concentration of all aethalometer BC readings. The  $\sigma_{SG}$  values were then applied to the second time interval of BC concentrations and a statistical Analysis of Variance (ANOVA) conducted in Minitab on the adjusted readings in the second time interval to determine whether significant differences existed between the different aethalometers. The ANOVA test evaluates whether or not significant differences exist under the assumption that the responses, or measured BC concentrations in this case, are independent from one another, are normally distributed, and that the samples from each machine have equal standard deviations. Based on probability distributions, the ANOVA test determines whether the mean response for each machine deviates enough from the mean response of all machines to be considered different. If differences were found based on the ANOVA test,  $\sigma_{SG}$  was adjusted until the test indicated no statistical difference between machines.  $\sigma_{SG}$  values were only adjusted using time segments where all machines were similar in concentration-trends. Selecting only segments displaying the same behavior eliminates influences of readings that deviated significantly from the others. BC

readings were averaged over ten minutes to reduce noise in the calibration. Values for  $\sigma_{SG}$  determined for the two simultaneous runs were averaged and used for the study readings.



**Figure 7.1 Personal Environmental Monitor (PEM) shown deployed on top of the protective housing with the sampling pump and sound proofing material inside.**

The original proposal called for 3 to 5 sonic anemometers to be deployed within the study area to determine wind speed and direction. However, delays in the contracting process and the State of California Stop-Work-Order which occurred at the beginning of the project delayed the field deployment so that these units were no longer available. Local weather stations deployed by other entities (weather underground and fire department stations) were used to collect the needed meteorological data. In addition, two meteorological instruments were deployed for some of the IOPs during this study: an EBAM weather station and an ultrasonic anemometer. The Met One Instruments, Inc. E-BAM (Beta Attenuation Monitor) 9800 Rev K, borrowed from the San Luis Obispo Air Pollution Control District (SLO APCD) was used to measure  $PM_{10}$  and meteorological parameters. The E-BAM was operated using the standard  $PM_{10}$  measurement mode, which uses a flow rate of 16.7 L/min, and  $PM_{10}$  measurements were taking at 10 minute and 1 hour intervals. Wind speed and direction were measured using a wind combination sensor Model 034B mounted on the E-BAM; the ambient temperature sensor has a range between -50 and 50°C with an accuracy of 0.1°C; and the Model EX-593 relative humidity sensor has a range between 0 and 100 percent with an accuracy of 3 percent (Met One Instruments, Inc., 2001).

For this study, the E-BAM recorded meteorological data at the Cambria California Department of Fire (CDF) station at an elevation of 227 feet within a field approximately with adequate clearance on 3 sides and about 30 feet away from the closest trees and fences on the fourth side. While the Met One Instruments, Inc. manual (2001) recommends placement at least 20 meters from the drip line of trees, due to particle deposition on tree surfaces, such a large amount of space was unavailable within the study area. Before operation, the E-BAM was flow and leak checked, the temperature was compared to an external thermometer, and the E-BAM was properly aligned. Because the E-BAM is capable of withstanding even rainy conditions, the E-BAM was left to run during and in between IOPs, starting with IOP 4b. Although meteorological data was recorded for the last seven IOPs, and instrument error occurred during IOP 9b which prevented PM<sub>10</sub> measurements.

Additional meteorological data was collected using a Young Model 81000 Ultrasonic Anemometer which was used to measure meteorological data within the study area during IOPs 8b, 9b, and 10b. The ultrasonic anemometer is capable of high resolution readings, up to 32 Hz and its wind speed threshold is 0.2 m/s (any lower wind speeds are read as 0 m/s). Wind speed accuracy between 0 and 30 m/s is  $\pm 0.05$  m/s and wind direction between 1 and 30 m/s is  $\pm 2^\circ$ . The ultrasonic anemometer tracks temperature ranges between -50 and 50°C to correct for wake effects caused by the anemometer structure and agrees with ambient temperature within 2°C. For this reason, the anemometer temperature was used as a proxy for ambient temperature.

During the IOPs, the anemometer was placed in the backyard of a Cambria resident at an elevation of 207 feet approximately 5 feet away from any obstructions. While fewer obstructions would have been preferred; options were limited based on the configuration of the yard. Before operation, the anemometer was aligned with true north and the temperature was compared to a thermometer. The sonic anemometer was run during three of the nine IOPs (8b-10b) taking measurements 4 times each second. The ultrasonic anemometer was co-located with an aethalometer and a PEM.

In addition to the meteorological data collected at the sampling sites, statistical and dispersion modeling analyses also used data collected from existing stations near the study area. Cambria weather data was available through the Weather Underground website which provides free historical and real-time weather data in both national and international locations. In addition to providing meteorological data from its own stations, Weather Underground's Personal Weather Station (PWS) project allows any resident, organization, or business to contribute meteorological measurements in their area to the Weather Underground website. While PWSs are typically not certified, Weather Underground provides free meteorological archives.

PEMs, aethalometers, and meteorological instruments were distributed as evenly as possible over the whole the study area. Sampling locations were restricted to volunteers' homes and locations where the PEMs would be less likely disturbed. The sample arrangement from IOP 7b is displayed in Figure 7.2. The original proposal also specified collecting filter samples at the nearest regional monitoring stations, however there are no APCD monitoring stations within the Cambria area. Table 7.1 below summarizes sampling period date and time, number of PEMs and aethalometers deployed, and meteorological instruments used.

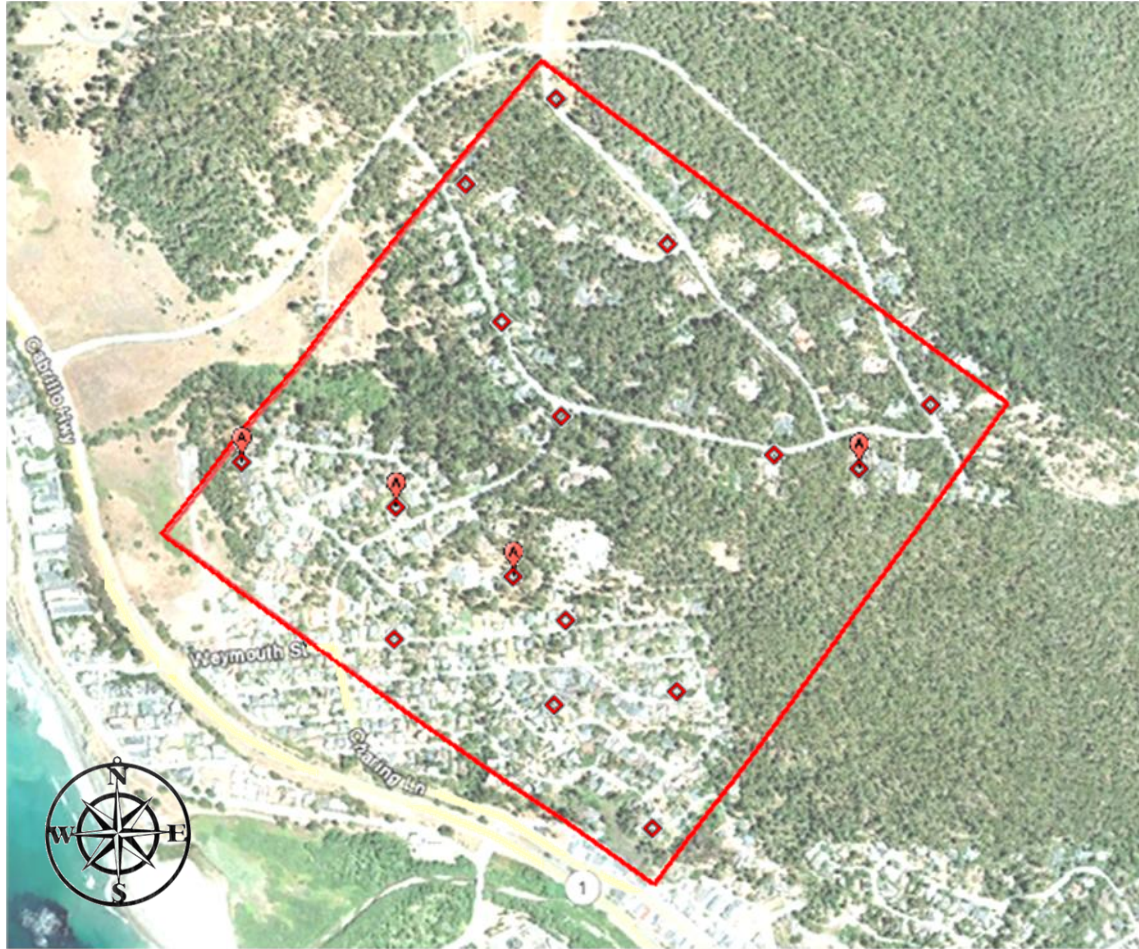


**Figure 7.2** Sampler arrangement for IOP 7b showing locations of 12 hour integrated filter samplers (PEMs) and aethalometers within the Cambria, CA study area.

The identification of wood burning sources was conducted using a Fluke Ti25 Thermal Imager. The Fluke Ti25 can measure the temperature of objects ranging from  $-4^{\circ}\text{F}$  to  $662^{\circ}\text{F}$  within accuracy of  $\pm 2^{\circ}\text{C}$  or 2% and capture thermal images. To identify wood burning sources, the Fluke Ti25 was used to determine chimney temperature. Chimney temperatures detected above  $75^{\circ}\text{F}$  were considered to be burning wood and images of burning sources were captured. A sample image from IOP 3b taken on January 30<sup>th</sup> is displayed in Figure 7.3.

## **7.2 Summary of Intensive Operational Periods**

Several statistical analyses were conducted to understand BC variability and interactions with meteorology and site characteristics. BC variability was observed through averages, medians, and standard deviations at each sampling location, between sampling locations, and between IOPs. Spatial variability between meteorological data at different sites was observed through averages, medians, and standard deviations for wind speeds, wind directions, temperature, and humidity.



**Figure 7.3** Sample infrared camera image showing the chimney base at 48.8F with a peak temperature of approximately 130F at the spark arrestor on top of the chimney

### **7.3 Variability of Real Time Measurements**

BC variability was determined for each IOP using 30 minute averaged aethalometer readings. Table 7.2 details the average, median, and standard deviation these BC concentrations over each IOP. In general, the variability within IOPs increases when average black carbon concentrations are elevated and decreases at lower concentrations. The temporal and spatial variability can be seen in the aethalometer BC concentrations versus time graph for IOP 7b shown in Figure 7.4 for the different aethalometer locations shown in Figure 7.5. This graph indicates that at each location there is a significant temporal variation in concentration at all locations and a significant spatial variation during the early evening hours when concentrations are higher. Comparison of IOPs 5b through 9b, all containing the same number of aethalometers, in Table 7.2, indicates that although the number of aethalometers in operation may affect the magnitude of the standard deviation since averaging BC at more sites increases the spatial variability captured by the statistic, it is not the dominate consideration. Spatial variability likely accounts for a smaller portion of the standard deviation, because typical differences in BC concentration between locations are much smaller than the differences between the highest and lowest BC concentrations measured at a single location. This effect can also be seen when analyzing the data collected every minute. For one minute BC concentrations over all IOPs the standard deviation was much larger, 2,640 ng/m<sup>3</sup>, than for the 30 minute data, 438 ng/m<sup>3</sup>. The high standard deviation in the data is likely the result of turbulent fluctuations when the source is near the receptor, but also includes the effect of higher measurement noise in the one minute readings.

**Table 7.1 Summary of instruments deployment and sampling times of Intensive Operational Periods (IOPs) for the field study conducted in Cambria, CA.**

| IOP         | Date            | Sample Time | Number of Outdoor PEMs | Number of Outdoor Aethalometers | Meteorological Data (Yes=y, No=n) |            |
|-------------|-----------------|-------------|------------------------|---------------------------------|-----------------------------------|------------|
|             |                 |             |                        |                                 | EBAM                              | Ultrasonic |
| Winter 2009 |                 |             |                        |                                 |                                   |            |
| 1a          | Jan 31 - Feb 1  | 6 PM - 6 AM | 9                      | 2                               | n                                 | n          |
| 2a          | Feb 18 - Feb 19 | 6 PM - 6 AM | 11                     | 2                               | n                                 | n          |
| 3a          | Feb 26 - Feb 27 | 6 PM - 6 AM | 8                      | 1                               | n                                 | n          |
| 4a          | Feb 27 - Feb 28 | 6 PM - 6 AM | 11                     | 2                               | n                                 | n          |
| 7a*         | Mar 15 - Mar 16 | 6 PM - 6 AM | 12                     | 1                               | n                                 | n          |
| 8a*         | Mar 20 - Mar 21 | 6 PM - 6 AM | 12                     | 2                               | n                                 | n          |
| Winter 2010 |                 |             |                        |                                 |                                   |            |
| 2b          | Jan 23 - Jan 24 | 6 PM - 6 AM | 11                     | 3                               | n                                 | n          |
| 3b          | Jan 30 - Jan 31 | 6 PM - 6 AM | 16                     | 3                               | n                                 | n          |
| 4b          | Feb 13 - Feb 14 | 5 PM - 5 AM | 15                     | 3                               | y                                 | n          |
| 5b          | Feb 28 - Mar 1  | 5 PM - 5 AM | 15                     | 4                               | y                                 | n          |
| 6b          | Mar 4 - Mar 5   | 5 PM - 5 AM | 14                     | 4                               | y                                 | n          |
| 7b          | Mar 11 - Mar 12 | 5 PM - 5 AM | 15                     | 4                               | y                                 | n          |
| 8b          | Mar 15 - Mar 16 | 6 PM - 6 AM | 15                     | 4                               | y                                 | y          |
| 9b          | Apr 3 - Apr 4   | 6 PM - 6 AM | 15                     | 4                               | y                                 | y          |
| 10b         | Apr 23 - Apr 24 | 6 PM - 6 AM | 15                     | 3                               | y                                 | y          |

*\*These IOPs were not included in some results and analyses due to a high prevalence of PEM BC concentrations lower than the detection limit.*

Over the course of the study, aethalometers were placed at five different locations, labeled A through E in Figure 7.5. Variability by sampling site across all IOPs is displayed in Table 7.3 and Figure 7.6 based on aethalometer black carbon measurements averaged over 30 minutes. The highest BC average and standard deviation were observed at site B where the

highest BC concentrations were also detected. However, the median at B was similar to the medians at other sites. This difference is due to the fact that the average for site B is highly influenced by data from IOPs 4b and 5b when a home adjacent to the site was burning and influence from this source created very high concentrations. The average and median concentration for sites A, C, and D were fairly similar, while the median concentration at site E was lower. Standard deviations were also fairly similar with the clear exception of site B and a slightly higher standard deviation for site A.

**Table 7.2 Aethalometer black carbon (BC) concentrations averages and variability for 12 hour sampling periods over thirteen Intensive Operational Periods (IOPs) conducted in Cambria, CA during the winters of 2009 and 2010.**

*Statistics are based on 30 min averaged BC concentrations measured during each IOP*

| <b>IOP #</b>   | <b>Number of Outdoor Aethalometers in Operation</b> | <b>Average (ng/m<sup>3</sup>)</b> | <b>Median (ng/m<sup>3</sup>)</b> | <b>Max (ng/m<sup>3</sup>)</b> | <b>Min (ng/m<sup>3</sup>)</b> | <b>Standard Deviation (ng/m<sup>3</sup>)</b> |
|----------------|---|-----------------------------------|----------------------------------|-------------------------------|-------------------------------|--|
| 1a             | 2   | 385                               | 359                              | 902                           | 238                           | 132  |
| 2a             | 2   | 110                               | 69                               | 397                           | 32                            | 88   |
| 3a             | 1   | 54                                | 32                               | 139                           | 14                            | 42   |
| 4a             | 2   | 137                               | 99                               | 883                           | 7                             | 191  |
| 2b             | 3   | 141                               | 125                              | 298                           | 77                            | 47   |
| 3b             | 3   | 184                               | 91                               | 1060                          | 4                             | 245  |
| 4b             | 3   | 626                               | 237                              | 16720                         | 13                            | 1996   |
| 5b             | 4   | 511                               | 194                              | 18160                         | 7                             | 1843   |
| 6b             | 4   | 167                               | 77                               | 1063                          | 7                             | 227  |
| 7b             | 4   | 151                               | 131                              | 896                           | 4                             | 99   |
| 8b             | 4   | 141                               | 82                               | 2006                          | 7                             | 252  |
| 9b             | 4   | 192                               | 100                              | 4134                          | 4                             | 461  |
| 10b            | 3   | 144                               | 123                              | 553                           | 87                            | 62   |
| <b>Average</b> |   | 226                               | 132                              | 3630                          | 38                            | 438  |

**Table 7.3 Black carbon (BC) concentrations averaged by sampling location for all IOPs using 30 minute averaged aethalometer data. Note: Aethalometers were not deployed at all locations for every IOP**

| Site           | Cases | Average (ng/m <sup>3</sup> ) | Median (ng/m <sup>3</sup> ) | Std Dev |
|----------------|-------|------------------------------|-----------------------------|---------|
| A              | 11    | 214                          | 144                         | 228     |
| B              | 10    | 381                          | 125                         | 1632    |
| C              | 6     | 157                          | 112                         | 169     |
| D              | 9     | 175                          | 126                         | 168     |
| E              | 3     | 128                          | 50                          | 151     |
| <b>Average</b> |       | 211                          | 111                         | 470     |

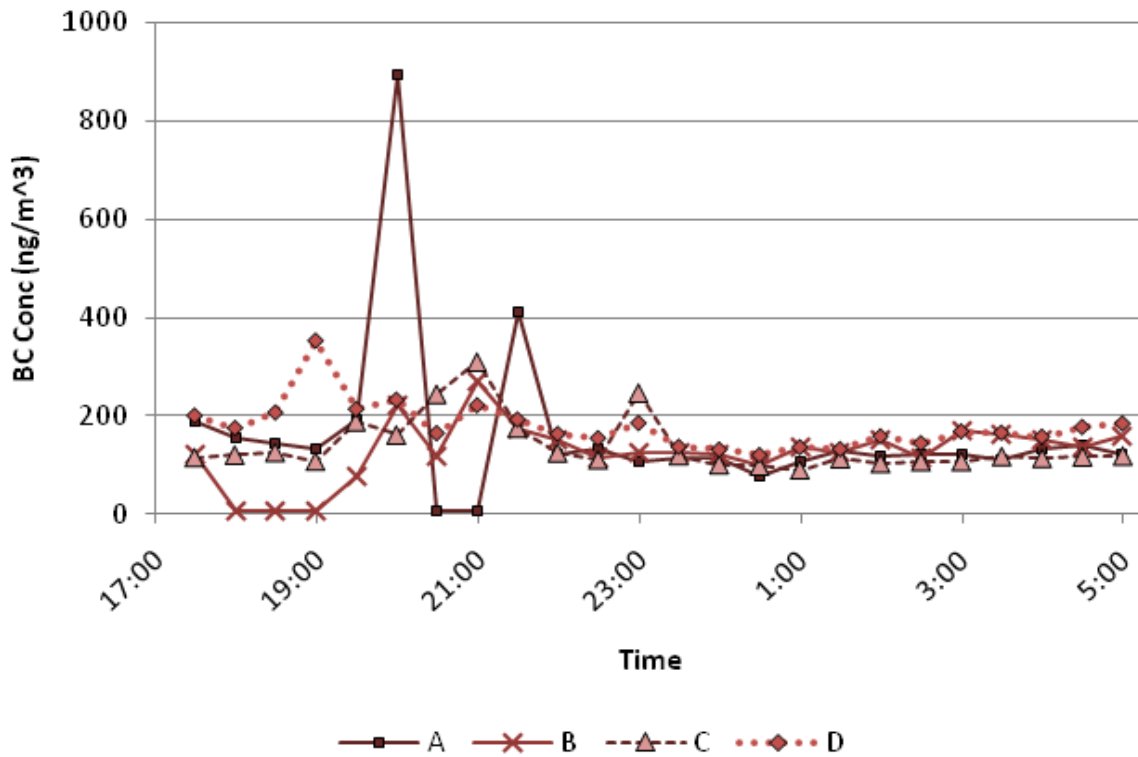


**Figure 7.4 30 minute average aethalometer black carbon concentrations at 4 locations within the study area, as shown in Figure 7.5, during IOP 7b (collected from 5pm 3/11/10 to 5am 3/12/10)**



**Figure 7.5 Aethalometer sampling locations used during the Intensive Operational Periods (IOPs).  
Note: Aethalometers were not deployed at all locations during every IOP.**

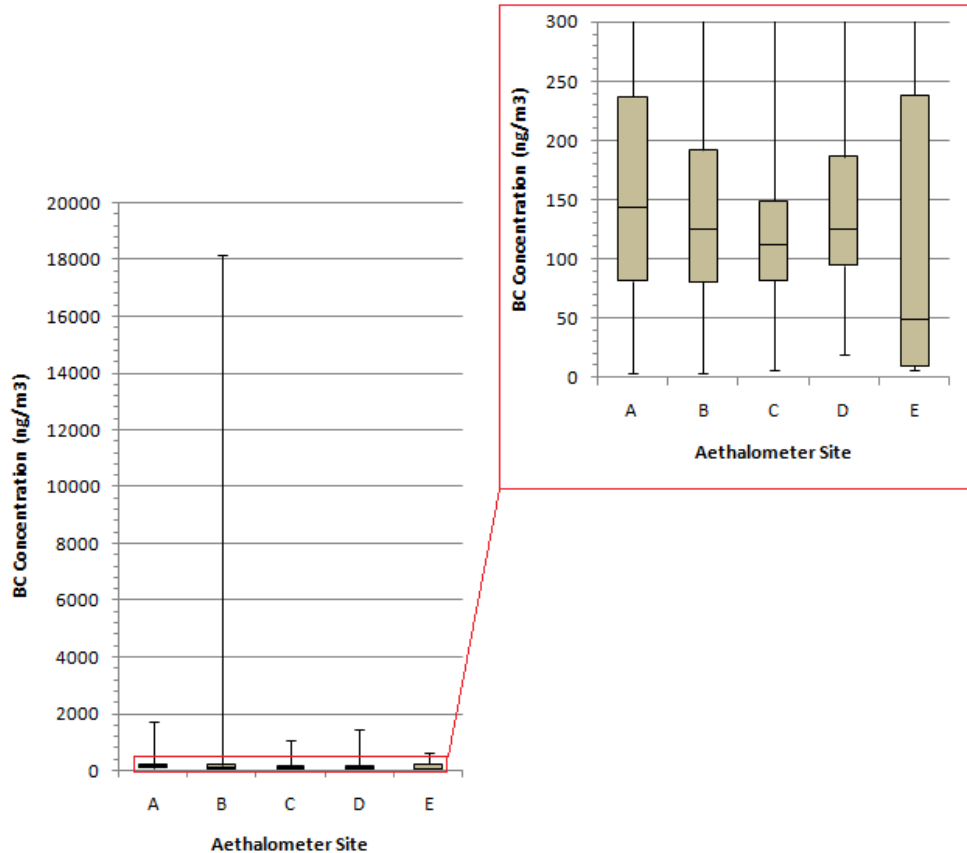


**Figure 7.6** Box plot comparing aethalometer black carbon (BC) concentrations between sites, as shown in Figure 7.5, over all IOPs. Note: Aethalometers were not deployed at all locations during every IOP

*Boxes denote the 1<sup>st</sup> and 3<sup>rd</sup> quartile and median value for all concentrations. The whiskers indicate the maximum and minimum values.*

#### 7.4 Variability of Filter BC Measurements

During each IOP, between 8 and 16 Personal Environmental Monitors (PEMs) successfully collected 12 hour outdoor filter samples within the study area. These filters were subsequently analyzed using light attenuation and the results were used to determine black carbon (BC) concentration, as well AAE values. Figure 7.7 shows all of the PEM sampling locations used during the study. Not all sites were used for all IOPs. Although PEM locations were kept as consistent as possible between IOPs, location changes occurred between sampling seasons and sites sometimes shifted due to access issues.

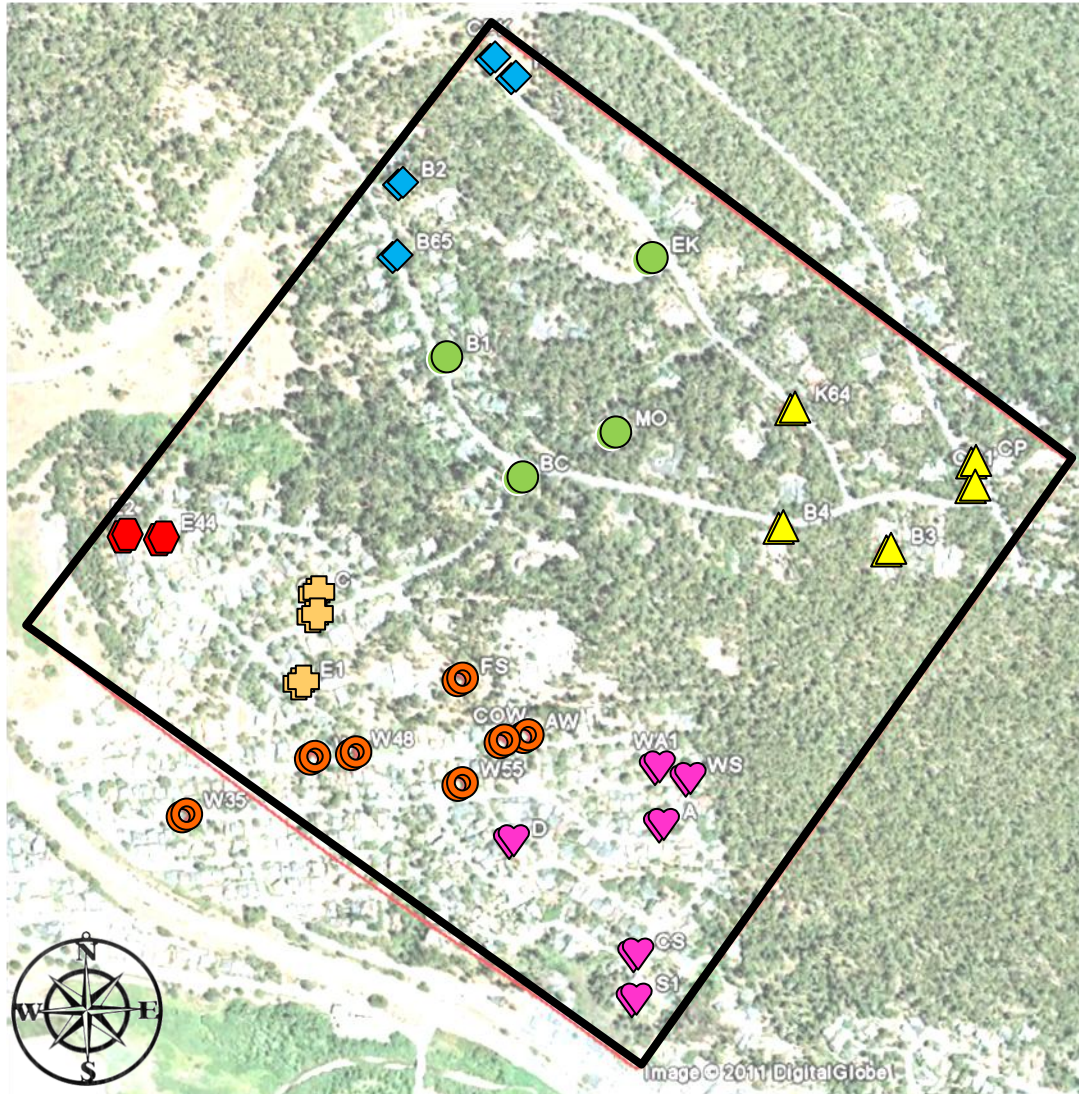


**Figure 7.7 Labels for all PEM sample locations used during the study. Only a subset of these locations was used for each Intensive Operational Period (IOP). Location symbols are coded to assist with grouping of results.**

The average PEM BC concentration over all locations and IOPs was  $224 \text{ ng/m}^3$  with a standard deviation of  $262 \text{ ng/m}^3$ . IOPs 7a and 8a were excluded from most analyses due to the high number of samples below the detection limit. The low concentrations during these runs are attributed to higher wind speeds and wind gust speeds during the early evening when sources were active and the lack of an inversion during IOP8a. Table 7.4 summarizes PEM BC averages, medians, and standard deviations by IOP. Figure 7.8 shows box plots for each IOP, illustrating that PEM concentrations tended to vary widely between sites for a single IOP with most concentrations much lower than the maximum concentrations for each IOP.

Figure 7.9 shows PEM BC concentrations for all sites and IOPs. Although there is a high degree of concentration variability between sites, there is also a general tendency for some sites to have higher concentrations than others. In addition to general variability, a small subset of samples exhibit concentrations that are much higher than any other samples during that IOP. It is expected that these very high concentrations are strongly influenced by a single nearby source

impinging onto the sampler. A general concentration trend can be seen more clearly when concentrations for all IOPs are averaged by site (Figure 7.10). In general, samples taken nearer the northeastern edge of the study area tended to have lower concentrations than those in the southwestern portion of the study area. There are several topographic differences between the two areas which could contribute to the observed differences. For instance, the northeastern portion has more tree coverage, lower housing/source density, and a higher elevation than the southwestern area. A potentially more important factor is that the winds most often entered the study area from the north or east during the IOPs. Consequently, black carbon from sources within the study area would be expected to increase in concentration within the air mass as the relatively clean entering air encountered sources within the study area. This gradient in concentration is apparent in several of the IOPs, such as IOP 3b shown in Figure 7.11. However, this trend was not always consistent and for some IOPs, such as IOP 1 shown in Figure 7.12, there was no concentration gradient. By visual inspection, for the 15 IOPs in this study, 6 showed a concentration gradient with concentrations generally increasing for locations toward the southwestern portion of the study area, 3 showed a slight but inconsistent concentration gradient, 4 showed no perceptible concentration pattern, and 2 had concentrations too low to determine if a pattern existed.

**Table 7.4 Black carbon concentrations for 12 hour PEM filter samples averaged by Intensive Operational Period (IOP)**

| <b>IOP</b>       | <b>Number of PEMs in Operation</b> | <b>Number of Sources Detected</b> | <b>Average (ng/m<sup>3</sup>)</b> | <b>Median (ng/m<sup>3</sup>)</b> | <b>Standard Deviation</b> |
|------------------|------------------------------------|-----------------------------------|-----------------------------------|----------------------------------|---------------------------|
| 1a               | 9                                  | 5                                 | 371                               | 343                              | 60                        |
| 2a               | 11                                 | 7                                 | 165                               | 86                               | 223                       |
| 3a               | 8                                  | 5                                 | 82                                | 76                               | 32                        |
| 4a               | 11                                 | 9                                 | 308                               | 262                              | 185                       |
| 7a*              | 16                                 | 11                                | 60                                | 30                               | 36                        |
| 8a*              | 12                                 | 10                                | 33                                | 30                               | 6.7                       |
| 2b               | 11                                 | 18                                | 82                                | 30                               | 86                        |
| 3b               | 16                                 | 15                                | 203                               | 181                              | 168                       |
| 4b               | 15                                 | 7                                 | 330                               | 281                              | 214                       |
| 5b               | 15                                 | 8                                 | 441                               | 273                              | 651                       |
| 6b               | 14                                 | 10                                | 220                               | 174                              | 183                       |
| 7b               | 15                                 | 14                                | 272                               | 159                              | 251                       |
| 8b               | 15                                 | 7                                 | 187                               | 154                              | 111                       |
| 9b               | 15                                 | 5                                 | 136                               | 119                              | 48                        |
| 10b              | 15                                 | 12                                | 81                                | 88                               | 47                        |
| <b>Average**</b> |                                    |                                   | <b>221</b>                        | <b>171</b>                       | <b>174</b>                |

\*These IOPs were not included in analyses due to a high prevalence of PEM BC concentrations lower than the detection limit. Average concentrations listed in this table assume values lower than the detection limit to be the average of a zero concentration and the detection limit (60.5 ng/m<sup>3</sup>), or 30.2 ng/m<sup>3</sup>.

\*\*IOP 7a and 8a are excluded.

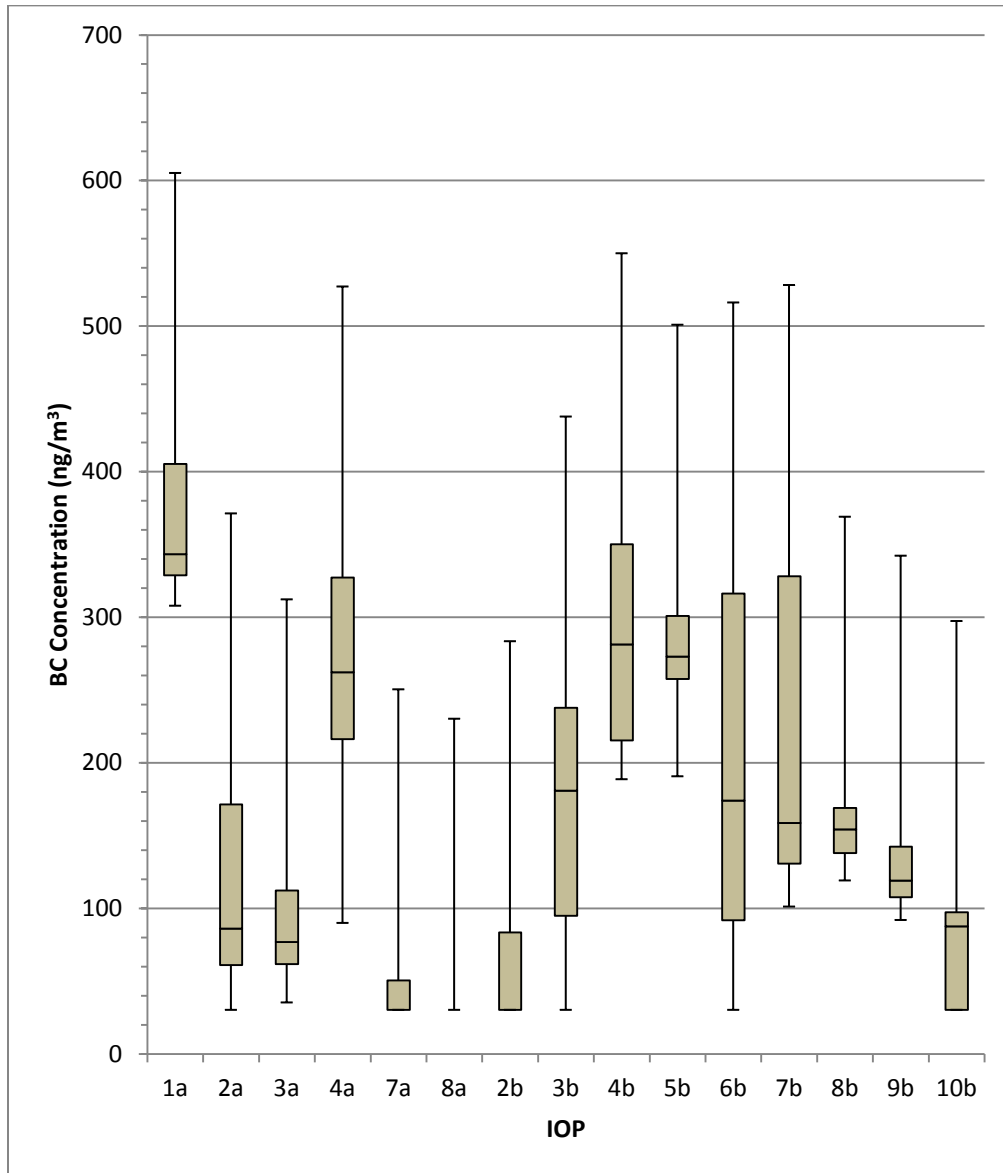


**Figure 7.8** Box plots showing black carbon concentrations for 12 hour PEM filter samples by Intensive Operational Period (IOP)  
*Box plots denote 1<sup>st</sup> quartile, median, and 3<sup>rd</sup> quartile values. The whiskers indicate the maximum and minimum values*

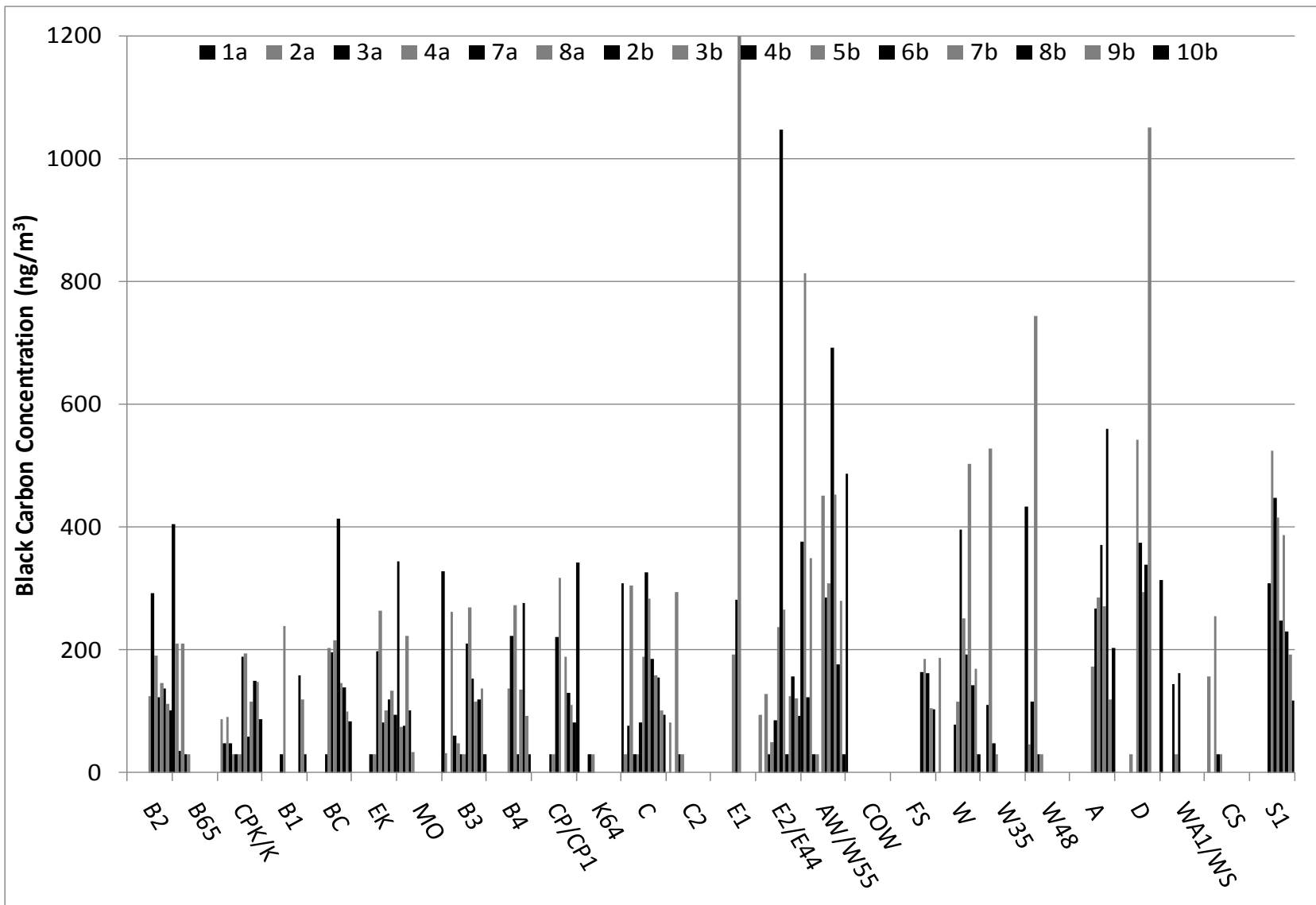


**Figure 7.9 Black carbon concentrations for 12 hour PEM 2.5 filters samples by location and Intensive Operational Period (IOP). Sampling locations names are shown in Figure 7.7 Note that the concentration for E1 IOP5b exceeds the graph limits and equals 2790 ng/m<sup>3</sup>**

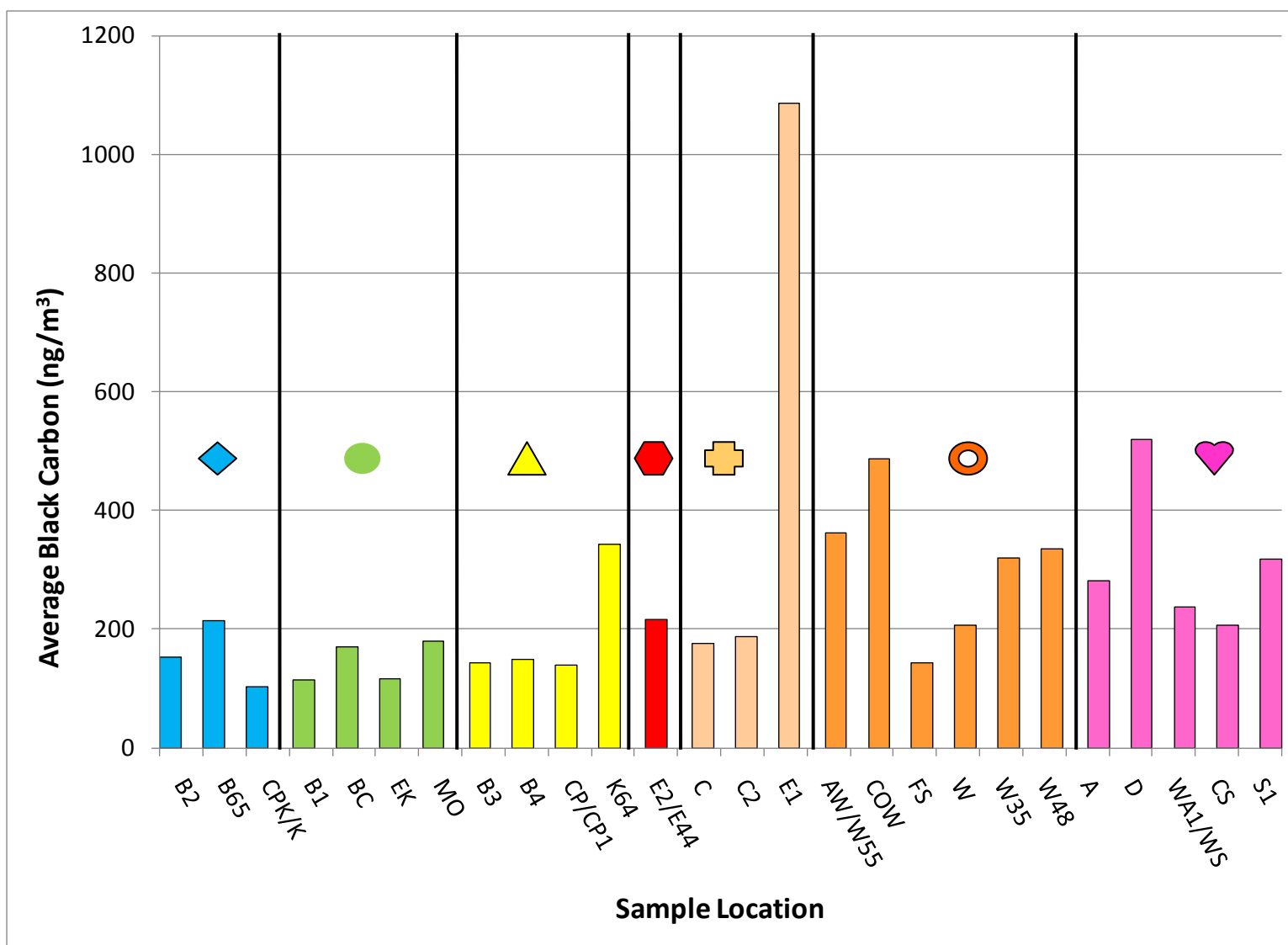
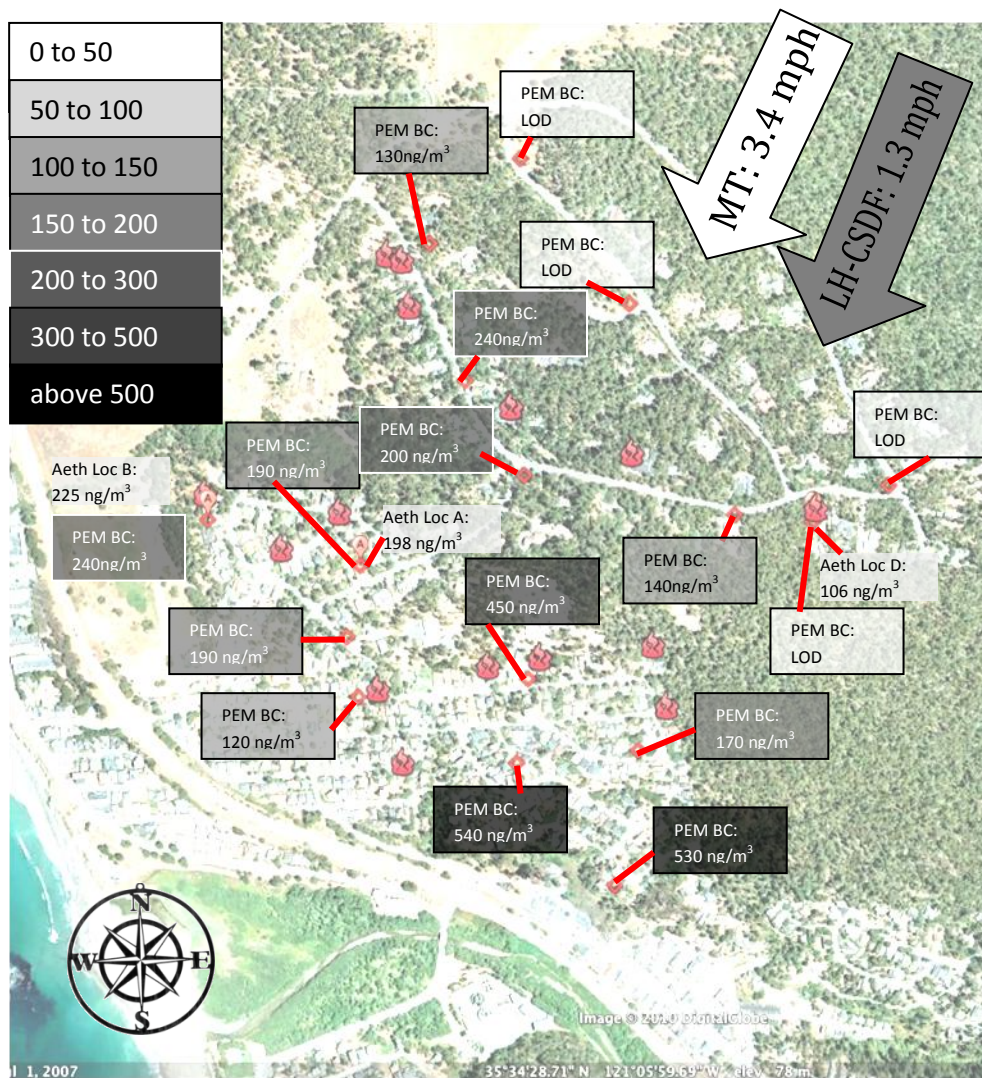


Figure 7.10 Average 12 hour PEM filter black carbon concentration averaged by sampling location for all IOPs. Section symbols match markers on Figure 7.7.

Note: IOPs 7a and 8a were excluded due to a high number of samples below the detection limit. Not all sites were used for all IOPs.



**Figure 7.11** 12 hour PEM filter and 12 hour average aethalometer black carbon PEM 2.5 concentrations (ng/m<sup>3</sup>) for IOP 3b collected from 6pm 1/30/10 to 6 am 1/31/10. Results have been shaded by concentration, using the schematic in the upper left, to aid in visualization. Arrows represent average wind speeds and directions for two local meteorological stations. Flame icon denotes location of a detected burning source



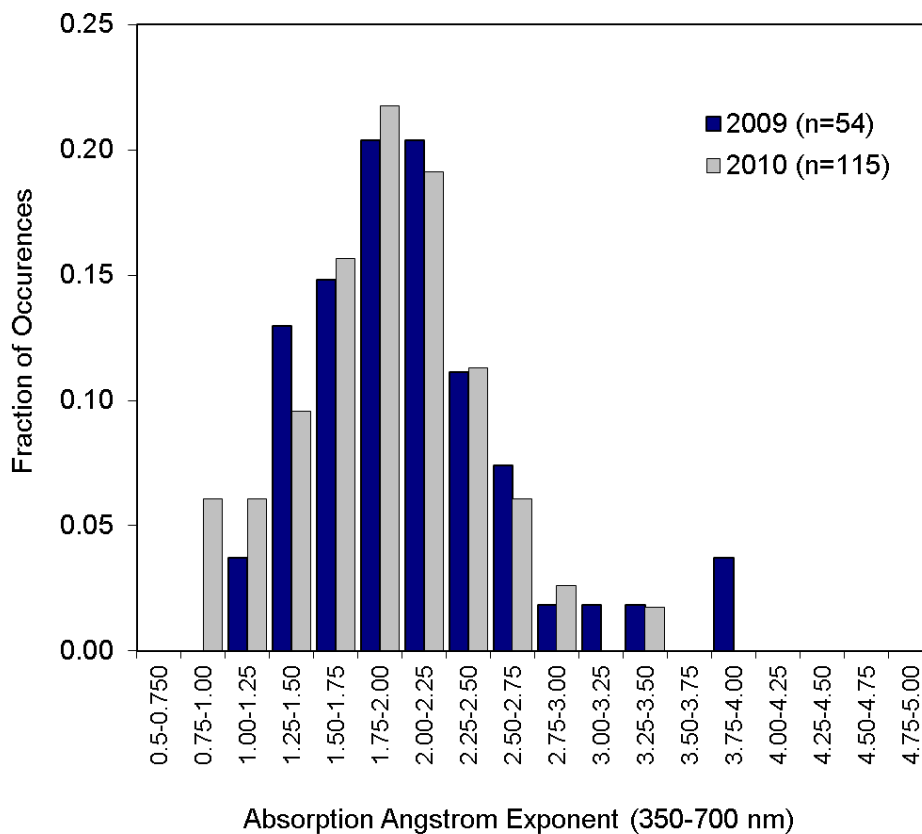


**Figure 7.13 Distribution of Absorption Ångström Exponents (AAE) of particulate matter samples collected in 2009 and 2010. AAE values are based on statistical regression of light transmission measurements of samples over the 350-700 nm spectrum**

AAE values ranged from slightly less than 1 to nearly 4. This wide range may be the result of the variability in the optical (and chemical) properties of particles in wood smoke. As noted above, the composition (e.g., OC/EC ratio) of wood smoke depends on wood type and combustion condition. Lower AAE values are typical of fires emitting particulate matter with lower OC content. The lowest values of AAE exhibited by a minority of samples in this study may be indicative of periods when motor vehicle exhaust – which exhibits AAE values approximately 1 – contributed appreciably to the particulate matter, either due to motor vehicle activity in the study region or to transport of particulate matter emitted outside of the study region.

In Figure 7.14 the AAE values and BC concentrations determined from each sample collected in 2010 are compared. There is no systematic relationship between AAE and BC concentration, but it is interesting that the nine samples with the lowest AAE values ~1 were associated with low BC concentrations. It is noteworthy that these nine samples were collected on the same day, 15-March. Excluding these nine samples, AAE values were greater than 1.25 for 95 and 96% of samples in 2010 and 2009, respectively, which strengthens our conclusion that wood smoke was the dominant source of particulate matter during this study.

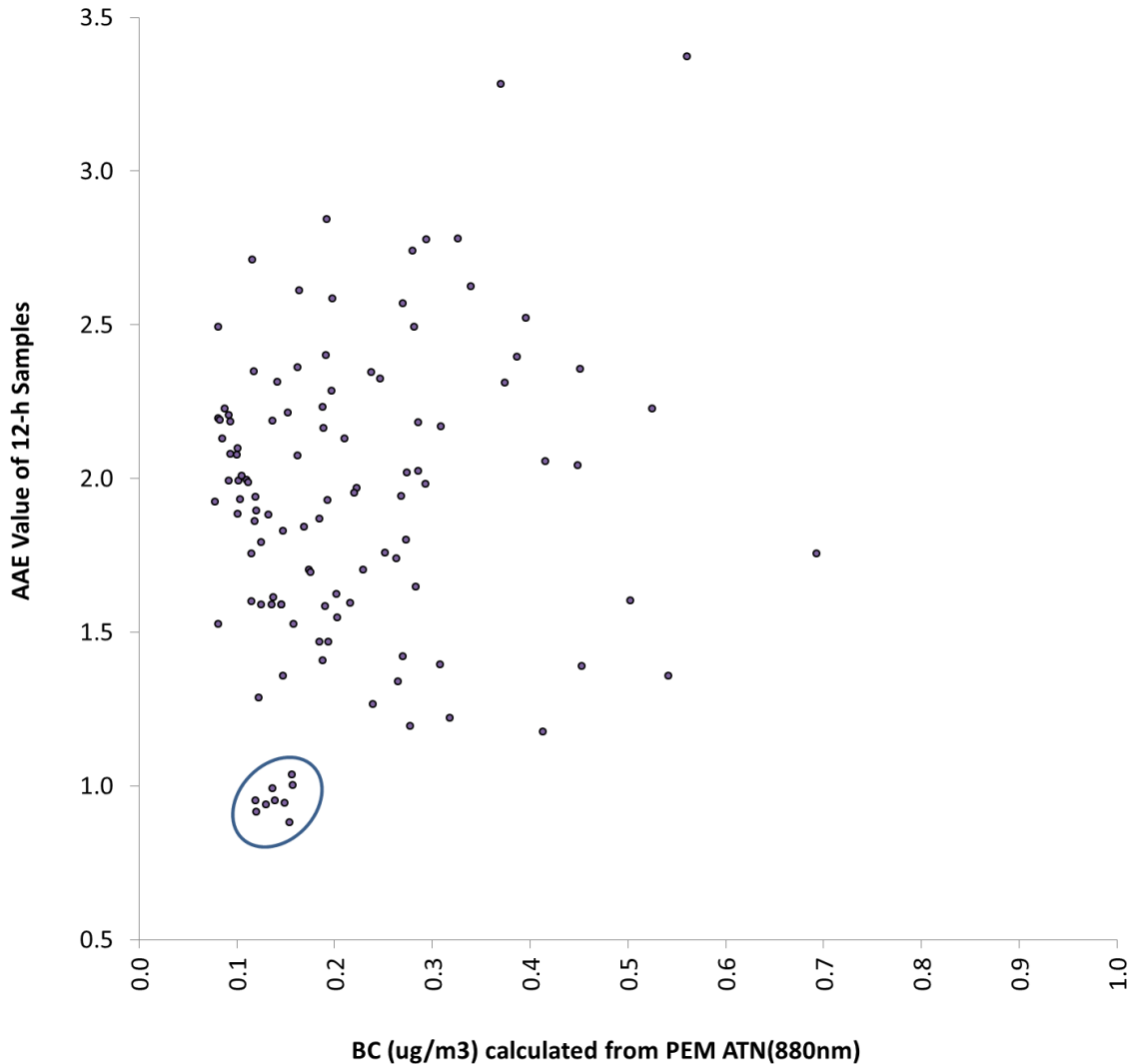


**Figure 7.14 Relationship between Absorption Ångström Exponents (AAE) and BC concentrations of particulate matter samples collected in 2010. The oval surrounds the nine samples with the lowest AAE values**

It is intriguing that, while PM samples at nine sampling locations exhibited the lowest AAE values on 15-March, the sample collected on the same day at location A exhibited the highest AAE value observed in 2010 of nearly 3.5. An examination of the temporal trend in BC concentrations, which were calculated from optical attenuation of the PEM samples at 880 nm, reveals that the BC concentration at location A was particularly high. Thus, it would seem that at location A, unlike other locations on that day, the air quality was very much impacted by wood smoke.

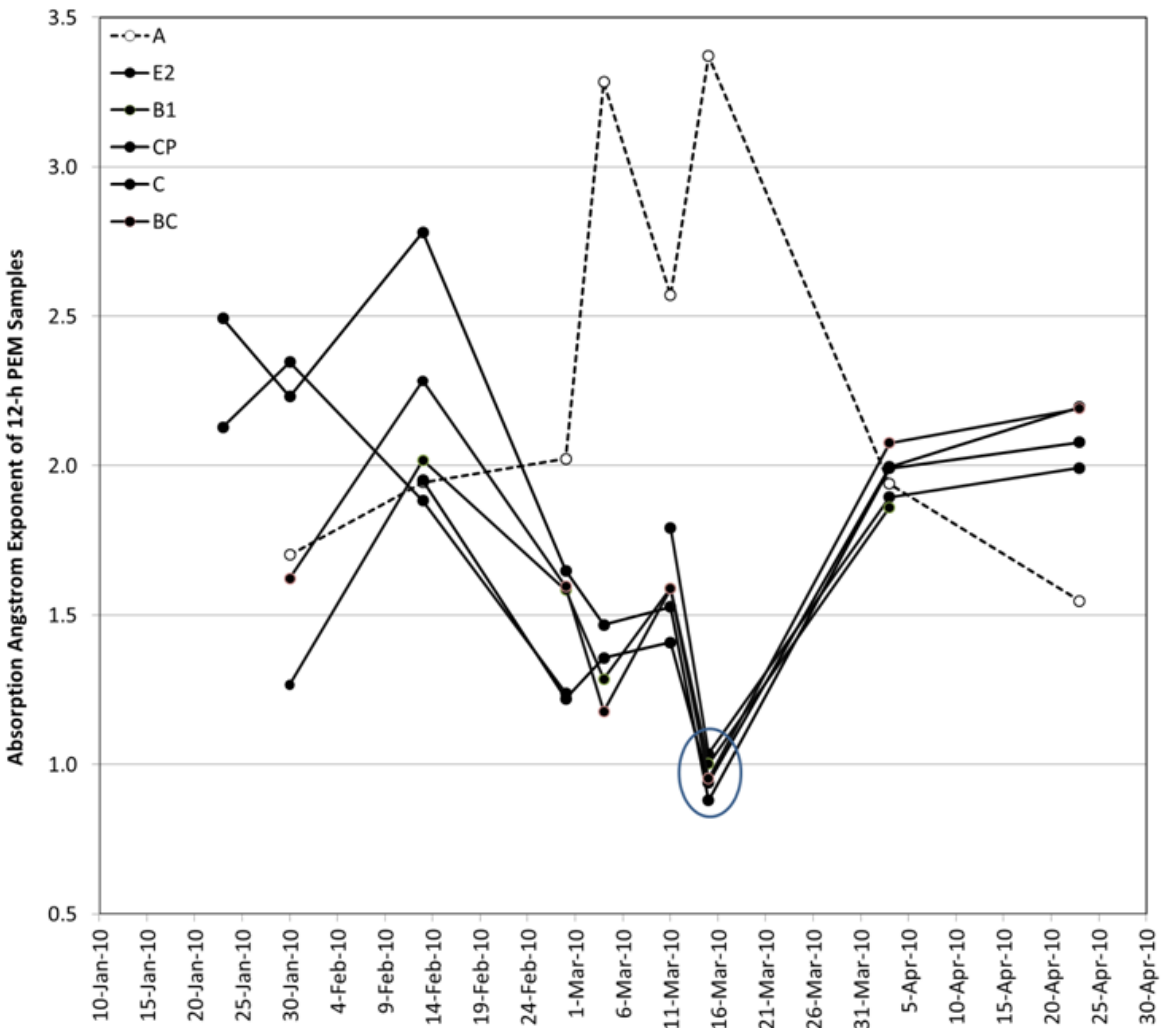


**Figure 7.15** Time series of Absorption Ångström Exponents (AAE) of particulate matter samples collected at several locations in 2010. The oval highlights samples with the lowest AAE values, all of which were collected on 15-March, 2010

## 7.6 Spatial Variability of Meteorological Stations

Meteorological stations are typically used to represent regions of many square miles, however wind speed and direction near the surface can vary substantially over shorter distances depending on terrain and obstructions. Due to the low stack heights, prevalence of inversions, and short distances between sources and receptors in this study, local meteorology is expected to be a significant factor in dispersion.

In addition to the equipment deployed for this study, Cambria weather data was available through the Weather Underground website which provides free historical and real-time weather data in both national and international locations. The site provides meteorological data from its own stations, as well as Weather Underground's Personal Weather Station (PWS) project which allows any resident, organization, or business to contribute meteorological measurements in their area to the Weather Underground website. While PWSs are typically not certified, Weather

Underground provides free meteorological archives in areas within close proximity to the Cambria study area. Two Weather Underground PWS stations located southeast of the study site were chosen to use in the statistical analysis, one in the Marine Terrace neighborhood and one in the Lodge Hill neighborhood. The Marine Terrace station is located about 2 miles from the study area on the roof of a home located in a residential neighborhood close to the coast. The Lodge Hill station is located at the Cambria Community Services District Fire Department (LH CSDF) that is 1.8 miles from the study site. LH CSDF contains trees on the west side of the fire station building, but because the meteorological instruments are located on the fire station radio tower, approximately 25 feet above the ground, there are fewer physical obstructions. Data from an additional meteorological station was available in the Lodge Hill neighborhood at Whispering Pines Bed and Breakfast (LH BaB) about 2.8 miles from the study area, but because the station, located on the roof of the bed and breakfast house, is surrounded by woods which would act as obstructions to wind movement, the station was not used for analysis in this study. The elevations for the Marine Terrace and LH CSDF stations are 53 and 260 ft, respectively, and meteorological readings are recorded every 10 minutes and every 30 minutes for Marine Terrace and LH CSDF, respectively.

Figure 7.16 provides a map of the meteorological stations in relation to the study area.

While the LH CSDF station has not undergone certification similar to many other PWS stations, it has been evaluated for quality control through the National Oceanic and Atmospheric Administration (NOAA) Meteorological Assimilation Data Ingest System (MADIS) project, providing information about data accuracy. The results have been posted on the Citizen Weather Observer Program (CWOP) website and have indicated that over the largest available analysis period of the previous 52 weeks (approximately one year), pressure and wind vectors are correctly calibrated, while dew point readings and temperature readings demonstrated large errors (CWOP, 2010). For this reason, LH CSDF site dew point and temperature were not used. The LH CSDF station was expected to be most representative of the study area among available Weather Underground stations due to its similarity to the study area in topography, terrain, and proximity to the ocean.

Despite the relatively short distances between stations, significant differences were found between meteorological stations. As shown in Figure 7.17 the Marine Terrace (MT) station wind speeds on average were almost twice as high as CSDF wind speeds, and more than three times as high as Sonic and EBAM stations. The lower EBAM and Sonic wind speeds are likely due to their placement closer to ground level (approximately breathing height), where obstructions may readily slow velocities. On average over stations, wind direction did not vary as widely for the MT, CSDF, and EBAM stations, but the Sonic station on average originated from the opposite direction with the exception of one case. Observing each IOP's dominant wind direction, for almost all cases, dominant wind directions for each station were not greater than 90 degrees away from the dominant wind directions of other stations. Temperature, with measurements available at all stations but CSDF, was fairly consistent over all locations, varying about  $\pm 5$  °F over all IOPs. Humidity across all sites was also similar in standard deviation (about 20 percent), but the averages differed in a consistent manner. The highest humidity was always found at the CSDF site, which is also most inland of all stations, followed by the EBAM site which is second most inland, and then the MT site which is closest to the coast and had the lowest humidity. Figure 7.17 summarizes meteorological variability for all stations over each IOP.



Figure 7.16 Map of meteorological stations in Cambria, CA area relative to the study area, as shown by the box in the northern portion of the map

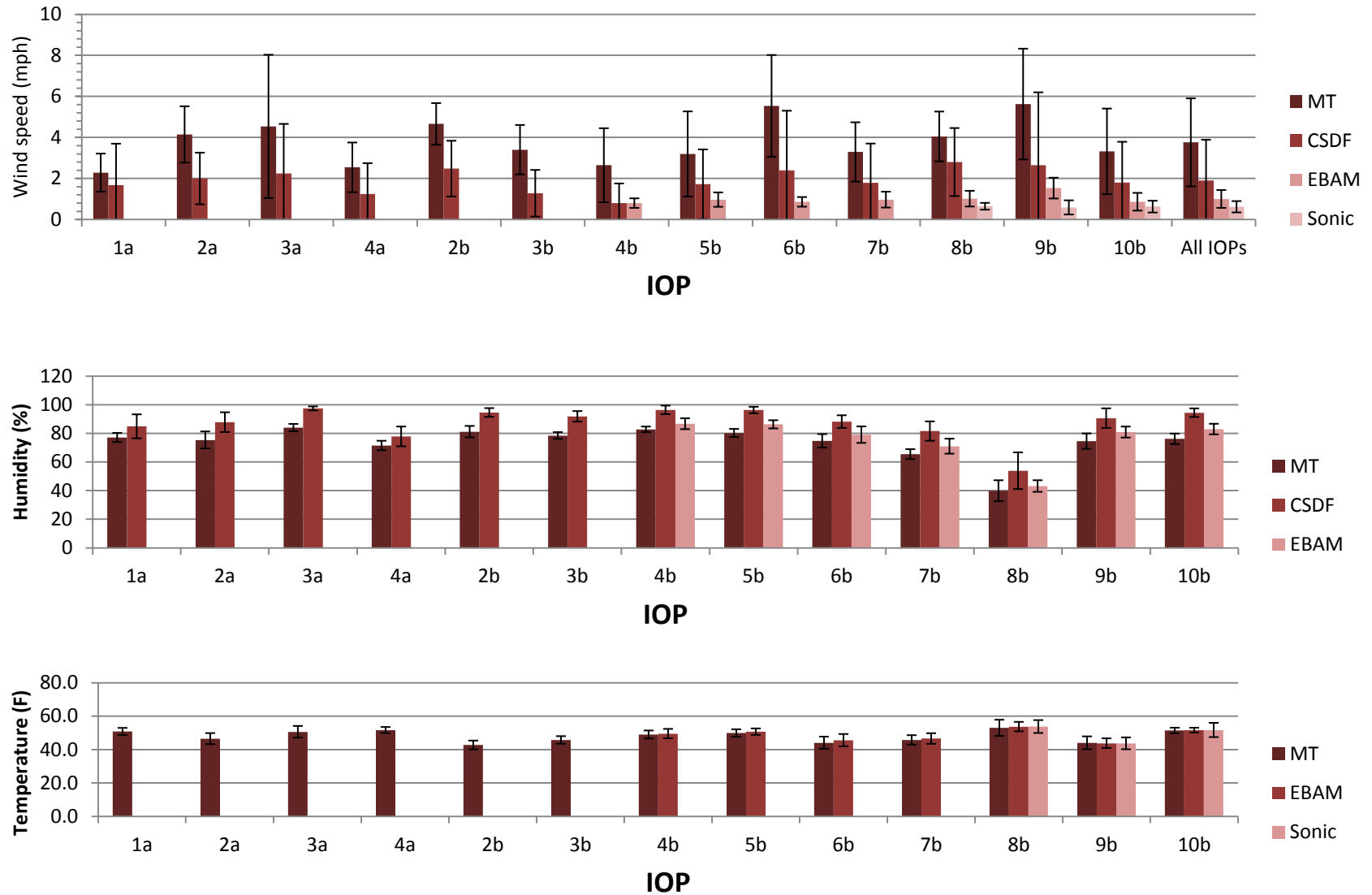


Figure 7.17 Meteorological parameter (wind speed, relative humidity, and temperature) averages and standard deviations during each Intensive Operational Period (IOP) for the stations shown in Figure 7.16

## 8 Quality Assurance and Quality Control

Quality assurance and quality control (QA/QC) were an integral part of the design and execution of this field project. Measures and procedures were instituted at every stage of the project, from training to data verification, to assure the effectiveness of the sampling plan and the accuracy of the data obtained.

### 8.1 Quality Assurance

The primary focus of the quality assurance plan was the development of procedures for sampler handling, sampler placement, burning site identification, and field protocols. Another key component was the training of personnel working on the project to follow the procedures put into place. Individuals involved in sampling were trained in the appropriate procedures for cleaning PEMs, loading filters, programming samplers, sampler placement, sampler retrieval, unloading filters, and filter storage and shipment.

Special care was taken in the handling of PEM filters to prevent contamination. The quartz filters used in the PEMS were pre-baked to remove organics and placed in sealed containers until placement in the PEM sampler. Before every sampling period, the PEMs were thoroughly cleaned with methanol and allowed to dry completely. This ensured that any carbon remnants from the previous sampling period were removed. The PEM impactor was subsequently cleaned and greased with mineral oil, providing a “sticky” surface for particles to deposit. The filters were meticulously placed in the PEM with special tweezers, minimizing the risk of contamination. After securing the top, each PEM was placed in an individual plastic zip top bag to transport to the field. After sampling, PEMS were placed back in their plastic zip top bag for the return trip to the lab. In the lab, filters were unloaded into individual, labeled plastic Petri dishes and sealed. The Petri dishes for each IOP were wrapped together in foil and shipped to Berkeley for analysis.

The placement of PEMs and aethalometers was designed to minimize external flow impacts. PEMs and aethalometers were placed as far away from fences, walls, or other structures and trees when possible. Due to security of instruments and property limitations, structures and trees were not always avoidable. To capture variability throughout the study area, PEMs were placed in an array that was as evenly distributed throughout the area as possible within the limitations of accessibility. Sample locations were recorded on field maps and identified by both address and landmarks. Originally GPS locations were to be used, however physical addresses and descriptions were found to provide a more reliable means for assuring consistent placement.

Burning sites (locations with active wood burning during an IOP) were identified using an infrared camera (Fluke Ti25 Thermal Imager). The camera detects heat on surfaces, but not elevated air temperatures. Therefore, burning sources were detected based on the presence of elevated temperatures at the chimney outlet. Several procedures were used to aid in identifying burning sites. First, personnel visited the field study area during daylight hours to help locate chimneys and the best angles to view them. Second, personnel trained with the camera using known sources prior to using the camera in the field. Finally, during field surveys, a minimum of two people were deployed: one to slowly drive the vehicle and a second to use the camera to scan roof tops and instruct the driver to maneuver the car into the best viewing angle. The nearly complete lack of vehicle traffic in the study area was very helpful in this task.

## 8.2 Quality Control

Quality control procedures were implemented to achieve optimum precision and accuracy whenever possible. Quality control measures were employed both for the analytical procedures utilized and for all instruments deployed during IOPs: PEM systems, aethalometers, ultrasonic anemometer, and E-BAM.

The light transmission method was used to determine filter attenuation and absorption Ångström exponents of particulate matter samples collected on filters. ATN was calculated from measured sample light transmission (T):  $ATN = 100\ln(1/T)$ , where T was defined as  $(I_s/I_{s,o}) \times (I_{r,o}/I_r)$ .  $I_s$  and  $I_{s,o}$  are the measured intensities of light transmitted through a quartz filter sample prior to and after removal of carbonaceous material by heating to 800 °C in oxygen,  $I_r$  and  $I_{r,o}$  are the intensities of light transmitted through a reference quartz filter measured at the same time as  $I_s$  and  $I_{s,o}$ , respectively. In using this method, the following steps were taken to ensure data accuracy.

- 1) Measurements of  $I_s$  and  $I_{s,o}$  were made using the same quartz filter rather than using another blank quartz filter to measure  $I_o$  because light transmission through quartz filters may vary.
- 2) A reference filter was used to correct for possible instrumental variability, such as changes in the brightness of the light source or detector response, during the interval of time between measurements of  $I_s$  and  $I_{s,o}$ .
- 3) Prior to measuring T, the spectrometer lamp was allowed to warm up and stabilize for a period of 20 minutes.
- 4) A subset of samples was analyzed twice to insure consistency in the measurement method, as illustrated in Figure 8.1.

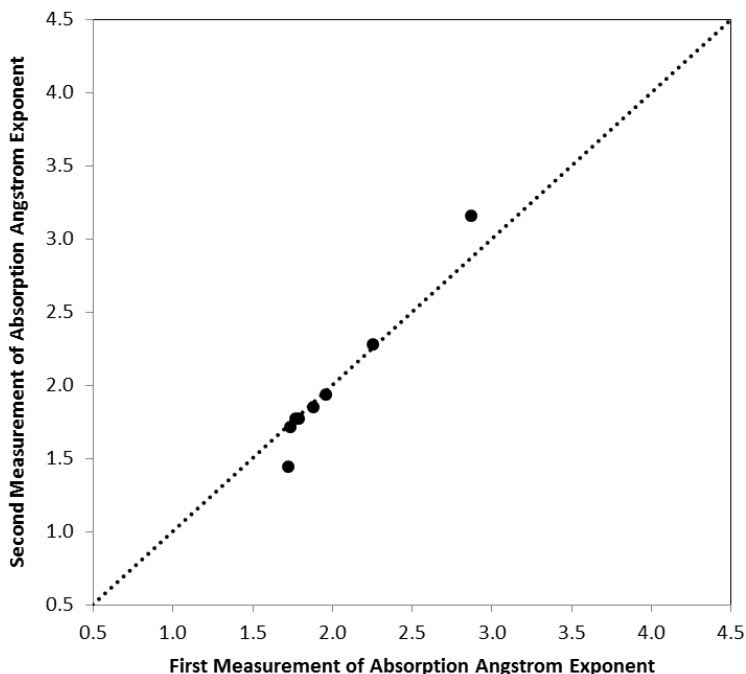


**Figure 8.1 Comparison of Absorption Angstrom Exponent from duplicate analyses performed on a subset of filter samples for QA/QC purposes.**

When performing thermal optical analysis for determining EC and OC contents of collected particulate matter samples using the thermal-optical analysis instrument at Lawrence Berkeley National Laboratory, the following steps were taken to ensure data accuracy.

- 1) Prior to analyzing samples, the instrument was “baked out” and the lamp was allowed to warm up and stabilize for a period of 60 minutes. The “bake out” is a 30 minute period during which the catalyst and sample furnace temperatures are increased to and held at 800 °C, which removes residual carbon in the system.
- 2) The system was calibrated by analyzing the carbon content of samples spiked with known amounts of potassium hydrogen phthalate (KHP). KHP is commonly used for this purpose because its carbon content is known and it is not volatile. Spiked samples were prepared by micro-pipetting aqueous solutions of KHP onto clean quartz filters. Solutions of various concentrations were prepared by dissolving measured amounts of KHP (a solid at room temperature) into measured amounts of pure water.

Method blanks and field blanks were collected during selected IOPs. After PEM assembly, the sample randomly designated the method blank would not be removed from the plastic bag., but instead be left unexposed. Field banks were exposed to the same conditions as other samples, lying adjacent to an active sampler but without air being drawn into the PEM, and were collected the next day. Both field blanks and method blanks were analyzed using the same light attenuation method used for the other filters. None of the filter blanks had a detectable black carbon concentration.

Aethalometers and PEMs used for BC concentration measurement utilize pumps to collect air particles. To ensure the proper operation of equipment, the flow for aethalometers and flow-controlled pumps attached to PEMs were calibrated using a Model DC-HC-1 Bios DryCal DC-2 calibrator. Aethalometer flows were recorded for calibration and PEM pumps were adjusted to 10.0 L/min to allow for proper operation of PEMs. Aethalometer BC measurements and flow readings were recorded for all IOPs to check for any operational interruptions, and PEM pump histories were collected and analyzed for all operating pumps after each IOP.

To ensure similarity between aethalometer BC measurements, aethalometers were simultaneously run side-by-side and then calibrated periodically during the winters of 2009 and 2010. For each side-by-side aethalometer run, the specific attenuation cross-section values for each aethalometer was reduced or increased over one time interval of measured BC concentrations to achieve the average BC concentration of all aethalometer BC readings. The specific attenuation cross-section values were then applied to the second time interval of BC concentrations and a statistical Analysis of Variance (ANOVA) conducted in Minitab on the adjusted readings in the second time interval to determine whether significant differences existed between the different aethalometers. The ANOVA test evaluates whether or not significant differences exist under the assumption that the responses, or measured BC concentrations in this case, are independent from one another, are normally distributed, and that the samples from each machine have equal standard deviations. Based on probability distributions, the ANOVA test determines whether the mean response for each machine deviates enough from the mean response of all machines to be considered different. If differences were found based on the ANOVA test, specific attenuation cross-section was adjusted until the test indicated no statistical difference between machines. Specific attenuation cross-section values were only adjusted using

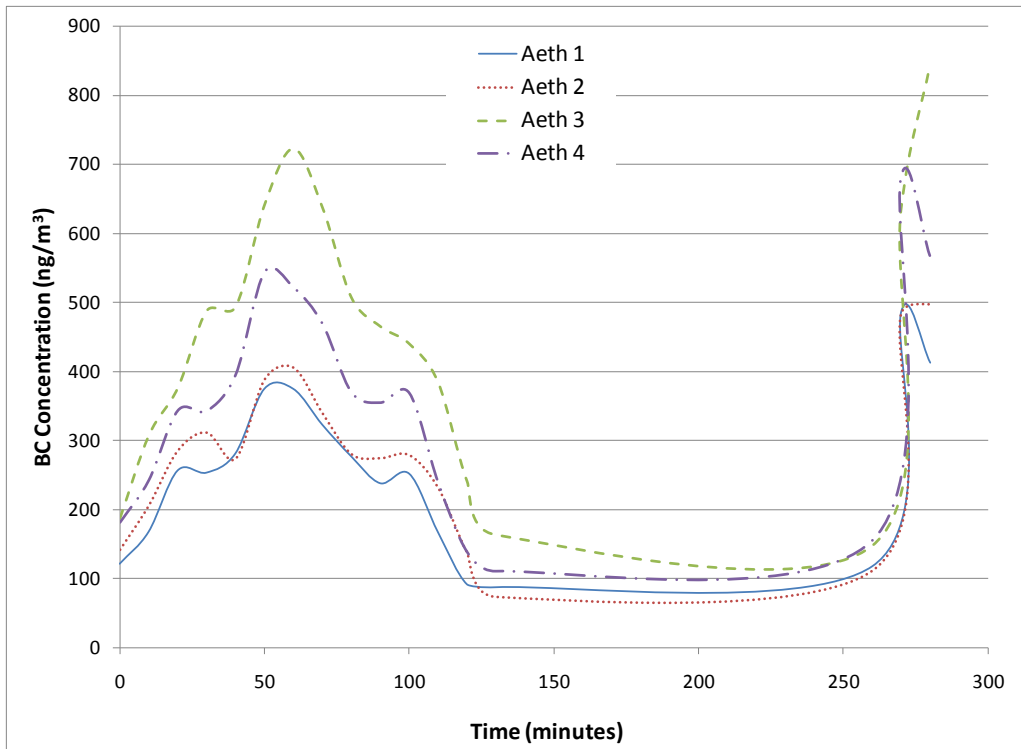


**Figure 8.2 Black carbon concentrations prior to adjustment of the specific attenuation cross-section values for a calibration run on January 19, 2010**

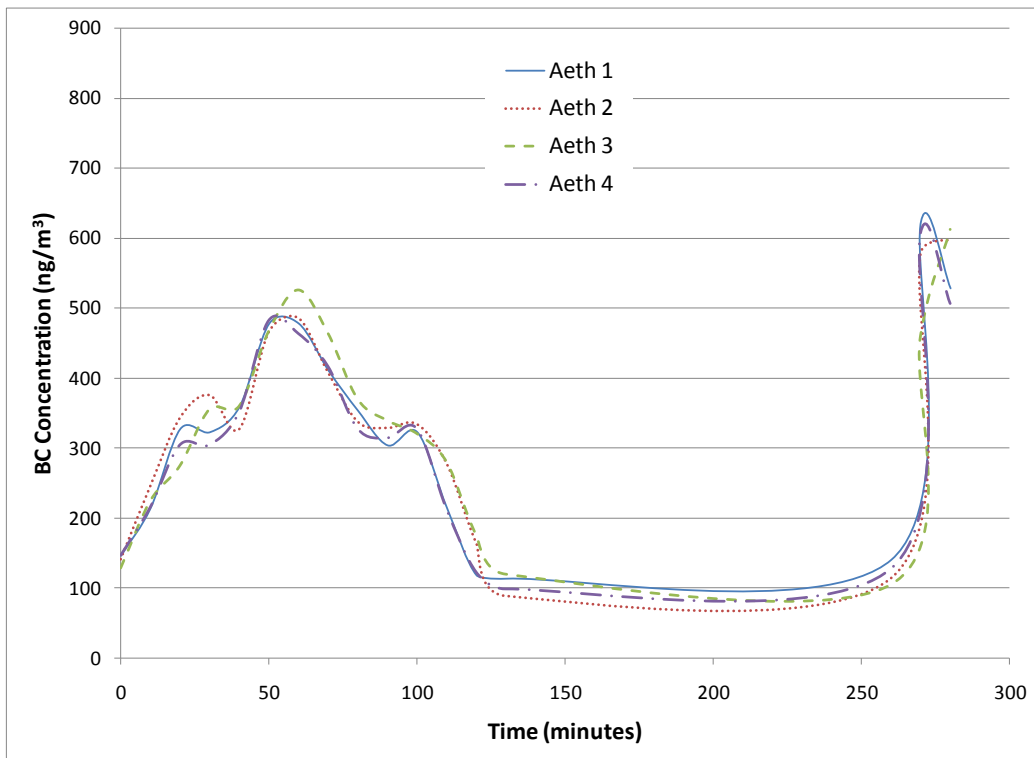


**Figure 8.3 Black carbon concentrations after adjustment of the specific attenuation cross-section values for a calibration run on January 19, 2010 (shown prior to adjustment in Figure 8.2)**

time segments where all machines were similar in concentration-trends. Selecting only segments displaying the same behavior eliminates the influence of readings that deviate significantly from the others. BC readings were averaged over ten minutes to reduce noise in the calibration. Values for specific attenuation cross-section determined for the two calibration runs were averaged and used for the study readings.

To ensure proper operation of meteorological instruments, both E-BAM and ultrasonic anemometer set-up procedures were followed precisely and temperature readings were compared to a thermometer. For the E-BAM, flow checks were automatically conducted and calibration leak checks were performed regularly. For both the E-BAM and ultrasonic anemometer, a compass was used to determine directional placement, with correction for magnetic to true north. Instruments were also placed as far away as possible from trees and structures to minimize downwash impacts on wind speed and direction readings for both instruments and PM<sub>10</sub> readings for the E-BAM. The E-BAM's beta particle detector window was cleaned periodically to ensure that there was no debris build-up that would affect PM<sub>10</sub> measurements.

Weather Underground stations located in Cambria, CA were selected based on a minimum criterion: meteorological instruments must be unobstructed by tall trees or structures. Owners of the meteorological station were also contacted when possible to inquire regarding the accuracy of meteorological stations. While most Cambria stations have not undergone quality control analysis, the CSDF station has been evaluated for quality control through the National Oceanic and Atmospheric Administration (NOAA) Meteorological Assimilation Data Ingest System (MADIS) project, providing information about data accuracy. The results have been posted on the Citizen Weather Observer Program (CWOP) website and have indicated that over the largest available analysis period of the previous 52 weeks (approximately one year), pressure and wind vectors are correctly calibrated, while dew point readings and temperature readings demonstrated large errors (CWOP, 2010). For this reason, CSDF site dew point and temperature were not used.

## 9 Statistical Modeling

Models based on ambient sampling data typically utilize pollutant concentrations at measured sites to estimate concentrations at other locations or under other conditions. The simplest of these models are mathematically linear, but more complex, non-linear models have emerged to improve predictions where linear relationships are inappropriate. An evaluation of PM<sub>10</sub> prediction methods in the large city of Greece, Thessaloniki, inhabited by 16,000 people tested the statistical performance of four methods: Multiple Linear Regression (MLR), Classification and Regression Trees (CART), Principle Component Regression (PCR), and the Multi-Layer Perceptron type of neural network (NN) (Slini et al., 2006). Amongst these methods, MLR and PCR are linear, while NN and CART are non-linear.

MLR is a parametric method (assumes a certain probability distribution for the data) that aims to predict a desired variable Y using other predictor variables such as wind speed and temperature. The CART method is nonparametric and allows for the consideration of a pool of predictor variables that may or may not be used. The selection of predictor variables occurs through binary recursive partitioning (a continuous splitting of data into two groups) that is based on the satisfaction of conditions previously set. The conditions are modified based on what yields the most accurate predictions and based on previous knowledge about the variables. PCR is a combination of Principle Component Analysis (PCA) and a linear regression. PCA evaluates the relationship between variables using a covariance matrix, selecting variables that

are most independent (have little or no relationship to one another) and account for the most variance. Selected variables are then used in a linear regression analysis. NN methods typically employ weights and functions in series that yield a predicted value. The major advantage to NN methods is that information about errors in predictions is used to improve the applied weights and functions through the use of algorithms.

In application of the four forecasting methods to Thessaloniki, a densely populated city with many traffic and industrial sources and complex topography, PM<sub>10</sub> and meteorological data from 1994 through 2000 was used. Slini et al.'s (2006) evaluation found NN to have the most reliable predictions containing the smallest errors in modeling performance and parameters, yet NN was unable to predict peak PM<sub>10</sub> values and may sometimes underestimate concentrations. PCR and MLR, alternatively, were able to correctly predict actual episode days and did so with a low percentage of false positives. However, MLRs had the highest significant differences between predicted and observed values. The statistical evaluation of modeling methods evaluated by Slini et al. demonstrated advantages and disadvantages to each of the methods. Perez et al. (2000) also demonstrated more accurate predictions for PM<sub>2.5</sub> concentrations using NN in comparison to MLR, although prediction errors were more similar for both methods than in Slini et al.'s research. Still, while NN offered the most accurate predictions, its inability to identify peak concentrations can make it less suitable for some practical purposes. Method selection should be based on the intended use of predicted values.

All four methods have advantages and disadvantages when compared to one another. This study will use MLR analysis because it is a simple linear model that is readily interpretable and operated (Pires et al., 2008), while also being relatively robust or flexible to deviations from model assumptions (Demuzere & van Lipzig, 2010). Many studies have tested MLR's ability to explain pollutant variability, though often on a larger-than-neighborhood scale and not always with an emphasis on PM<sub>2.5</sub> (PM<sub>10</sub> has instead been the focus of some MLR studies). These studies reveal that MLR models are site specific, though similarities between developed models offer information more generally applicable to other locations. Tai et al. (2010) used MLR to model daily PM<sub>2.5</sub> concentration throughout the United States using air quality and meteorological data collected from 1998 to 2008. They found meteorological parameters including surface air temperature, relative humidity, precipitation, cloud cover, geopotential height at 850 hPa, local rate of change of sea-level pressure, surface wind speed, a east-west wind direction indicator (cosine of wind direction), and a north-south wind direction indicator (sine of wind direction) to be significant predictors. These parameters accounted for up to 50 percent of variability in PM<sub>2.5</sub> concentration. Vukovich & Sherwell (2002) also used MLR to evaluate PM<sub>2.5</sub> variability from 1991 through 1997 data, but on a small scale at two specific sites located in Washington, DC and Shenandoah National Park, Virginia. At the Washington, DC site, dew point accounted for the most PM<sub>2.5</sub> variability, 53 percent, and the addition of sky cover and SO<sub>2</sub> emissions increased explained variation to 77 percent. At the Shenandoah site, temperature accounted for the most variability in PM<sub>2.5</sub>, 59 percent, and the addition of a solar radiation parameter resulted in a model that accounted for 82 percent of PM<sub>2.5</sub> variability. A principle component analysis also showed wind speed and temperature to demonstrate similar variation with PM<sub>2.5</sub> concentrations at both sites.

Studies relating meteorology to PM<sub>10</sub> have found similar meteorological parameters to explain variation in PM<sub>10</sub> concentrations. Variability in daily winter PM<sub>10</sub> concentrations have been correlated to meteorological conditions using MLRs for sites within the Netherlands (Demuzere et al., 2009) and within parts of the western Alpe-Adria region in central Europe

(Stadlober et al., 2008). Meteorology accounted for 23 percent of PM<sub>10</sub> variability in areas within the Netherlands based on data collected between 2001 and 2006 and between 55 and 70 percent of variability within cities of the Alpe-Adria region based on data collected during different time intervals within 2001 and 2007. Wind speed and direction, maximum temperature, shortwave downward radiation, lagged wind speed and direction, lagged cloud cover, precipitation, relative humidity, and lagged precipitation were all significant predictors for Netherland sites, while Alpe-Adria region MLR models indicated lagged PM<sub>10</sub> concentration, inversion, day of week and month, winds speed, and precipitation to be significant predictors.

Site specific predictors inevitably result due to differences in the location's terrain and the characteristics of the local population. Despite differences in the percentage of variability accounted for in different MLR models, relative humidity, temperature, precipitation, and wind speed tended to be significant predictors in many of the studies. Developing a MLR model for this study allows for the determination of parameters that effect local PM<sub>2.5</sub> variability. In addition to understanding the relationship between meteorological and source impacts and PM<sub>2.5</sub> variation at the study site, an evaluation of the MLR method on a neighborhood scale will offer information about its performance for future PM<sub>2.5</sub> applications.

## 9.1 Background

Multiple linear regression (MLR) and non-linear multiple regression (NMR) analyses were used to evaluate the effect of meteorological and wood burning source parameters on average BC concentrations and BC deviations. The MLR model, a first-order multiple regression model, determines the impact of explanatory, or independent, variables on a response, or dependent, variable as demonstrated below for k explanatory predictors.

$$y = \beta_0 + \beta_1x_1 + \beta_2x_2 + \beta_3x_3 + \dots + \beta_kx_k + \varepsilon \quad (9.1)$$

In Equation 9.1, y is the response variable, x<sub>i</sub> represents the independent variable i, β<sub>i</sub> is a partial slope of variable i, and ε is random error. The partial slopes, β<sub>i</sub>, represent the expected change in the response variable, y, with each change in the explanatory variables, x<sub>i</sub>. β<sub>0</sub>, alternatively, is the value of y when all x<sub>i</sub>'s are equal to zero. The random error, ε, accounts for the difference between the model-predicted value and the actual value, and often represents variation in y that cannot be explained by the x<sub>i</sub>'s (explanatory variables). MLR assumes that explanatory variables are linearly related to the response variable, all explanatory variables are independent of one another, and that the residuals, or error between predicted and actual y values, are normally distributed about zero. To determine the MLR model that explains the most variation with the least amount of error, the least-squares method was used. This method first examines the sum of the squared errors that result when different β<sub>i</sub> and β<sub>0</sub> values are used. The β<sub>i</sub> and β<sub>0</sub> values that result in the lowest sum of squared error are then selected for the MLR model. The NMR follows the same principles as the MLR except that the explanatory variables, x<sub>i</sub>, may represent more complex, non-linear functions.

The 2010 version of the statistical analysis program, Minitab version 16.1.1 (Minitab Inc.) was used to determine the best regression models for this study. BC concentrations and deviations were used as response variables while meteorological data, number of sources, distance from sources, and tree coverage were tested as explanatory variables when suitable. Data from individual meteorological stations and combinations of meteorological stations were used in the analyses, where weather station groups use data that is the average of values available

for the stations it combines. Weather stations were grouped based on their geographic proximity and characteristics relative to the study site. Both Weather Underground stations, Marine Terrace and LH CSDF were combined due to their location within Cambria but outside the study area. The weather stations thought to be most representative of the study area, LH CSDF and E-BAM, were grouped. Finally, both stations located within the study area, E-BAM and Sonic, were evaluated as a combination. Meteorological parameters evaluated for all sites and combinations are summarized in Table 9.1.

Aethalometer and PEM BC data both offered different characterizations of pollutant concentrations and variability within the study area. Because aethalometers provided BC data at high resolution during each IOP, a larger sample size is available to determine the relationship between BC concentration and weather characteristics. For this reason, it was possible to use aethalometer data to evaluate all meteorological stations and determine the meteorological station most capable of explaining variability in BC concentrations. PEM BC concentrations were also evaluated in a similar manner but for 12 hour averaged BC concentrations and deviations with 12 hour averaged meteorological data. EBAM and Sonic stations could not be evaluated for PEMs due to a shortage of data, since they only operated during a subset of the IOPs. The differences and/or similarities between PEM and aethalometer relationships to weather data from different stations provided information about time averaging's impact on BC concentrations and variability.

While the time resolution of the PEMs (12 hours) was much lower than that of the aethalometers (1 minute), spatial resolution for the PEMs was higher than spatial resolution for aethalometers. Each IOP contained between 8 and 16 outdoor PEMs in different locations, while only between 1 and 4 aethalometers were operated in different outdoor locations during each IOP. PEM BC concentrations were thus used to evaluate the impact of distance from burning sources, number of burning sources, and site characteristics on BC concentration and variability.

**Table 9.1 Meteorological data available at each station**

| <b>Station/<br/>Combination</b> | <b>Measurement<br/>intervals</b> | <b>Wind<br/>Speed<br/>(mph)</b> | <b>sin<br/>(WD<sup>#</sup>)</b> | <b>cos<br/>(WD<sup>#</sup>)</b> | <b>Humidity<br/>(%)</b> | <b>Temp (F)</b> | <b>Wind<br/>Gust<br/>Speed<br/>(mph)</b> | <b>Vertical<br/>Wind<br/>Speed<br/>(mph)</b> | <b>Average<br/>Difference<br/>between Wind<br/>Direction</b> |
|---------------------------------|----------------------------------|---------------------------------|---------------------------------|---------------------------------|-------------------------|-----------------|--|--|--|
| <b>Marine Terrace<br/>(MT)</b>  | 10 min                           | X                               | X                               | X                               | X                       | X               | X  |  |  |
| <b>LH CSDF</b>                  | 30 min                           | X                               | X                               | X                               | X                       |                 | X  |  |  |
| <b>E-BAM</b>                    | 10 min                           | X                               | X                               | X                               | X                       | X               |  |  |  |
| <b>Sonic</b>                    | < 1min                           | X                               | X                               | X                               |                         | X               |  | X  |  |
| <b>MT &amp; LH<br/>CSDF</b>     | 30 min*                          | X                               | X                               | X                               | X                       |                 | X  |  | X  |
| <b>E-BAM &amp; LH<br/>CSDF</b>  | 30 min*                          | X                               | X                               | X                               | X                       |                 |  |  | X  |
| <b>E-BAM &amp; Sonic</b>        | 10 min*                          | X                               | X                               | X                               |                         | X               |  |  | X  |

<sup>#</sup> WD: Wind Direction

\*The measurement intervals used for combinations were based on the station with the lowest resolution. For example, for the MT and LH CSDF combination, meteorological data is available at 10 and 30 minute resolutions, respectively, so 30 minute intervals were used.

## 9.2 Regression Analysis of Aethalometer Black Carbon

Meteorological data collected from Weather Underground and available meteorological instruments were evaluated with aethalometer results to determine the meteorological data which best accounted for variability in BC concentration and BC deviation. For the analysis of aethalometer data, two response variables were evaluated: BC concentration averaged over 30 minutes ( $BC_{ave}$ ) and the weighted deviation function ( $BC_{dev}$ ) described as:

$$BC_{dev} = \frac{std\ dev_t}{BC_{t,ave}} \quad (8.2)$$

where  $std\ dev_t$  is equal to the standard deviation of all operating aethalometers at time  $t$  and  $BC_{t,ave}$  is the average BC concentration of BC measurements from all operating aethalometers at time  $t$ . Concentration variability is most appropriately considered as a percentage of the measurement. For instance, a standard deviation of  $40\text{mg/m}^3$  implies much more variability when the average concentration is  $40\text{ ng/m}^3$  than it does when it is  $1000\text{ ng/m}^3$ .  $BC_{dev}$  allows for comparison of BC standard deviation over a wide range of concentration and the use of the weighted deviation function reduces the bias toward high concentrations. Both averaged BC concentrations and deviations were additionally transformed as necessary to normalize residuals about zero.

To satisfy the independence assumption for MLR models, BC concentrations were averaged over 30 minutes to eliminate major time correlations between BC readings and a BC concentration delayed (or lagged) by one time point was included as an explanatory variable in the regression models. The presence of time correlations was evaluated using the Autocorrelation Function (ACF) and the Durbin-Watson statistic in Minitab. For the ACF, potential explanatory variables were used to develop a regression model and the residuals were stored. Residuals are the difference between the observed response variable (in this study BC concentration or deviation) and the response variable resulting from the regression model. ACF then computes the correlation between residuals by comparing a residual at time  $t$  to the data point at time  $t+k\Delta$ , where  $\Delta$  is 30 minutes in this study and  $k$  is any constant. Minitab produces ACF statistics and a graph that indicates whether correlations exist between the response variable at times  $t$  and  $t+k\Delta$ . A comparison of  $t$  and  $t+1\Delta$  (where  $k$  is equal to 1) is referred to as “lag 1,” and comparing  $t$  to  $t+2\Delta$  (where  $k$  is a value of 2) is called “lag 2,” and so forth. Figure 9.1 is a sample graph of residuals resulting from the use of the CSDF meteorological station parameters in conjunction with average BC concentration. The red dotted lines indicate the 95 percent confidence intervals where time correlations are insignificant. An ACF value above the top of or below the bottom of the red dotted line indicates that correlations exist. In the case shown in Figure 9.1, a lag 1 correlation exists and must be accounted for in the model. For this reason, BC concentration or deviation lagged by one time point was included as an explanatory variable. To run the ACF analysis, missing meteorological data at single time points were assumed to be the average of the previous and following time point value. Because there were very few missing single time points, their effect on the models should be undetectable. When larger intervals of data were missing, the data set had to be excluded from the ACF analyses. Data sets where the ACF could not be conducted were assumed to be correlated at similar lags as data sets where the ACF was used. Large time intervals of missing data were rare, so their impact on all data sets should not be significant.

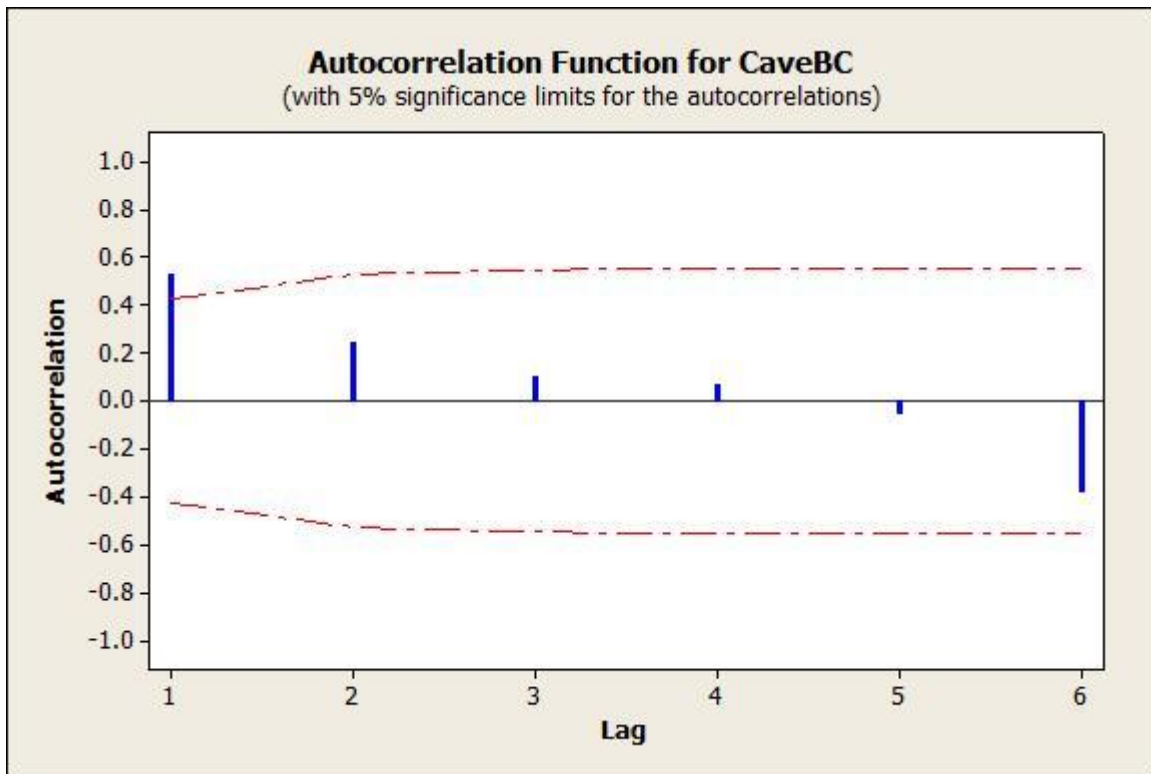


**Figure 9.1** ACF analysis results for the time lag of the 30 minute average aethalometer black carbon concentration using data from the CSDF meteorological station. Autocorrelations that exceed the dotted horizontal lines are considered significant.

In developing a suitable regression model, the Durbin-Watson (DW) statistic was also evaluated. While similar in purpose to the ACF analysis, the DW statistic checks only for correlations in the lag 1 situation and differs mathematically. Critical values developed by Durbin and Watson (1951) indicate when negative and positive correlations exist based on the fact that squared differences in sequential residuals will be smaller for positive correlations and larger for negative correlations. A DW statistic of 2 generally indicates no serial correlation while values less than 2 and greater than 2 suggest positive and negative correlations, respectively (Ott & Longnecker, 2010). Because DW cutoffs for determining correlations are limited to sample sizes of 200 or less (Savin & White, 1977), specific DW cutoffs could not be used for this study's data sets which in most cases contained sample sizes greater than 300. For this reason, the DW statistic observed in developed aethalometer models was assumed to have no time correlations if close to the value of 2. This approximate use of the DW statistic offers additional support to the ACF conclusion. ACF tests alone are considered to be sufficient on their own due to their ability to evaluate correlations at multiply lags.

Suitable meteorological predictors for BC averages or deviations were determined by first including potential predictors for each meteorological station or combination in the regression models and then eliminating variables that had p-values greater than 0.05, the significance level. The significance level determines the percent confidence with which the interval of each partial slope can be determined. At a significance level of 0.05, the confidence of the partial slopes can be determined using one minus the significance level, or 95 percent confidence in this case. To account for diurnal variations in BC concentration, a predictor

representing the number of time intervals passed during the sampling period was used. For example, when using 30 minute averaged BC concentrations, the first 30 minutes of the sampling period is time interval 1, the second 30 minute period is time interval 2, and so forth. A “lack of fit” test was also used to indicate whether interactions or curvature existed in the models. If interactions or curvature were found, modifications were made to account for these properties resulting in nonlinearity of the model(s).

### 9.2.1 Predictors for Aethalometer Average Black Carbon Concentration

While the relationship between BC concentrations and meteorological predictors is typically not linear, a MLR model can still be used by linearizing, or normalizing, BC concentrations through the use of a transformative function. To normalize average BC concentrations ( $BC_{ave}$ ), a transformation that best linearized BC concentrations, raising average BC concentration to the  $-0.7^{th}$  power, was determined and used for the MLR model. Figure 9.2 compares the normal probability plots and histograms of average BC concentration (left) to its transformed counterpart  $(BC_{ave})^{-0.7}$  (right). A straight sloping line following the blue line is needed for the normal probability plot and a bell shaped pattern is desired for the histogram. However, it is important to note that because the normalizing power is negative, higher concentrations will lead to lower values of the normalized parameter.

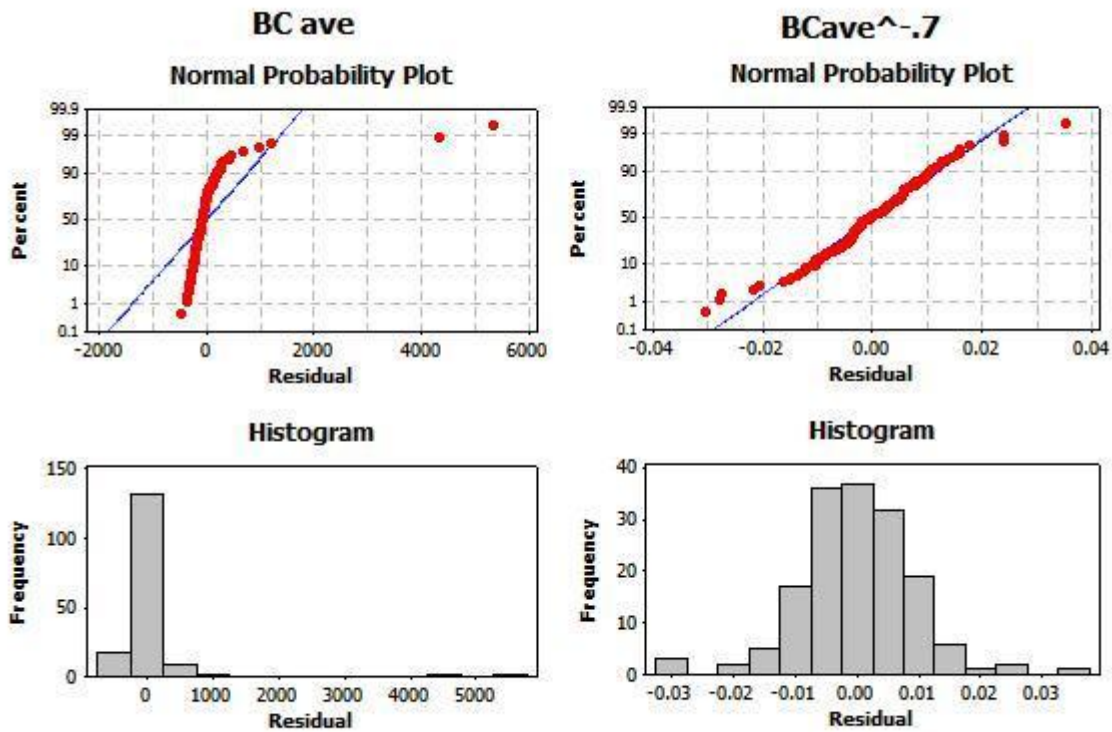


**Figure 9.2 Comparison between residual charts for un-normalized ( $BC_{ave}$ ) and normalized ( $BC_{ave}^{-0.7}$ ) black carbon concentration shows that the transformation yields a normal distribution of residuals**

When using meteorological parameters from each station or combination to determine a model for average BC concentration, it was found that only two meteorological stations or combinations contained parameters well correlated with average BC concentration: the EBAM station and the EBAM and LH CSDF station combination. Table 9.2 summarizes the results of the Minitab analyses including the partial slopes for significant parameters and the coefficients of determination ( $R^2$ ) for each model. The  $R^2$  value indicates the percent of variability in the average BC concentration accounted for by the explanatory variables included in the model. The  $R^2$  value for the average BC concentration models ranged from 52 to 54 percent, with the EBAM and LH CSDF combination explaining the most variability for both linear and non-linear models. Among tested explanatory variables, humidity and wind speed were the only significant meteorological predictors for aethalometer BC average. Average BC concentration lagged by one time interval (Lag 1  $(BC_{ave})^{-0.7}$ ) and time interval, accounting for time of day, also significantly accounted for average BC concentration after transformation.

Although the model  $R^2$  values were found to account for more than 50% of average BC variability, lack of fit tests conducted in conjunction with Minitab analyses suggest that the models need improvement. All models poorly represent average BC concentration at higher values of  $x_i$  (i.e. higher wind speeds and humidity). Additionally, all linear models were found to have potential curvature and/or interactions. Figure 9.3 displays plots of  $(BC_{ave})^{-0.7}$  versus EBAM meteorological parameters in addition to applied trend lines. The figure indicates that only a weak relationship exists between  $(BC_{ave})^{-0.7}$  and the parameters, time interval and humidity. The concentration tends to generally decrease as time interval increases (indicated by a lower  $BC_{ave}^{-0.7}$ ) with a fairly noisy relationship. The pattern for relative humidity is difficult to determine since relative humidity did not vary between 50 and 70% during sampling periods and most samples were collected when relative humidity was higher. The linear correlation with Lag 1  $(BC_{ave})^{-0.7}$  most probably exists because the values directly correspond to  $(BC_{ave})^{-0.7}$  values. Figure 9.4 displays  $(BC_{ave})^{-0.7}$  versus explanatory predictors for the EBAM-CSDF combination in addition to applied trend lines. The response variable,  $(BC_{ave})^{-0.7}$ , had similarly ambiguous relationships with humidity and time interval, and wind speed also seems to demonstrate a noisy distribution with a mild upward slope. This upward sloping relationship between  $(BC_{ave})^{-0.7}$  and wind speed indicates the impact of increasing wind speed for increasing pollutant dispersion.

The unclear relationship between the meteorological and time parameters likely resulted in the detection of possible interactions and curvature by the lack of fit tests. Different functions and variations of the variables were tested to better normalize residuals and find better regression models. Non-linear models were also explored to eliminate the "poor fit" detected to attempt to account for possible interactions and curvature. In the cases of the EBAM and EBAM-CSDF combinations, converting the linear model into a non-linear model did not improve the model's  $R^2$  value dramatically. Mild improvements to the  $R^2$  values may be the result of increasing the number of explanatory variables or only mildly improving the fit. The former is suspected because the standard errors for the linear models tend to be smaller than the standard deviations for the non-linear models relative to their coefficients. Smaller variations in the linear models suggest higher accuracy than non-linear models. For this reason, the linear models are likely a more suitable model for understanding average aethalometer BC concentration than the non-linear models. In using the linear models, potential interaction detected in the Lag 1  $(BC_{ave})^{-0.7}$  predictor and possible curvature in time interval and humidity variables for the EBAM meteorological station were noted. For the meteorological data combining the EBAM and CSDF stations, potential interactions in the Lag 1  $(BC_{ave})^{-0.7}$  and wind speed predictors were observed.

**Table 9.2 Resulting coefficients and fit from multiple regression models for normalized 30 minute average aethalometer black carbon concentration  $(BC_{ave})^{-0.7}$  using the EBAM station and a combination of the EBAM< and CSDF stations**

*The table below summarizes explanatory predictors determined to be significantly correlated to  $(BC_{ave})^{-0.7}$  based on Minitab analysis.*

| Met Station    | Model Type | Explanatory Variable                             | Coefficient ( $\beta_i$ ) | Std Dev of Coefficient | R <sup>2</sup> (%) |
|----------------|------------|--|---------------------------|------------------------|--------------------|
| EBAM           | Linear     | Lag 1 $(BC_{ave})^{-0.7}$                        | 5.3E-01                   | 6.5E-02                | 52                 |
|                |            | Time Interval                                    | 4.0E-04                   | 1.2E-04                |                    |
|                |            | Humidity (%)                                     | -2.1E-04                  | 5.8E-05                |                    |
|                |            | Constant, $\beta$                                | 2.5E-02                   | 5.4E-03                |                    |
|                | Non-linear | Lag1 $(BC_{ave})^{-0.7}$                         | 2.5E-01                   | 1.4E-01                | 54                 |
|                |            | Time Interval                                    | -3.8E-04                  | 3.8E-04                |                    |
|                |            | $(Lag\ 1\ (BC_{ave})^{-0.7}) * (Time\ Interval)$ | 2.2E-02                   | 1.0E-02                |                    |
|                |            | $(Humidity\ \%)^2$                               | -1.4E-06                  | 4.5E-07                |                    |
|                |            | Constant, $\beta$                                | 2.8E-02                   | 5.1E-03                |                    |
|                |            |  |                           |                        |                    |
| EBAM & LH CSDF | Linear     | Lag 1 $(BC_{ave})^{-0.7}$                        | 5.1E-01                   | 6.5E-02                | 53                 |
|                |            | Time Interval                                    | 3.8E-04                   | 1.2E-04                |                    |
|                |            | Wind Speed (mph)                                 | 2.3E-03                   | 9.4E-04                |                    |
|                |            | Humidity (%)                                     | -1.7E-04                  | 6.1E-05                |                    |
|                |            | Constant, $\beta$                                | 2.1E-02                   | 5.9E-03                |                    |
|                | Non-linear | Lag1 $(BC_{ave})^{-0.7}$                         | 2.5E-01                   | 1.3E-01                | 55                 |
|                |            | Time Interval                                    | -4.5E-04                  | 3.7E-04                |                    |
|                |            | $(Lag\ 1\ (BC_{ave})^{-0.7}) * (Time\ Interval)$ | 2.3E-02                   | 1.0E-02                |                    |
|                |            | Wind Speed (mph)                                 | 2.2E-03                   | 9.3E-04                |                    |
|                |            | Log(Humidity %)                                  | -8.3E-03                  | 4.0E-03                |                    |
|                |            | Constant, $\beta$                                | 5.3E-02                   | 1.8E-02                |                    |
|                |            |  |                           |                        |                    |

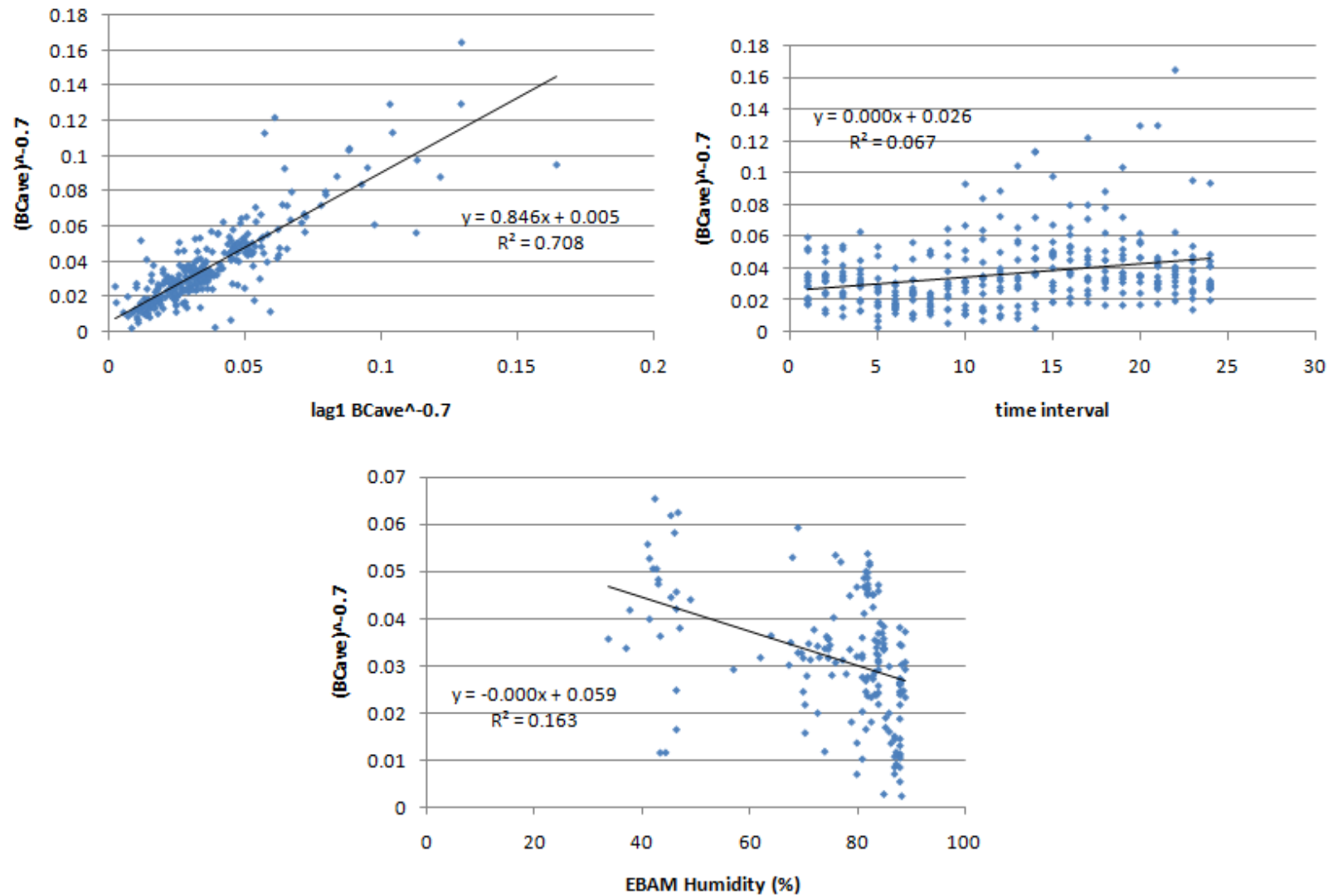


**Figure 9.3** Parameter plots from the multiple linear regression model for normalized 30 minute average aethalometer black carbon concentrations when modeled using meteorological data from the EBAM station

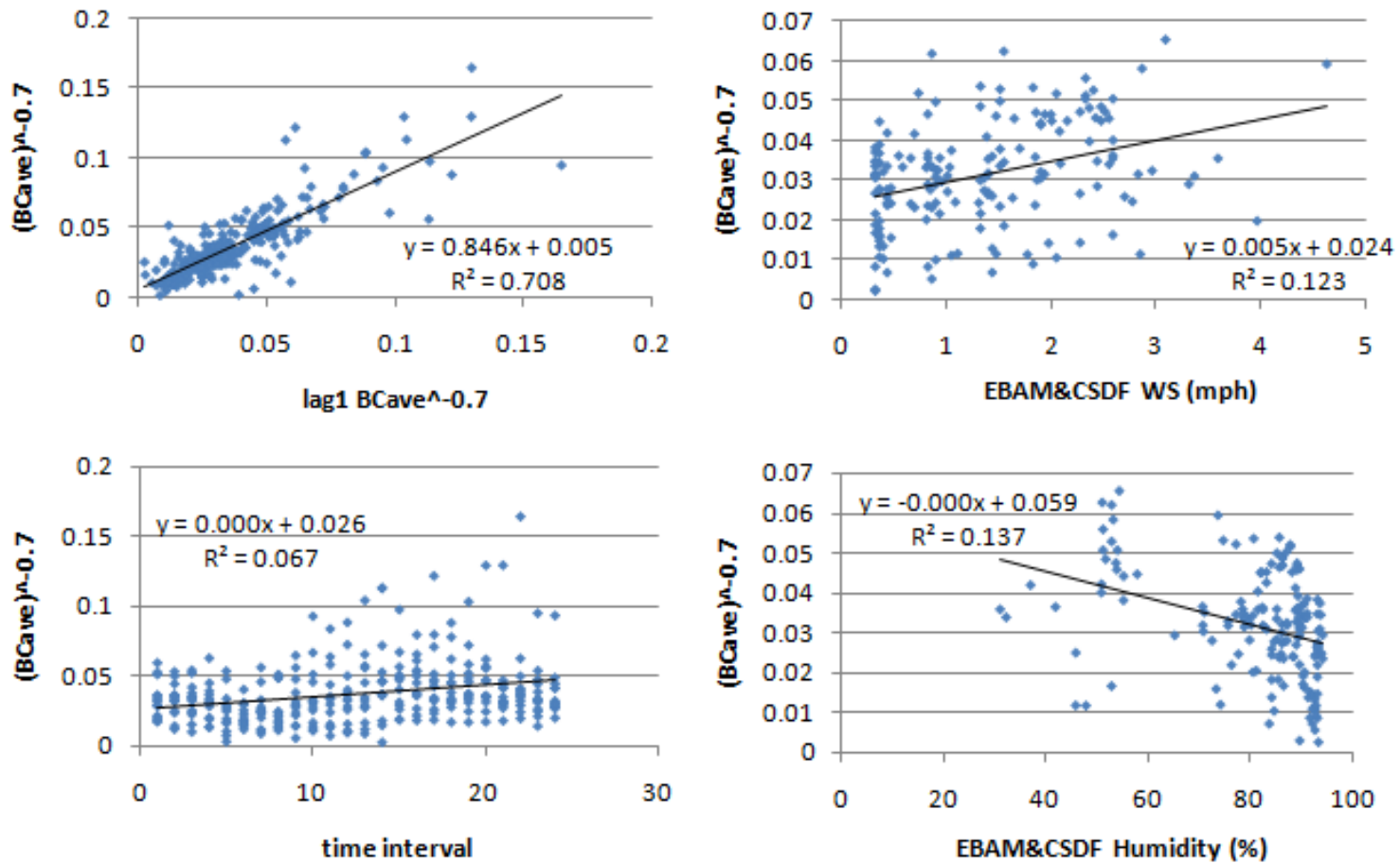


Figure 9.4 Parameter plots from the multiple linear regression model for normalized 30 minute average aethalometer black carbon concentrations when modeled using meteorological data from the EBAM and LH-CSDF combined stations

While the results of the models suggest that the EBAM and CSDF combination account for more of the BC variation than the EBAM station alone, the difference is small. This may indicate that a near ground level station within the near-field exposure area would be sufficient to represent average BC concentration when using the above models. However, the lack of fit using the LH CSDF station alone suggests that even nearby meteorological stations may not be capable of providing explanatory data for near-field concentrations. The small improvement in  $R^2$  values for the EBAM and LH CSDF combination versus EBAM alone may have resulted from the addition of the wind speed predictor in the EBAM and CSDF combination model or because using additional information from the LH CSDF station helps to account for upper air meteorology (in addition to EBAM's ground level meteorology).

### 9.2.2 Predictors for Aethalometer Black Carbon Deviation

BC deviation ( $BC_{dev}$ ) and meteorology were evaluated to determine whether meteorology was correlated with BC standard deviation, or variance. To linearize BC deviation ( $BC_{dev}$ ), as done with average BC, the best transformation was BC deviation raised to the 0.5<sup>th</sup> power. Only the LH CSDF meteorological station's parameters were found to be suitable predictors of BC deviation. Table 9.3 summarizes the results of the Minitab analysis including the partial slopes for significant parameters and the coefficient of determination ( $R^2$ ) for the resulting linear model. The  $R^2$  value for the LH CSDF model was 47.3 percent, with wind speed and humidity as significant meteorological predictors of variation in BC deviation and Lag 1 ( $BC_{dev}$ )<sup>0.5</sup> as a variable intended to account for time correlations.

**Table 9.3 Resulting coefficients and fit from the multiple regression model for normalized 30 minute average aethalometer black carbon concentration deviation ( $BC_{dev}$ )<sup>0.5</sup> using the LH-CSDF station**

| Met Station | Model Type | Explanatory Variable                | Coefficient ( $\beta_i$ ) | Standard Deviation of Coefficient | $R^2$ (%) |
|-------------|------------|-------------------------------------|---------------------------|-----------------------------------|-----------|
| LH CSDF     | Linear     | Lag 1 ( $BC_{dev}$ ) <sup>0.5</sup> | 6.1E-01                   | 4.5E-02                           | 47        |
|             |            | Wind Speed                          | -2.8E-02                  | 8.3E-03                           |           |
|             |            | Humidity                            | -2.3E-03                  | 1.1E-03                           |           |
|             |            | Constant, $\beta$                   | 4.7E-01                   | 1.1E-01                           |           |

The BC deviation model contained possible curvature (for Lag 1  $BC_{dev}$ <sup>0.5</sup>) and potential interactions (for relative humidity), but attempts to account for the curvature and interaction were unsuccessful. Figure 9.5 shows plots of ( $BC_{dev}$ )<sup>0.5</sup> versus LH CSDF wind speed, humidity, and Lag 1 ( $BC_{dev}$ )<sup>0.5</sup> as well as applied trend lines. While the Lag 1 ( $BC_{dev}$ )<sup>0.5</sup> predictor demonstrates a general upward sloping trend, the wind speed and humidity relationships with BC deviation are much less apparent which is similar to the trends for the average BC concentration models. The detection of possible curvature and interactions by the lack of fit tests may have resulted from the unclear relationships between the BC deviation and the meteorological parameters..

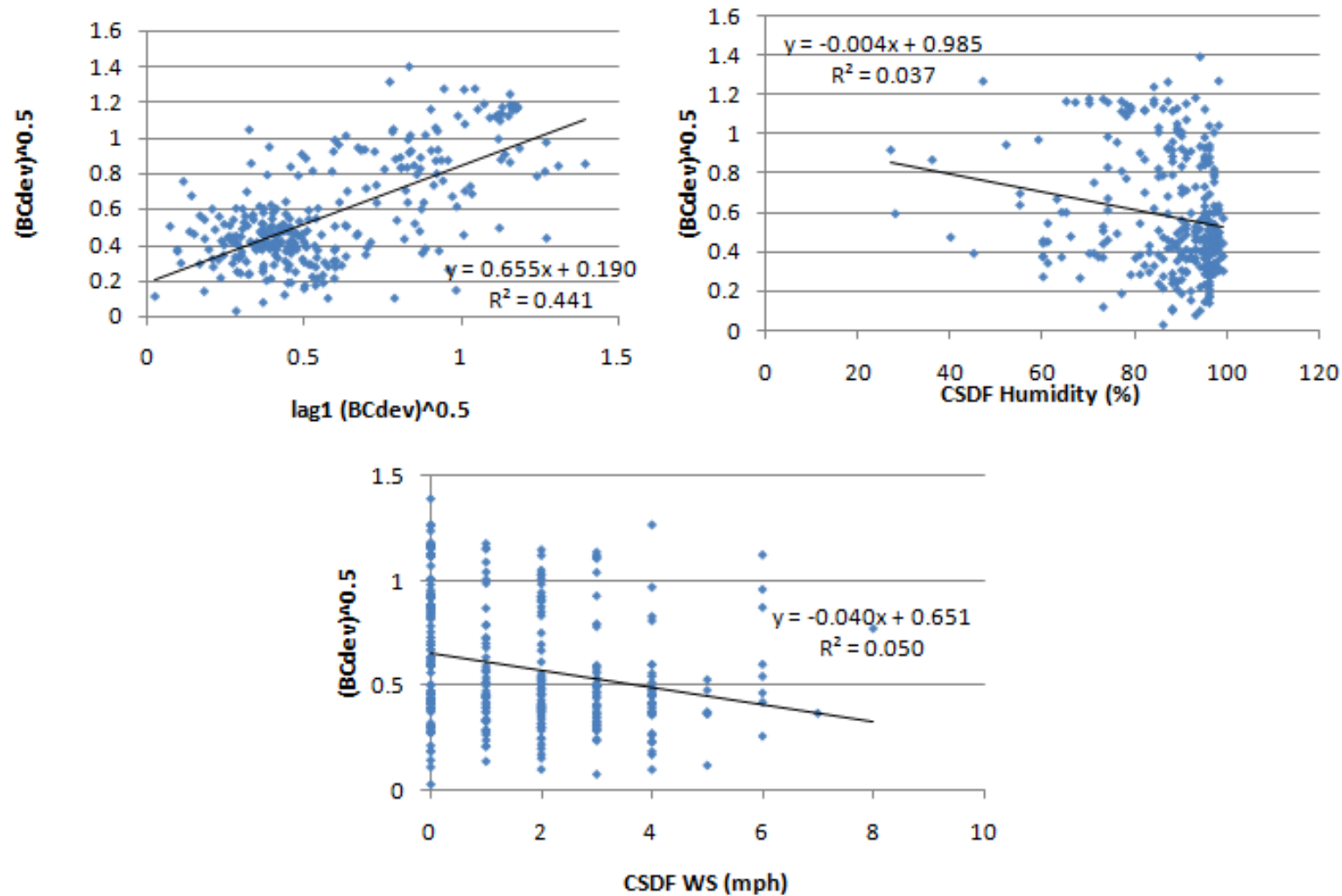


Figure 9.5 Parameter plots from the multiple linear regression model for normalized 30 minute average aethalometer black carbon concentration deviation ( $BC_{dev}^{0.5}$ ) when modeled using meteorological data from the LH-CSDF station

### 9.3 Regression Analysis of Integrated Black Carbon Measurements

Two different MLR analyses were conducted for the integrated black carbon (PEM BC) data. Similar to the analyses for aethalometer BC data, the first test evaluated which meteorological data best accounted for variability in BC concentration and deviation. The second PEM BC analysis investigated the impact of wood burning sources on PEM BC concentration by focusing on geographic proximity to sources and relation to dominant wind direction. Average PEM BC and BC deviation were used as the response variables, while meteorological characteristics were used as explanatory variables. Because PEM and aethalometer resolution differed, response and explanatory variables were used in a modified manner for the PEM analysis. Instead of using average BC concentration and weighted deviation for every 30 minutes, the 12 hour integrated BC concentration measured for each PEM was averaged with the other PEMs operating during the same IOP to determine  $BC_{ave}$ . The standard deviation of those PEMs was then divided by  $BC_{ave}$  to find the  $BC_{dev}$  value. Meteorological data were also averaged over 12 hours for use as explanatory variables in the regression analyses. Because a significantly smaller sample size was available for PEM analysis than for aethalometer analyses, EBAM and Sonic meteorological stations, which were not available for all runs, were not used. Additional meteorological parameters, presence of inversion (yes or no) and difference in wind direction (for combined meteorological stations only), were included in the analysis. The number of wood burning sources detected on each night of sampling was also included as a predictor variable, while lagged BC concentration and deviation were not needed due to the larger time spans between sampling nights. PEM BC concentrations were assumed to be independent from one another and the DW statistical cutoffs determined by Savin and White (1977) were used to confirm independence.

#### 9.3.1 PEM BC Average Concentration and BC Deviation

To determine which meteorological station contained parameters that best explained PEM BC concentrations, a statistical approach similar to the one for aethalometer BC was used. The transformation best able to linearize BC concentrations was average BC concentration raised to the 0.4<sup>th</sup> power for the Marine Terrace station and the natural log of BC concentration for the LH CSDF station and the Marine Terrace and LH CSDF combination. For average PEM BC concentration, wind speed consistently accounted for variation. The sine of wind direction was found to also be a predictor for the Marine Terrace and the Marine Terrace and CSDF combination and the cosine of the wind direction was an additional predictor for the Marine Terrace station. Table 9.4 summarizes the results of the Minitab analysis including the partial slopes for significant parameters and the coefficient of determination ( $R^2$ ) for the resulting linear model. The  $R^2$  values for the average BC models ranged from 47.1 to 81.3 percent, with the Marine Terrace model explaining the most variability in average PEM BC concentration. Figures 9.6, Figure 9.7, Figure 9.8 show scatter plots and an applied trend line for the two stations separately, as well as their combined data, along with their significant parameters.

These results indicate that in the near-field, standard meteorological data may provide a means of estimating average black carbon concentrations. However, the actual fitting parameters would be expected to vary with local conditions and more data would be needed to reduce uncertainties. One possible reason that the statistical models do a better job of describing integrated concentrations than they do for real time measurements, may be the result of averaging out local turbulence and temporal fluctuations which can strongly influence time

resolved results. In addition, the increased spatial coverage achieved by the PEM sampling provides a more uniform representation of the study area, which may in turn improve the modeling results.

**Table 9.4 Linear regression parameters for normalized 12 hour filter (PEM) black carbon concentrations averaged by Intensive Operational Period (IOP) for 3 different meteorological data sets**

| Met Station              | Response Variable  | Explanatory Variable | Coefficient ( $\beta_i$ ) | Standard Deviation of Coefficient | R <sup>2</sup> (%) |
|--------------------------|--------------------|----------------------|---------------------------|-----------------------------------|--------------------|
| Marine Terrace           | $(BC_{ave})^{0.4}$ | Wind Speed           | -2.34                     | 0.48                              | 81.3               |
|                          |                    | sin(wind direction)  | 14.9                      | 5.5                               |                    |
|                          |                    | cos(wind direction)  | 12.8                      | 3.3                               |                    |
|                          |                    | Constant, $\beta$    | 17.9                      | 1.9                               |                    |
| LH CSDF                  | $\ln(BC_{ave})$    | Wind Speed           | -0.778                    | 0.249                             | 47.1               |
|                          |                    | Constant, $\beta$    | 6.71                      | 0.50                              |                    |
| Marine Terrace & LH CSDF | $\ln(BC_{ave})$    | Wind Speed           | -0.725                    | 0.142                             | 73.6               |
|                          |                    | sin(wind direction)  | 2.60                      | 1.02                              |                    |
|                          |                    | Constant, $\beta$    | 7.25                      | 0.41                              |                    |

No meteorological stations contained parameters capable of explaining variation in BC deviation. However, the number of wood burning sources was found to be a suitable predictor when a natural log transformation was applied to PEM BC deviation. The number of wood burning sources alone was able to account for 30 percent of the variability in PEM BC concentration. This may be because increasing the number of sources increases the probability that some samples will be more directly influenced by a nearby source, while others are not, thereby increasing variability. It could be hypothesized that if there were enough sources within a given area to influence most locations directly that this trend would reverse and samples would become more uniform. However, there were not enough burning sources within our study area to observe this effect. Table 9.5 and Figure 9.9 summarize the details of the model and plot the relationship with a trend line, respectively.

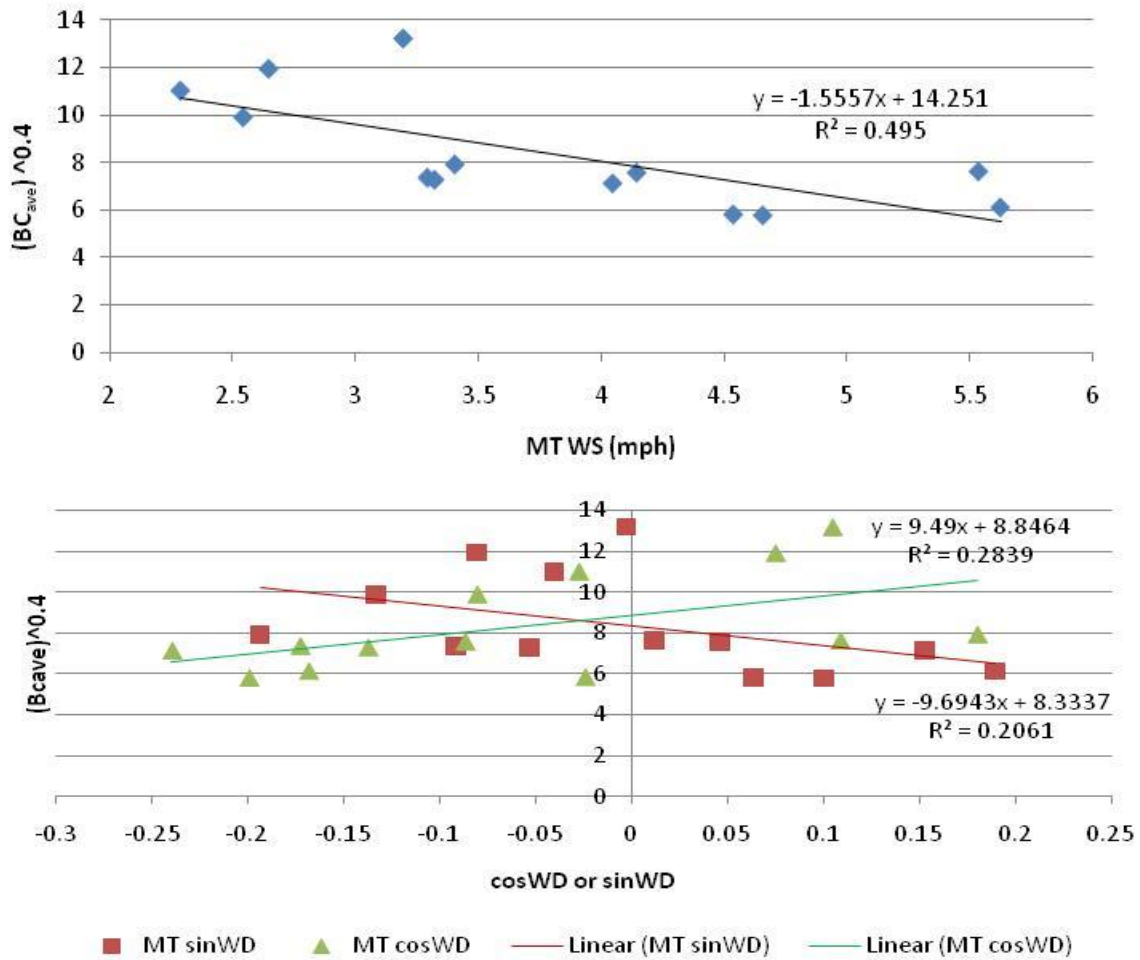


**Figure 9.6** Parameter plots from the multiple linear regression model for normalized 12 hour filter (PEM) black carbon concentrations  $(BC_{ave})^{0.4}$  averaged by Intensive Operational Period (IOP) when modeled using meteorological data from the Marine Terrace station

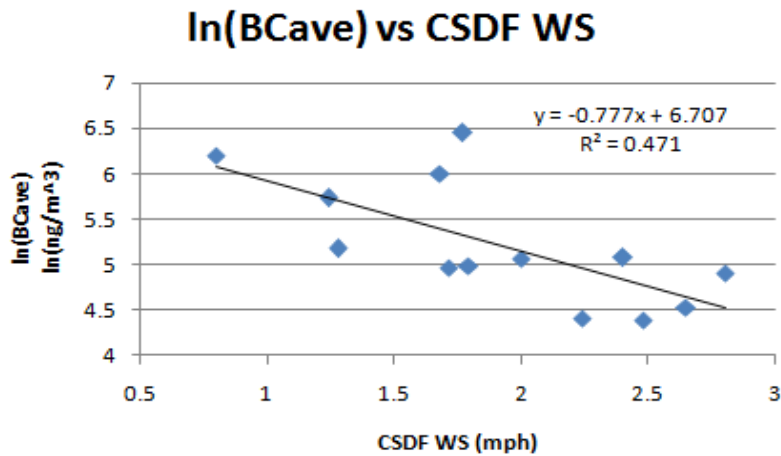


**Figure 9.7** Parameter plot from the multiple linear regression model for normalized 12 hour filter (PEM) black carbon concentrations ( $\ln(BC_{ave})$ ) averaged by Intensive Operational Period (IOP) when modeled using meteorological data from the LH CSDF station

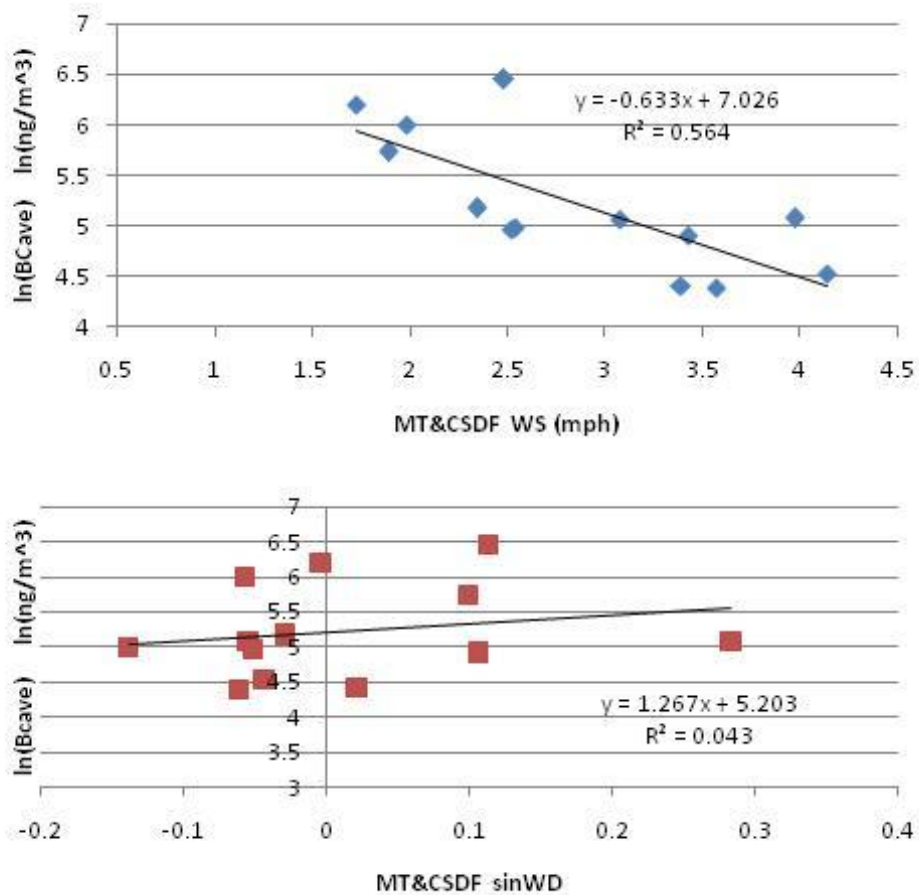


**Figure 9.8** Parameter plots from the multiple linear regression model for normalized 12 hour filter (PEM) black carbon concentrations ( $\ln(BC_{ave})$ ) averaged by Intensive Operational

**Period (IOP) when modeled using combined meteorological data from the LH CSDF and Marine Terrace (MT) stations**

**Table 9.5 Linear regression parameters for normalized 12 hour filter (PEM) black carbon deviation ( $\ln(BC_{dev})$ ) by Intensive Operational Period (IOP) as a function of number of burning sources**

| Response Variable | Explanatory Variable | Coefficient ( $\beta_i$ ) | Std Dev of Coefficient | $R^2$ (%) |
|-------------------|----------------------|---------------------------|------------------------|-----------|
| $\ln(BC_{dev})$   | Number of Sources    | 0.076                     | 0.035                  | 31        |
|                   | Constant, $\beta$    | -1.02                     | 0.35                   |           |

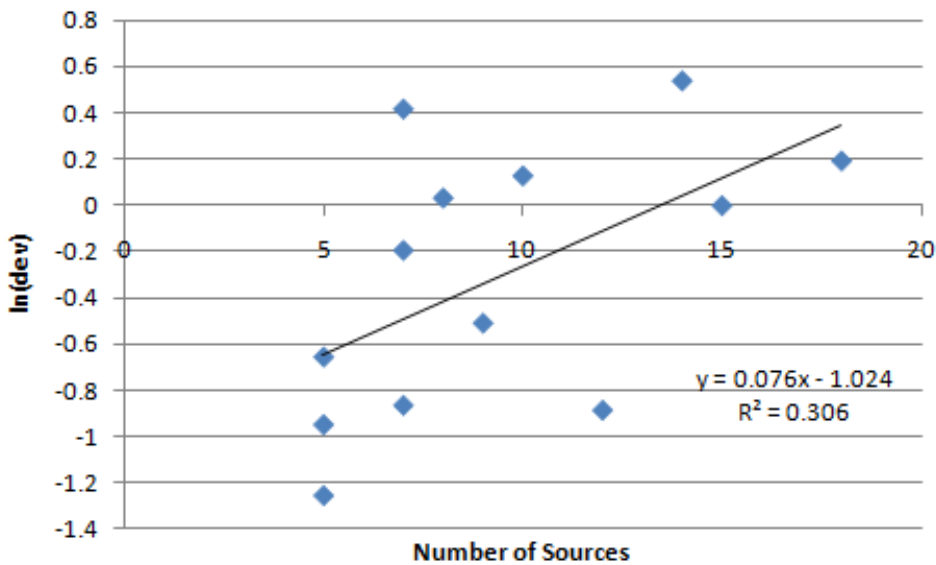


**Figure 9.9 Parameter plot from the multiple linear regression model for normalized 12 hour filter (PEM) black carbon concentration deviation ( $\ln(BC_{dev})$ ) by Intensive Operational Period (IOP) as a function of number of wood burning sources**

**9.3.2 Directional Effects on PEM BC**

Several factors were considered in the analysis of the relationship between PEM concentrations and directional/geographic impacts. To conduct the MLR analysis and identify characteristics that have the largest effect on PEM BC, the study area was first divided into sections and labeled as shown in Figure 9.10. The study area divisions distinguish between differences in geographic characteristics including tree coverage, elevation, and housing density which may impact pollutant dispersion. Section A typically is higher in elevation, contains more trees surrounding homes, and contains homes that tend to be fairly separated from one another. Section C alternately is lower in elevation, contains fewer trees than section A, and has homes in closer proximity to one another. Section B’s characteristics tend to be somewhat mid-way between section A and section C in elevation, tree coverage, and housing density, though tree coverage and housing density in section B share more similarities with section C. The

establishment of sections allows for the MLR model to take into account sectional differences in BC dispersion and better account for variability in average BC concentrations.

Having divided the study area into sections, the number of burning sources within each area was counted to observe potential relationships with PEM BC concentrations. The number of upwind burning sources was also considered, along with the closest distance of each sampler to any burning source and to any upwind burning source. Impacts of wind direction were considered by including the smallest angle between each sampling location and the IOP's dominant wind direction in the model. Impacts due to sampler site characteristics were observed through noting the sampling sites' proximity to the roads and the level of vegetation and structures surrounding the sampling instruments during operation. The level of vegetation and surrounding structures, mild, moderate, and heavy, was determined based on sampling location details. A mild level of vegetation and structures was assigned to PEM sites where surrounding vegetation was low and where virtually no structures were in close proximity. A moderate level was assigned where surrounding vegetation or structures taller than the PEM placement height were found on approximately 30 to 60 percent of the area surrounding the PEM. Lastly, a heavy level refers to PEM sites where vegetation taller than the PEM height in addition to rocks, trees, or fences were adjacent to PEM locations. The IOP during which each PEM BC concentration was sampled was also considered in the MLR to account for differences in burning behavior and site meteorology over each night.

Unlike MLRs conducted for relating BC and meteorology, the directional MLR used the categorical variables (non-numerical) location (A, B, and C), IOP (4b through 10b), and level of vegetation and structures (i.e. fencing) surrounding PEMs (mild, moderate, and heavy). For categorical variables, the MLR model assumes all options of the categorical variables but one to be a dependent variable,  $x_i$  (see Equation 8.1 repeated below), whose value is either 1 (true) or 0 (false). The partial slope,  $\beta_i$ , of the included variable evaluated then represents the difference between the included option and the excluded option. For example, when considering the categorical variable, 'location,' which has three options, A, B, and C, options A and B are represented by  $x_i$ 's in the MLR model, while option C is excluded. When a PEM is located in location A, the  $x$  representing location A is equal to 1 and the resulting partial slope is equal to the difference in BC concentration between location A and C (assuming the response variable is equal to BC concentration). The location B variable  $x$  would then be equal to 0 and would not be included for consideration in that particular sample. Categorical variables allow the MLR model to quantitatively account for differences between sampling conditions.

$$y = \beta_0 + \beta_1x_1 + \beta_2x_2 + \beta_3x_3 + \dots + \beta_kx_k + \varepsilon \quad (9.1)$$

Considering that wind direction played an important role in the variables for the directional analyses, IOPs were only evaluated if the most representative meteorological data was available. For this reason, only IOPs 4b through 10b were evaluated since aethalometer results indicated that EBAM meteorological data (measured only in IOPs 4b through 10b) was most representative for the study area. Due to the lower time resolution PEM data and smaller sample size, a significance level of 0.1 was used instead of the 0.05 level used for previous analyses.



**Figure 9.10 Study area divisions used for directional regression models**

The directional MLR was conducted by first linearizing the PEM BC data through the use of the best transformation, taking the natural logarithm of PEM BC concentration. The resulting model explained about 69 percent of the variability through the two categorical variables, location and IOP, as detailed in Table 9.6. Variables with "excluded" coefficients are the reference values. One way to describe this is to say that the excluded variables are built into the constant beta-0. Location B and IOPs not displayed in the table did not show a statistically significant difference from the reference variable. For instance, concentrations in location B and location C did not show a significant statistical difference in the model.

The final model indicates that significant differences were found between PEMs in locations A and C and over IOPs. Significant differences between IOPs and locations indicate that 90 percent confidence intervals for BC concentration do not overlap in value for the

locations and IOPs. The 0.10 alpha variable was used because the aethalometer regression model results demonstrated that the data had a low capacity for explaining black carbon concentration. Thus, the confidence interval was increased to identify variables that may potentially be significant, but difficult to identify. Still, differences in concentration between locations and IOPs may be small, on average around 1 ng/m<sup>3</sup> for each variable.

**Table 9.6 Multiple linear regression model parameters for normalized 12 hour filter (PEM) black carbon concentration (ln(BC)) for the directional model using the divisions in Figure 9.10**

| Response Variable | Categorical Variable | Option | Coefficient ( $\beta_i$ ) | Std Dev of Coefficient | R <sup>2</sup> (%) |
|-------------------|----------------------|--------|---------------------------|------------------------|--------------------|
| ln(PEM BC)        | Location             | A      | -0.26024                  | 0.05693                | 69.3               |
|                   |                      | C      | excluded                  |                        |                    |
|                   | IOP                  | 4b     | 0.4319                    | 0.1104                 |                    |
|                   |                      | 5b     | 0.4460                    | 0.1104                 |                    |
|                   |                      | 7b     | 0.2795                    | 0.1104                 |                    |
|                   |                      | 10b    | -0.9682                   | 0.1105                 |                    |
|                   |                      | 9b     | excluded                  |                        |                    |
|                   | Constant, $\beta$    | n/a    | 5.18631                   | 0.05674                |                    |

While the model seems to have explained a large percentage of variability, the model's residual versus fitted value plot as shown in Figure 9.11 does not clearly satisfy the MLR assumption of equal variance in the residuals. Residual values seem to be smaller at larger values, suggesting a potential non-linear relationship between the independent and dependent variables. Because the data used in the directional MLR did not clearly satisfy all MLR assumptions, even after transformation, the developed model may not be reliable and significant relationships may still exist between PEM BC concentration and other tested explanatory variables.

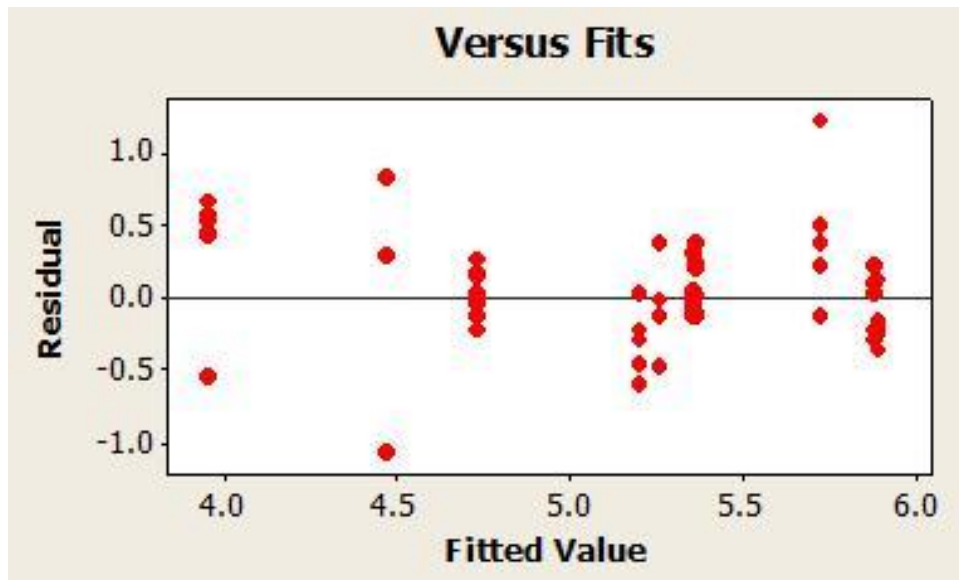


**Figure 9.11 Residual plot for the directional linear regression model for normalized 12 hour filter (PEM) black carbon concentration (ln(BC))**

Observing variables graphically suggests a potential significance of the variables level of vegetation and structures surrounding PEMs, number of burning sources in location, and number of upwind burning sources, after sorting for location and level of vegetation and structures surrounding PEMs. As shown in Figure 9.12, PEM BC concentration over different locations and under differing levels of vegetation and structures surrounding PEMs demonstrates that a notable relationship between PEM BC and number of burning sources in sampling location may be found. PEM BC concentrations measured in location C and at a site where vegetation and structures were minimal (“mild”) had a visible tendency to be higher as the number of burning sources in the location increase. A moderate level of vegetation and structures also seemed to have a similar pattern, though less clearly in comparison to the mild level. A similar relationship was seen for the dependent variable, number of upwind burning sources, as shown in Figure 9.13. Box plots showing differences in PEM BC concentrations are further detailed in Figure 9.14, showing a tendency for BC concentrations to be higher in location C and in instances of mild levels of surrounding vegetation and structures.

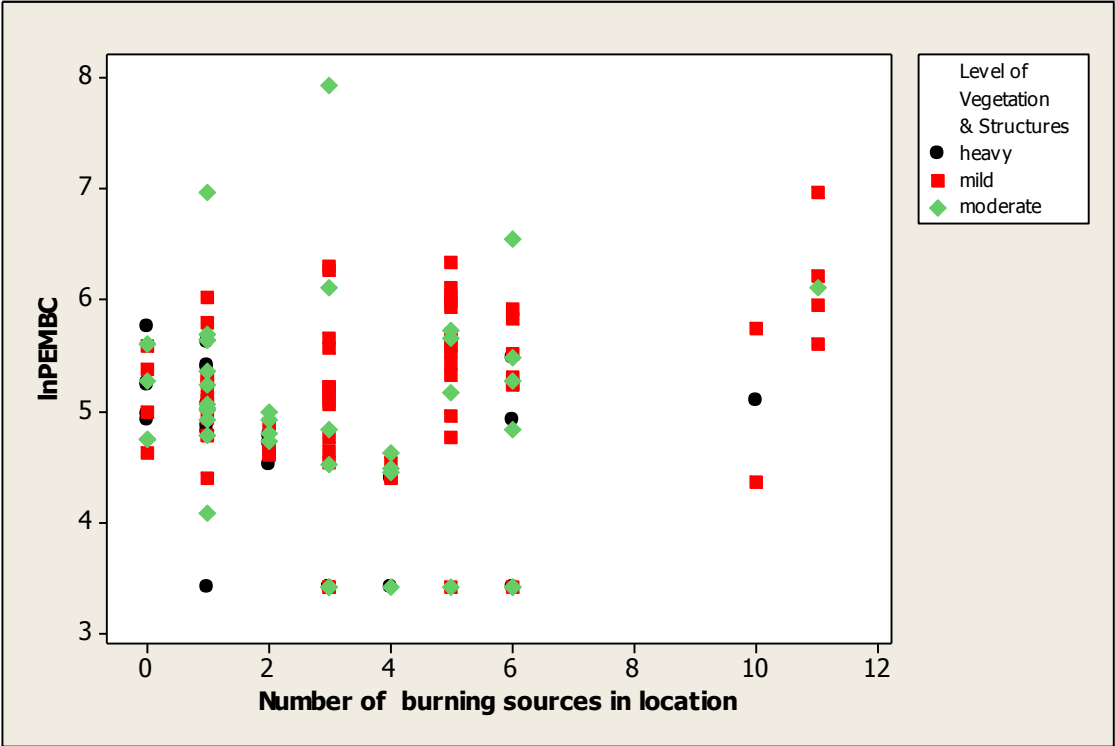
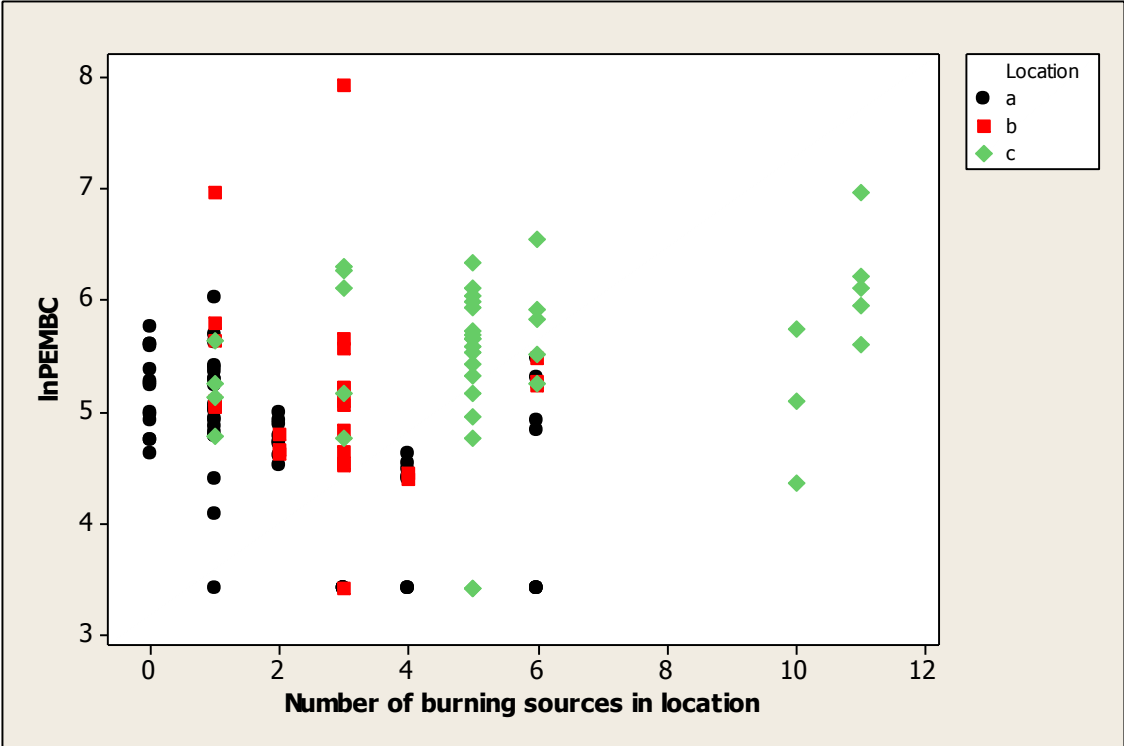


Figure 9.12 Normalized 12 hour filter (PEM) black carbon concentration (ln(BC)) versus number of burning sources in the division, as shown in Figure 9.10, sorted by location and level of vegetation and structures surrounding PEM for IOPs 2b through 10b

*The lnPEMBC transformation (as opposed to untransformed PEM BC concentration), makes the differences between variables more visible.*

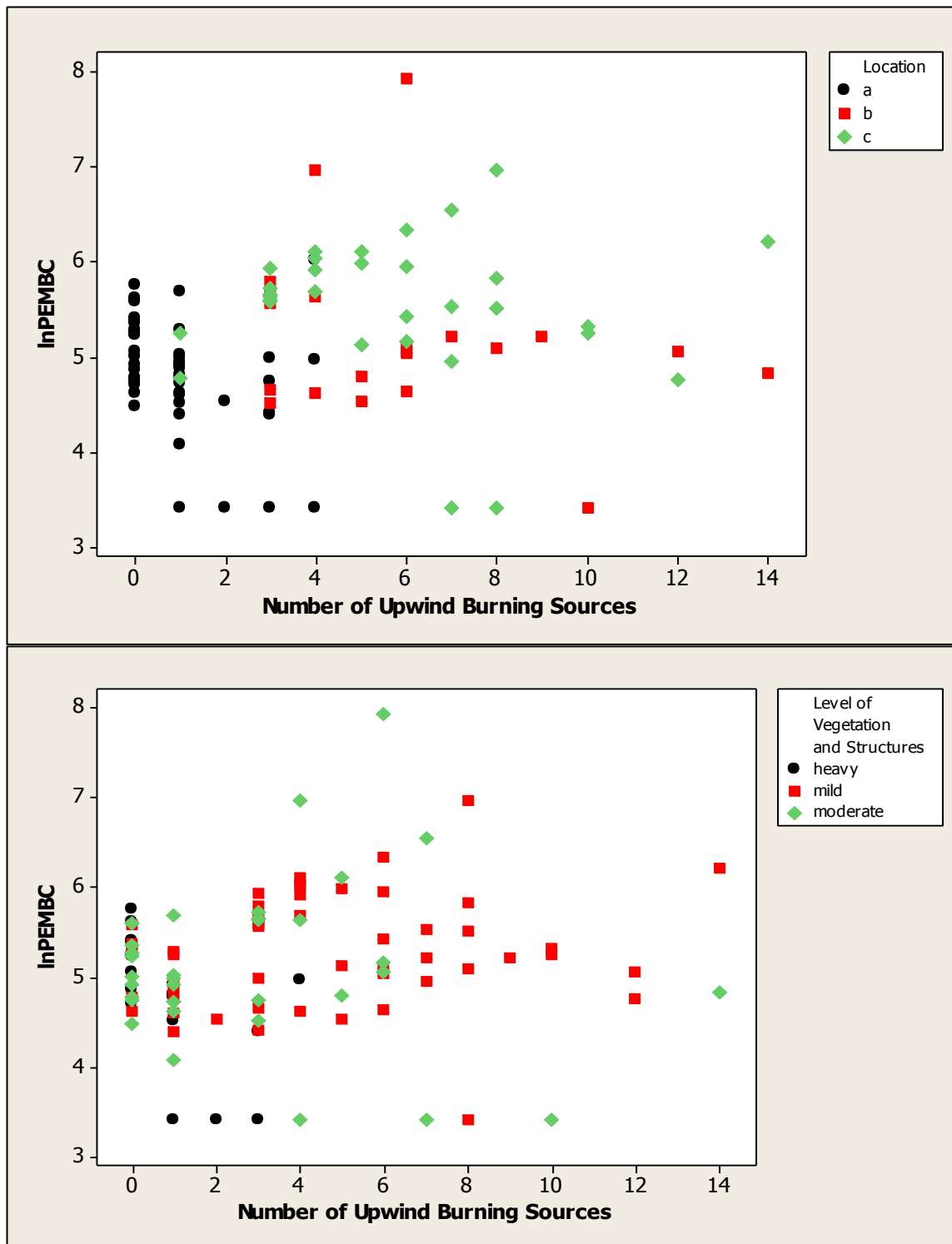
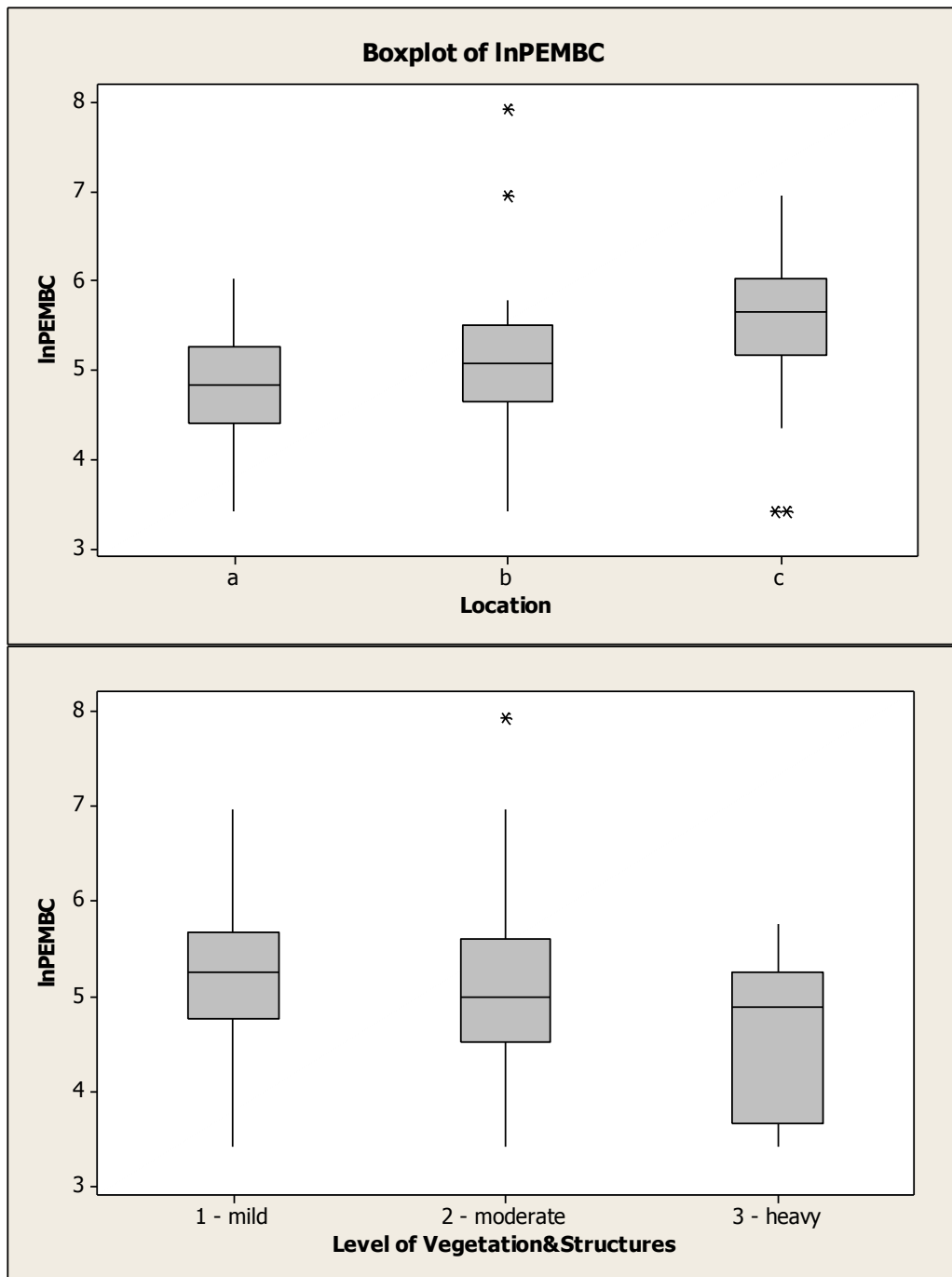


Figure 9.13 Normalized 12 hour filter (PEM) black carbon concentration ( $\ln(BC)$ ) versus number of upwind burning sources in location sorted by division, as shown in Figure 9.10, and level of vegetation and structures surrounding PEM for IOPs 4b through 10b

*The  $\ln$ PEMBC transformation (as opposed to untransformed PEM BC concentration), makes the differences between variables more visible.*



**Figure 9.14. Box plot showing normalized 12 hour filter (PEM) black carbon concentration (ln(BC)) by division, as shown in Figure 9.10, and degree of PEM obstruction for IOPs 2b through 10b**

*Box plots denote 1<sup>st</sup> and 3<sup>rd</sup> quartile, and median value for all concentrations. The whiskers indicate the maximum and minimum values. Each star represents an outlier identified by Minitab. The lnPEMBC transformation (as opposed to PEM BC concentration), makes the differences between variables more visible.*

## 10 Physical Modeling

Mechanical modeling methods can estimate pollutant concentrations with relatively high resolutions within small areas, however many models require highly detailed and accurate mechanistic information that may be economically impractical (Valari & Menut, 2010). Dispersion models belong to a category of mechanical models which rely on meteorological and geographical information which is often readily available. Dispersion models are mathematical simulations of pollutant travel as it leaves the original source location used to determine pollutant concentrations over differing spatial and time characteristics. Through the use of measured terrain, weather, and land use information, pollutant concentrations can be estimated for locations where air monitoring does not take place.

### 10.1 Background

Several models and model enhancements have been developed using dispersion as the basis for concentration predictions. American Meteorological Society/U.S. Environmental Protection Agency Regulatory Modeling System (AERMOD) is the current EPA-preferred dispersion modeling program for near-field regulatory application (US EPA, 2008), officially replacing its predecessor, Industrial Source Complex Short Term 3 (ISCST3), on December 9<sup>th</sup>, 2006. Both AERMOD and ISCST3 predict the highest concentrations over a selected averaging period and specified days and months based on source, terrain, and meteorological data input into the programs. To determine the highest pollutant concentration, both programs model all concentrations that result as the emission source constantly releases pollutants over the different meteorological conditions and as the plume interacts with the terrain.

ISCST3 was developed in 2002 by the US EPA as the third revision to the first ISCST program. Like ISCST and ISCST2, ISCST3 can evaluate plume rise and downwash for Good Engineering Practice stack heights and for shorter stacks, but it has also been refined to improve algorithms for area sources and dry and wet deposition for the purpose of calculating ground level pollutant concentrations at a one hour time-step or higher. The program assumes steady-state Gaussian plume dispersion from stationary point, line, area, or volume sources and is capable of considering conditions such as complex terrain, stack tip downwash, buoyancy induced dispersion, and final plume rise. To calculate ground level concentrations, ISCST3 considers meteorology, including wind profiles, vertical temperature gradients, and high or calm winds (US EPA, 1995).

With the help of Electric Power Research Institute (EPRI), the US EPA also developed ISC-Plume Rise Model Enhancement (ISC-PRIME), to improve predictions of building downwash where shorter stacks may cause plumes to become entrained around nearby structures. ISC-PRIME uses the same algorithms as ISCST3 with the exception of the building profile input program (BPIP), which has been shown to improve representation of the building downwash effect (EPRI, 1997). These improvements are largely a result of considering properties and interactions such as stack location relative to the building, streamline deflection over the building, speed deficits or shear impacts on a plume in a wake, and connections between two downwash algorithms (US EPA, 2003).

While a number of options are available on ISCST3 and ISC-PRIME (ISCST3 combined with BPIP), the program has several shortcomings often resulting in an overestimation of pollutant concentrations in unstable conditions (US EPA, 2003; Trinity Consultants, 2001). The American Meteorological Society/Environmental Protection Agency Regulatory Model Improvement Committee (AERMIC) was formed in 1991 to produce a program with more

representative modeling capabilities than the US EPA’s ISCST. The result of AERMIC’s work was AERMOD, designed to overcome ISCST3’s weaknesses while also being suitable for complex terrain and application over distances less than 50 km (40 CFR Part 51). While AERMOD’s modeling capabilities include a more complete representation of atmospheric conditions than ISCST3, it also requires a more extensive database of meteorological conditions. Table 10.1 summarizes the meteorological inputs required for each model.

**Table 10.1 Required Meteorological Inputs for ISCST3 and AERMOD**

| <b>ISCST3</b>              | <b>AERMOD</b>                   |
|----------------------------|---------------------------------|
| Hourly Flow Vector         | Hourly Flow Vector (deg.)       |
| Hourly Wind Speed          | Hourly Wind Speed (m/s)         |
| Hourly Ambient Temperature | Hourly Ambient Temperature (K)  |
| Hourly Stability Class     | Hourly Solar Radiation          |
| Hourly Rural Mixing Height | Hourly Cloud Cover              |
| Hourly Urban Mixing Height | Surface characteristics         |
|                            | Twice daily upper air soundings |

ISCST3 was ultimately selected for this study using model data available for Morro Bay, CA from the San Luis Obispo County Air Pollution Control District (SLO APCD) for the years, 1994, 1995, and 1996, which were the only years for which this data was available. Morro Bay is a coastal community with similar climate to Cambria and located approximately 12 miles to the southeast. Twelve hour Morro Bay meteorological data acquired from the SLO APCD was selected for each IOP based on its similarity to each IOP’s meteorology. The meteorology for each sampling period as detected by the Marine Terrace station was compared to similar hours of meteorology in Morro Bay. Days between the months of December through April where average and median wind speed and temperature were similar between Morro Bay and Cambria were selected for use.

Dispersion modeling was conducted using ISC-PRIME and ISCST3 through the BEEST version 9.74 (BEE-Line Software) user interface to predict BC concentrations within the 1 km<sup>2</sup> study area. Comparing results from the two programs allows for better understanding of the impact of building downwash; ISC-PRIME considers building downwash while ISCST3 does not. Both ISC-PRIME and ISCST3 were used to model 12 hour PEM BC concentrations over each IOP, the modeled concentrations were then compared to observed concentrations, and the results of ISC-PRIME and ISCST3 were compared to one another.

To conduct dispersion modeling in ISCST3 and ISC-Prime, several characteristics were categorized and assumptions were made where data was unavailable. The Cambria study area was characterized as a rural location due to the low percentage of residential land use, about 40 percent, highly forested terrain, and combination of simple and complex terrain. Homes, instead of all being represented individually, were represented as groups when homes were located close to one another, as shown in Figure 10.1

Because BC fireplace emission data is not readily available, BC emission rates were determined based on PM<sub>2.5</sub> emission data. When Purvis et al. (2000) tested standard and EPA-certified fireplace designs, they found total PM emission rates ranging between 10.3 to 58.4 grams per hr with PM<sub>2.5</sub> to constituting about 83 percent of total PM. Thus on average, Purvis et al. found PM<sub>2.5</sub> emissions of 32.9 grams per hour to result from fireplace wood burning. Gullet et al. (2003) in another study testing EPA-certified fireplaces and woodstoves found emission

rates to average 23.9 grams per hour, falling into the range observed by Purvis et al. The average of Gullet et al. and Purvis et al.'s observations, a  $PM_{2.5}$  emission rate of 28.4 grams per hour, was assumed in the models. Because BC emissions were measured, BC was assumed to average 5% of  $PM_{2.5}$  emissions, yielding a BC emission rate of 1.42 grams per hour per source.

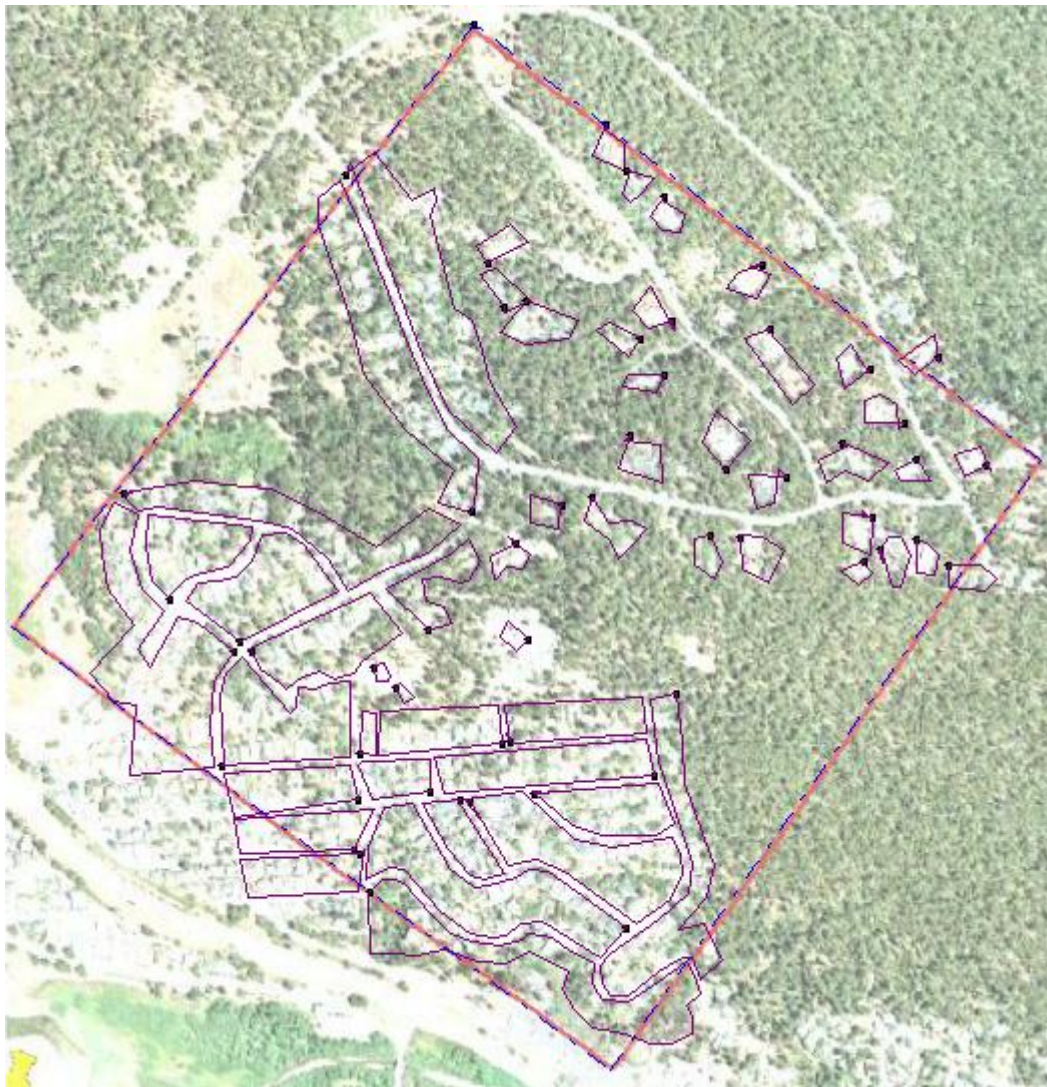


**Figure 10.1 Schematic of structure representations in BEEST for dispersion modeling**

Chimneys were assumed to have an exit velocity of 9.3 feet per second, the median velocity determined in Dasch's (1982) study of fireplace emissions. On average, homes were approximately 20 feet in height, chimneys were about 25 feet tall, and chimney exit diameters were estimated to be about 7.5 inches, a compromise between typical fireplace and wood stove diameters. A sensitivity analysis indicated small differences in modeled concentrations between exit diameters ranging between 6 and 12 inches for ISC-PRIME, but ISCST3 concentrations differed more widely. Because the "stacks" in the case of this study are chimneys located slightly above homes at heights much lower than specified for Good Engineering Practice in 40 CFR 51.100, the stacks in the study area were considered short stacks.

Once final BC concentrations were modeled by the ISCST3 and ISC-PRIME programs, BC concentrations had to be adjusted to account for the actual time period of source emissions. ISCST3 and ISC-PRIME assume each emission source to be emitting throughout the 12 hour averaging period, when in fact emissions occur over a much shorter time span. Based on aethalometer data, on average, source emissions occur over about 4.5 hours (37.5 percent) of each IOP, most often in the evening and early night time. To approximately adjust BC concentrations modeled by the ISC programs to represent actual emissions, 37.5 percent of the ISC modeled concentrations were taken as the 12 hours integrated average BC concentration in the area. It is important to note that taking a factor of the modeled concentration is an approximate method that does not account for diurnal meteorological variations. Because the ISC programs tend to choose the time interval where meteorological characteristics will yield higher concentrations (i.e. lower wind speeds and mixing height), modeled BC concentrations can be higher than would be expected under actual conditions. Modeled concentrations of zero were set to the average of zero and the lower detection limit, so that model zeros were assumed to be the same value used for non-detectable PEM samples ( $30.26 \text{ ng/m}^3$ ) to improve comparison with measured data.

## ***10.2 Dispersion Modeling Results***

Dispersion modeling using ISC-PRIME and ISCST3 for the Cambria study area resulted in a majority of under predicted concentrations. On average, the modeled-to-measured BC concentration ratio was 0.14, ranging from  $1.3 \times 10^{-5}$  to 2.14, and 0.09, ranging from  $1.2 \times 10^{-5}$  to 0.88, for ISC-PRIME and ISCST3, respectively. Box plots shown in Figure 10.2 demonstrate the distribution and prevalence of ratios between a 1<sup>st</sup> and 3<sup>rd</sup> quartile value of 0.02 and 0.14 for ISC-PRIME and 0.02 and 0.09 for ISCST3.

While both models tended to yield BC concentrations less than the measured BC PEM concentrations, ISCST3 underestimated concentrations more often than ISC-PRIME. The overall tendency to under predict concentrations was not expected for ISCST3, but has been seen to occur for ISC-PRIME. ISCST3 was expected to predict higher-than-observed concentrations under complex terrain as discussed by US EPA (2003) and Perry et al. (2005). When observing the modeled-to-measured BC ratio relative to the magnitude of measured BC concentrations for ISC-PRIME, as shown in Figure 10.3, BC concentrations over predicted by ISC-PRIME only resulted when measured concentrations were low. The same tendency was observed for ISCST3 predictions as shown in Figure 10.4. Both figures also show that the highest observed BC concentrations were always under predicted by both ISC-PRIME and ISCST3. Since very high concentrations result when a nearby source directly influences a sampler, this under prediction most likely results from an inability to capture this very localized effect in the models. High modeled-to-measured BC ratios are less than 5 percent of all observed ratios and high measured concentrations are less than 5 percent of all PEM concentrations.

The disparities between this study's results and the results of the previous studies likely resulted due to several assumptions made in the modeling process and the meteorological data used. Because emission rates and stack characteristics can vary widely, it was only within this study's means to use approximated values. Emission rates are highly variable not only amongst homes, but also amongst fireplaces and even between burning events in the same fireplace. In addition, all stacks were approximated to be identical, although it is likely that exit flue heights and diameters differ significantly throughout the area. The approximation of all of these characteristics reduced the accuracy of the modeled results. If assumptions such as source

strength, emission time, and BC fraction were significantly low then this could lead to model under prediction. Another factor that may lead to model inaccuracy is the complex terrain and surface features of the study area. Streets, trees, and other obstructions can lead to air flow channeling which may significantly divert flow patterns and downdrafts around these obstructions can lead to enhanced surface concentrations. These types of complex, near-field effects may not be well captured by the models.

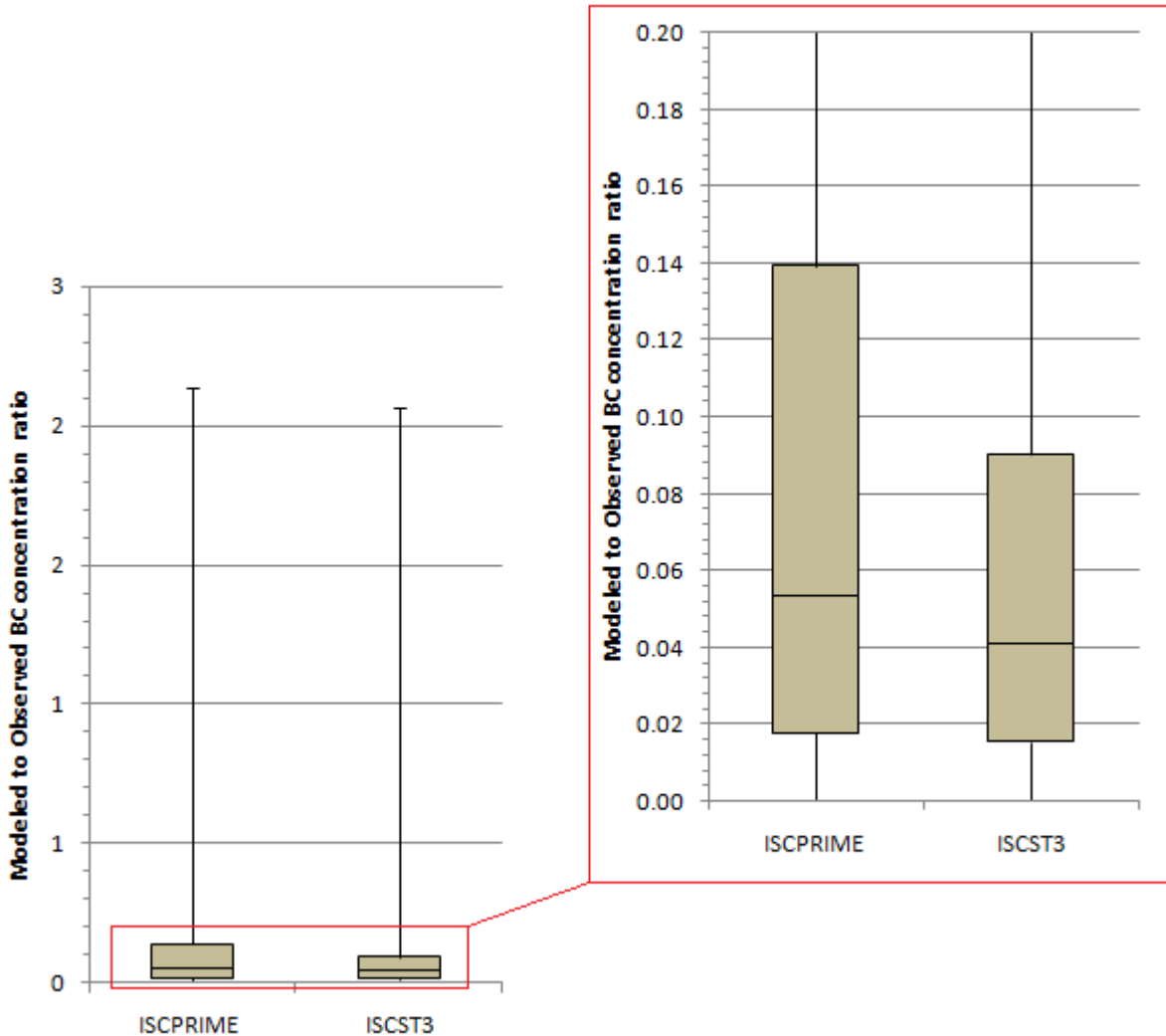


**Figure 10.2** Box plots showing the ratio modeled black carbon to measured black carbon for ISC Prime and ISCST3 for all 12 hour integrated filter samples over all intensive operational periods (IOPs)

*Box plots denote 1<sup>st</sup>, median, and 3<sup>rd</sup> quartile for all concentrations. The whiskers indicate the maximum and minimum values.*

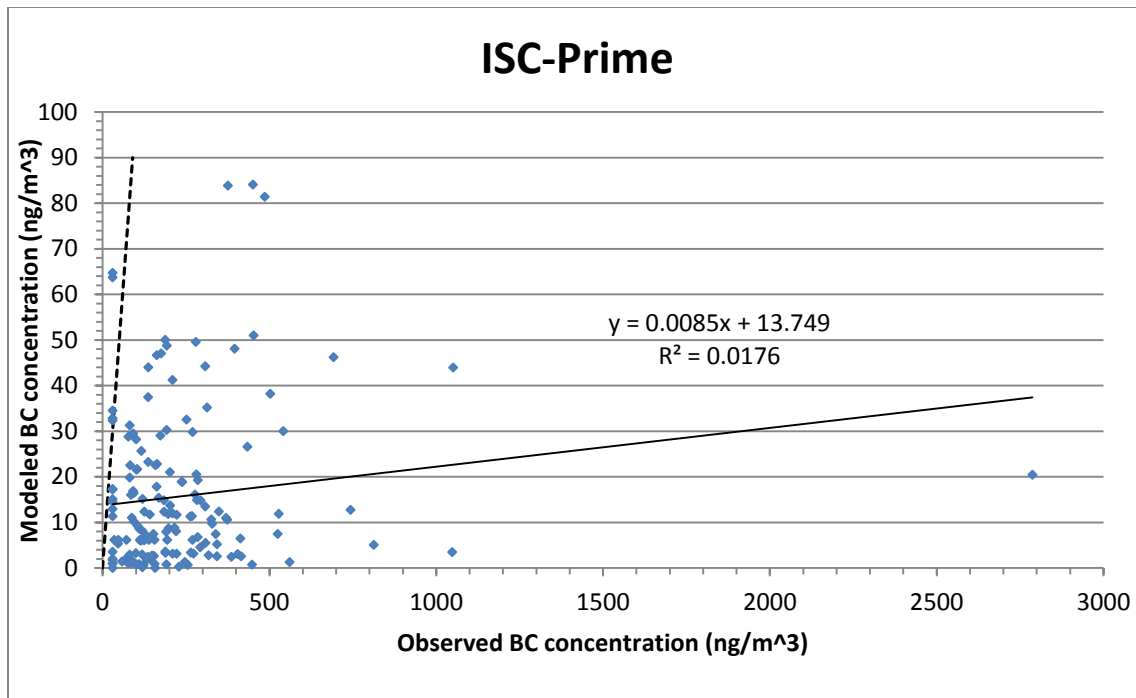


**Figure 10.3** ISC-PRIME modeled versus measured BC concentration for all samples over all IOPs. The dotted line represents a one-to-one ratio between measured and modeled BC concentrations. The solid line is an applied trendline with equation and  $R^2$  value shown.

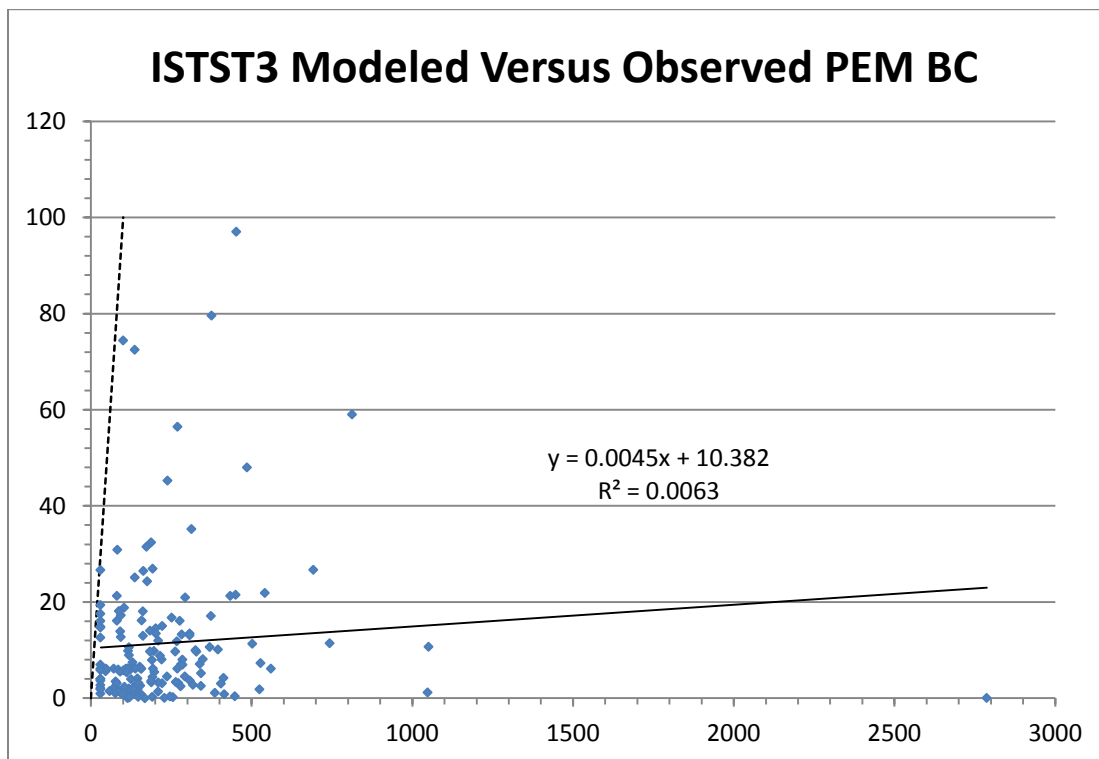


**Figure 10.4** ISCST3 modeled versus measured BC concentration for all samples over all IOPs. The dotted line represents a one-to-one ratio between observed and modeled BC concentrations. The solid line is an applied trendline with equation and  $R^2$  value shown.

In addition to model assumptions, the use of Morro Bay meteorological data may have contributed to low modeled BC concentrations. The Morro Bay meteorological data was selected based on similarity to the Marine Terrace data because of the similarity between the types of stations. However, the Marine Terrace data had average wind speeds between 3 to 5 times greater than the near ground level EBAM station which analysis of the aethalometer data showed was better able to explain BC concentrations. Therefore these lower elevation wind speeds may have a more significant influence on near-field ground level concentrations than the commonly used elevated meteorological measurements, leading to higher than predicted concentrations.

To aid in the analysis of the concentration patterns predicted by the models and patterns observed in measured concentrations, factors were determined that would bring average modeled BC concentrations close to the measured average. To accomplish this task, different factors were determined and applied to the modeled concentrations for each IOP such that the average measured BC concentration was equal to the average modeled BC concentration. Figure 10.5 shows the resulting modeled-to-observed BC concentration graphs.

For some IOPs, both the ISCST3 and ISC-Prime models yielded contours that were similar in many details. For instance, Figure 10.6 shows model contours for IOP 6b with measured PEM BC shown as circles with the concentrations denoted by using the appropriate color based on that contour map's scheme. For this IOP, both models yielded contour maps with similar shapes, although there is still some variability in the details. Each model predicted peak areas in similar locations and low concentrations in the northwestern portion of the study area. The measured concentrations show some features that are similar to the models, however measured concentrations tend to exhibit a wider spread of the contours, indicating more dispersion. On the other hand, for some IOPs the two models yielded very different contours. Figure 10.7 shows the modeled contour maps for IOP4b. In this instance, ISC-PRIME predicts relatively consistent concentrations over much of the study area with a single peak in the southwest. However, ISCST3 predicts a concentration ridge running along the southeast border of the study area. For this IOP, ISC-PRIME appears to do a better job of representing the measured concentrations, although the model predicts low concentrations where the PEM measurements were highest, in the south corner and west corner of the study area. Differences between ISC-PRIME and ISCST3 BC dispersion were usually small where average wind speed was less than 3 mph (IOP 4b), but increased when average wind speeds were above 3 mph (IOP 6b). This is an indication that building downwash becomes less significant when wind speeds are low. In general, both models were able to capture some of the features shown in the PEM measurements during some IOPs, but not during others. For instance, ISC-PRIME captured BC dispersion well for IOP 4A, but not as well for IOP 4B (Figure 10.8). Still, for IOP 4B, ISC-PRIME identified higher concentrations on the southwest part of the study area and then decreasing concentrations in the north east direction. ISC-PRIME was sometimes able to accurately predict the location where the highest BC concentration occurred, while ISCST3 was less often able to do so. Figure 10.9 shows two examples (IOPs 9B and 10B) where dispersion was not well modeled by both ISC programs. The locations of the highest measured BC concentrations were not identified by ISC-PRIME and ISCST3 and locations of low concentration were often identified as locations of high concentration.

When observing wind speeds for IOPs 4A, 4B, 9B, and 10B along with other IOP contours and their respective wind speeds, ISC-PRIME and ISCST3 seem to more accurately model pollutant dispersion at average wind speeds less than 3 mph. Based on the Marine

Terrace meteorological station, IOPs 4A and 4B had wind speeds of 2.5 and 2.6 mph, respectively, and IOPs 9B and 10B had wind speeds of 5.6 and 3.3 mph, respectively. Unfortunately, neither model consistently provided an accurate picture of variability within the study area.

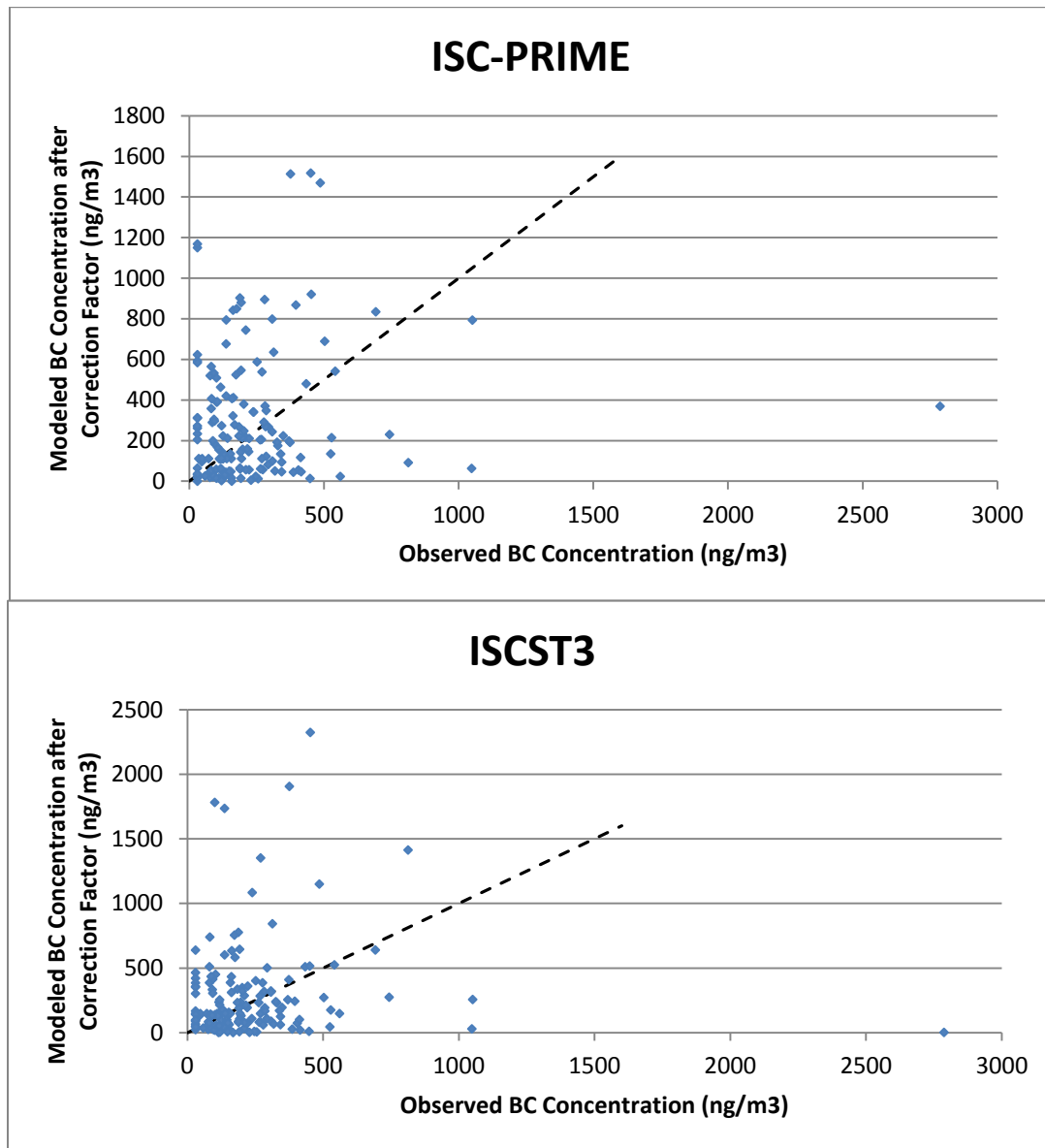


**Figure 10.5** Corrected modeled BC versus observed BC concentration for the ISC-PRIME and ISCST3 models after adjustment of average modeled values to match the average measured values. *The dotted line represents a one-to-one ratio between observed and modeled BC concentrations*

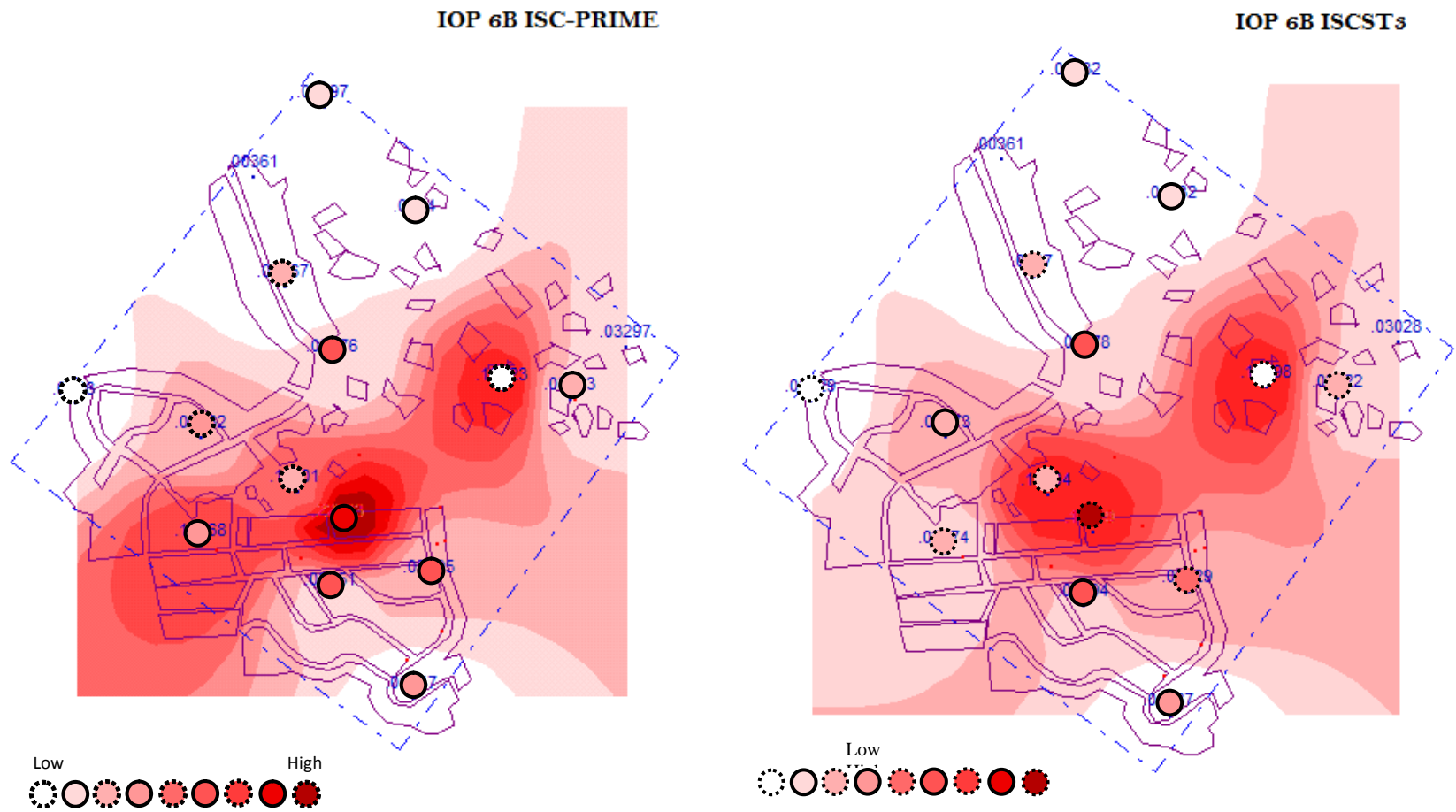


**Figure 10.6** ISC-Prime and ISCST3 dispersion model contour maps for IOP 6b. Modeled values have been adjusted so that the average modeled concentration equals the average measured concentration. Measured values are represented by circles shaded to match the concentration scale of the model.

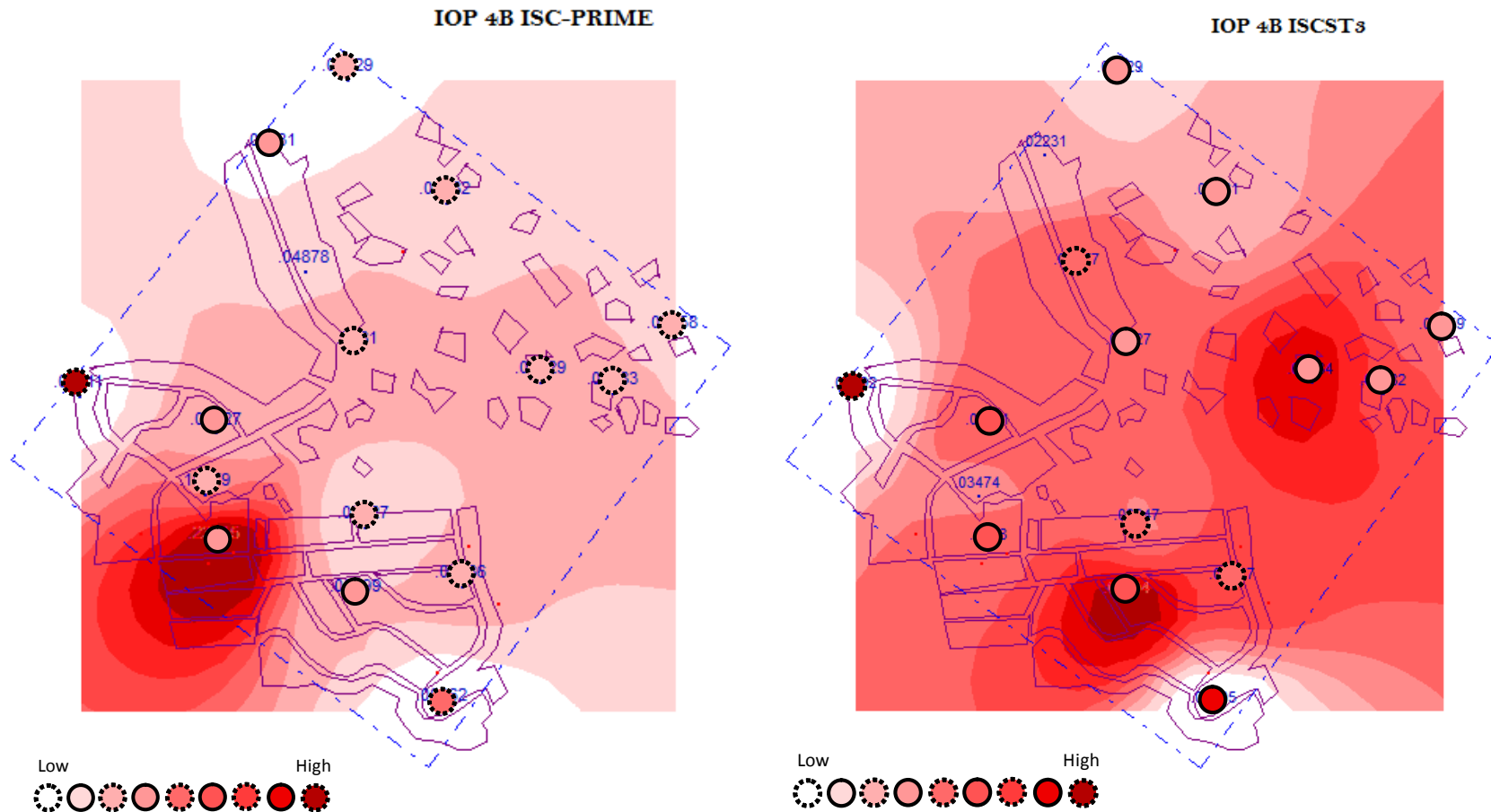


**Figure 10.7** ISC-Prime and ISCST3 dispersion model contour maps for IOP 4b. Modeled values have been adjusted so that the average modeled concentration equals the average measured concentration. Measured values are represented by circles shaded to match the concentration scale of the model.

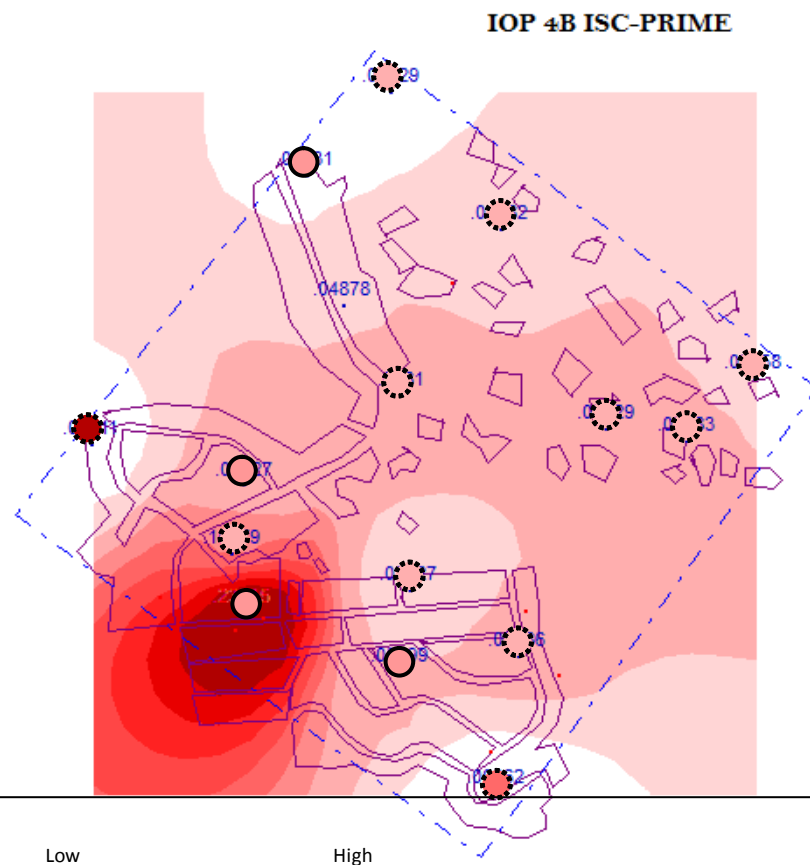
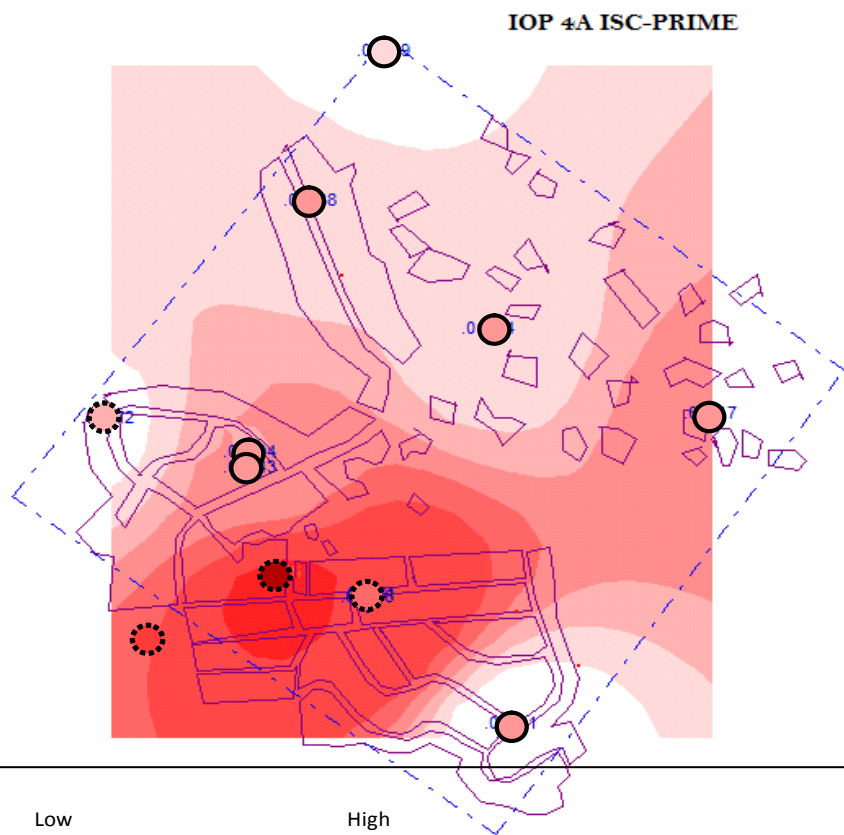


**Figure 10.8** ISC-PRIME contour plots for IOPs 4a and 4b. Modeled values have been adjusted so that the average modeled concentration equals the average measured concentration. Measured values are represented by circles shaded to match the concentration scale of the model.

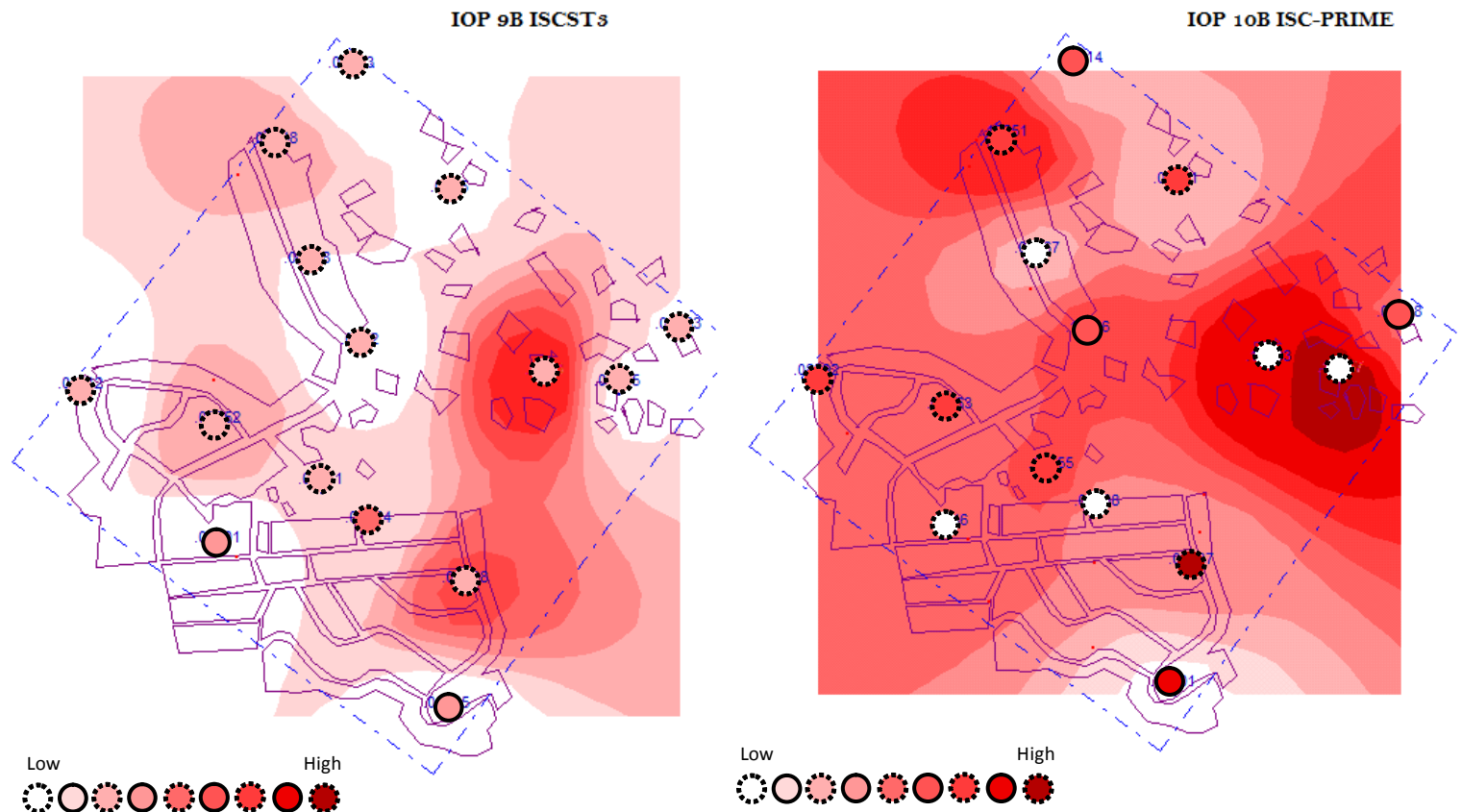


**Figure 10.9** ISCST3 contour plot for IOP 9b and ISC-PRIME contour plot for IOP 10b. Modeled values have been adjusted so that the average modeled concentration equals the average measured concentration. Measured values are represented by circles shaded to match the concentration scale of the model.

## 11 Transfer of Wood Smoke Indoors

Assessing the impact of wood smoke exposures on the local residential population requires an understanding of both indoor and outdoor concentrations since studies have shown that Californians spend eighty-seven percent of their time indoors (Jenkins et al., 1992). This is expected to be especially true for times when wood smoke concentrations are high (evenings, nights, and during cold weather) when people would be more likely to be inside their homes. So although ambient monitoring is a vital component of exposure assessment, the indoor concentration also plays a significant role.

### 11.1 Methods

The relationship between indoor and outdoor concentrations for a conservative tracer can be described using the mass balance equation shown in Equation 11.1.

$$\frac{\partial C_{in}}{\partial t} = (C_{out} - C_{in})\lambda_v \quad (11.1)$$

where  $C_{in}$  = indoor concentration ( $\mu\text{g}/\text{m}^3$ ),  
 $C_{out}$  = outdoor concentration ( $\mu\text{g}/\text{m}^3$ ),  
 $t$  = time (hr), and  
 $\lambda_v$  = air exchange rate ( $\text{h}^{-1}$ ).

Equation 11.1, however, does not account for the generation and loss processes that occur for non-conservative pollutants and in real environments. Figure 11.1 shows some of the processes which can influence concentrations of particles within residences. Equation 11.2 (Thatcher et al., 2001) shows a mass balance equation which accounts for these processes and can be used for particulate pollutants under most circumstances in the indoor environment.

$$\frac{\partial C_{in}}{\partial t} = (C_{out}P - C_{in})\lambda_v - C_{in}k_{dep} + G + S + F + K + H + R \quad (11.2)$$

where  $P$  = dimensionless penetration factor,  
 $k_{dep}$  = deposition loss rate ( $\text{h}^{-1}$ ),  
 $G$  = generation of particles from indoor sources ( $\mu\text{g}/\text{m}^3 \cdot \text{h}$ ),  
 $S$  = particle formation through gas/particle exchange ( $\mu\text{g}/\text{m}^3 \cdot \text{h}$ ),  
 $F$  = particle formation due to reaction ( $\mu\text{g}/\text{m}^3 \cdot \text{h}$ ),  
 $K$  = particle size change through coagulation ( $\mu\text{g}/\text{m}^3 \cdot \text{h}$ ),  
 $H$  = particle size change through hygroscopic growth ( $\mu\text{g}/\text{m}^3 \cdot \text{h}$ ), and  
 $R$  = generation of indoor particles from resuspension ( $\mu\text{g}/\text{m}^3 \cdot \text{h}$ ).

This study was designed so that most of the terms above can be assumed to be negligible despite the inherent complexity of the relationship between indoor and outdoor concentrations. By assuming that the wood smoke particles are inert and that resuspension is negligible (which is reasonable based on their submicron size), Equation 11.2 simplifies to Equation 11.3 (Hering et al., 2007) for a home without indoor generation.

$$\frac{\partial C_I}{\partial t} = C_O P \lambda_v - C_I (\lambda_v + k_{dep}) \quad (11.3)$$

The model described by Equation 11.3 has 2 concentration parameters (indoor and outdoor concentration) and three transport parameters (penetration, air exchange rate, and deposition loss rate). The penetration factor (P) refers to the fraction of particles that pass through the shell of the building with the infiltrating air. The deposition loss rate defines particle losses due to deposition onto all indoor surfaces (/hr). The final transport parameter is the air exchange rate which describes the airflow through the building divided by the building volume (/hr).

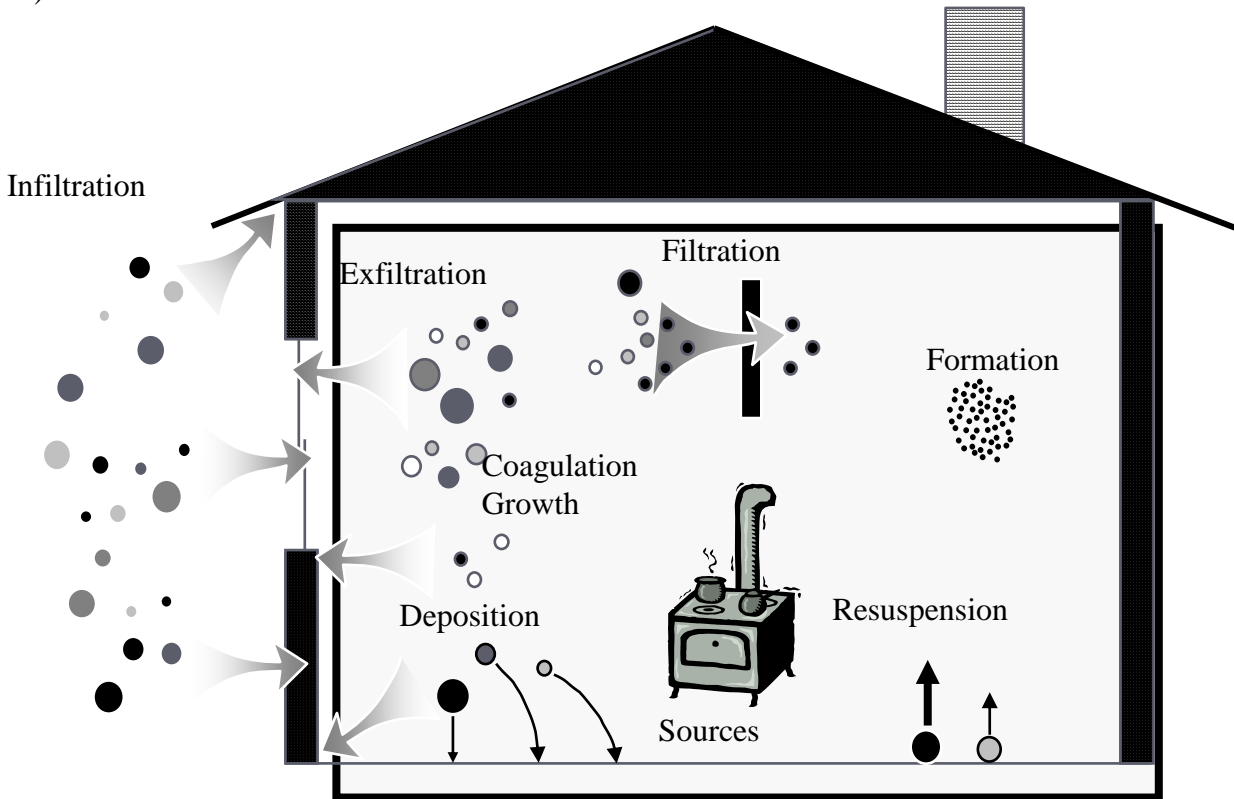


**Figure 11.1 Important processes which can influence the concentrations of particles in the indoor environment**

Because mechanical and natural ventilation were not present in the study homes, the only method of air exchange was infiltration through the building shell. The primary driving force for infiltration is indoor/outdoor pressure differences. These pressure differences arise from wind impacting on exterior surfaces and/or the temperature difference between the interior and exterior.

Due to homeowner concerns, we were unable to provide direct measurements of air exchange rate for the study home. Consequently, a series of testing using aethalometers placed indoors and outdoors at a residence were used to estimate the air exchange rate using a time dependent model. In addition, the values obtained from the aethalometer model were compared to the air exchange rate estimated using a model developed Lawrence Berkeley National Laboratory which estimates infiltration rates based upon the temperature difference, wind speed, and building and environmental factors (Sherman & Grimsrud, 1980). The model shown in Equation 11.4 describes infiltration rate ( $\text{hr}^{-1}$ ).

$$\lambda = 3600 \frac{A_{LEAK}}{A_{FLOOR}H} \sqrt{f_s^2 \Delta T + f_w^2 W^2} \quad (11.4)$$

where  $A_{leak}$  (m<sup>2</sup>) = the total leakage area of the building,  
 $A_{floor}$  (m<sup>2</sup>) = floor area of the building,  
 $H$  (m) = building height,  
 $f_s$  (ms<sup>-1</sup>K<sup>1/2</sup>) = the stack parameter determined by the geometry of the building,  
 $\Delta T$  (K) = absolute temperature difference,  
 $f_w$  (unitless) = the wind factor determined environmental shielding, and  
 $W$  (m/s) = the wind speed.

## 11.2 Indoor/Outdoor Ratios

The average indoor/outdoor ratio is a traditional and easy to use method for describing the relative concentration of a pollutant in the indoor environment. Typically the time integrated indoor and outdoor concentrations are measured and the ratio between them is used to estimate the indoor concentration for a given outdoor concentration. It is important to note that only long term averages are useful for determining the ratio. Since changes in outdoor concentration are transmitted slowly through the building shell (often described as an apparent time lag in the concentration series), the indoor/outdoor ratio at any particular time is more dependant on recent changes in outdoor concentration than on characteristics of the home or pollutant. Figure 11.2 illustrates the theoretical indoor concentration response for a spike in the outdoor concentration for a conservative pollutant when the air exchange rate is 0.5/hr. For a conservative pollutant with no indoor sources, the theoretical indoor outdoor ratio (I/O) is 1.0 for long sampling periods. In this example, the I/O for the 24 hours shown is close to the theoretical value at 0.98. However, for shorter sampling periods, the I/O ratio obtained is dependent on where the sampling period lies in relation to the outdoor concentration peak. Figure 11.3 illustrates the importance of choosing an appropriate sampling period by showing the dependence of I/O ratio on the start time for a hypothetical 8 hour sampling period. The I/O ratio has a minimum of 0.16 that occurs when samples are taken from hours 1.6 to 9.6. In that instance, sampling includes the start of the outdoor peak but concludes before the indoor concentration rises significantly. Conversely, the maximum I/O ratio of 6.8 is obtained for integrated samples taken between 10 and 18 hours. In this example, hour 10 is the point where the outdoor concentration has decreased and is equal to the indoor concentration. Since the indoor concentration decays slowly, the I/O ratio is artificially high.

In addition to the need to collect samples over an entire peak event, there are also inherent uncertainties introduced when extrapolating a given indoor/outdoor ratio to represent indoor concentrations under differing circumstances. This is illustrated in Equation 11.5 which is a rearrangement of Equation 11.3 for steady state conditions. This formulation assumes that indoor generation is negligible and the outdoor concentration is uniform across the building shell, a condition that is typically well satisfied for ambient pollutants but which may not hold when sources are near the building.

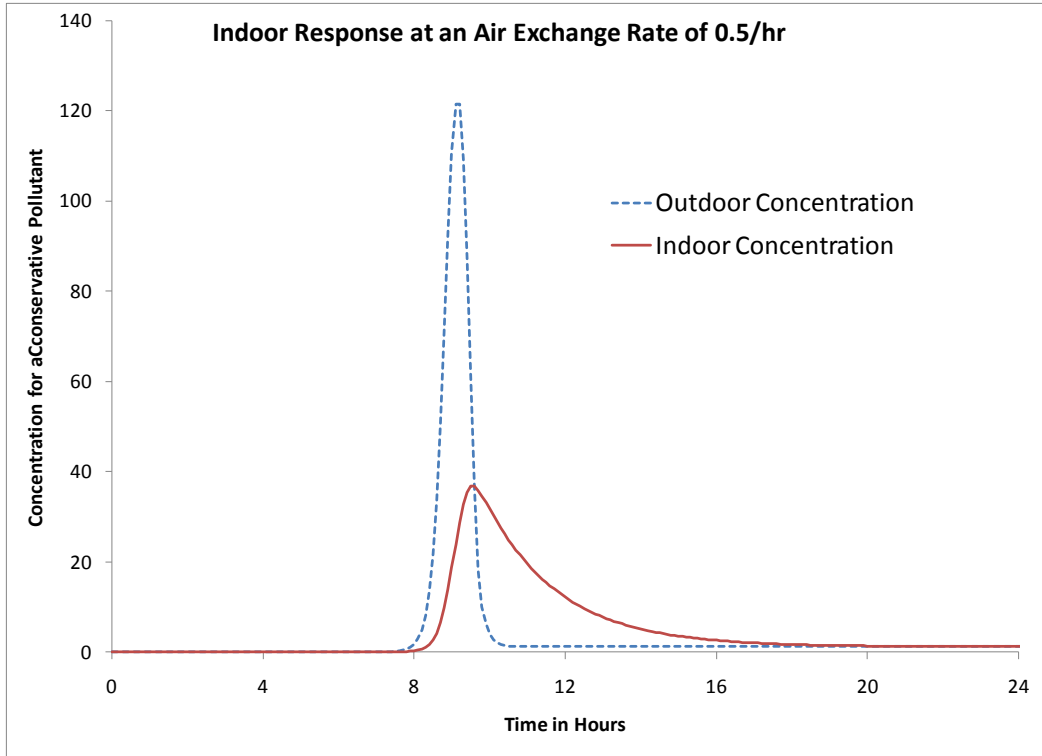


**Figure 11.2** Calculated indoor concentration response to a theoretical spike in outdoor concentration for a conservative pollutant with an air exchange rate of 0.5/hr (based on a mass balance model)

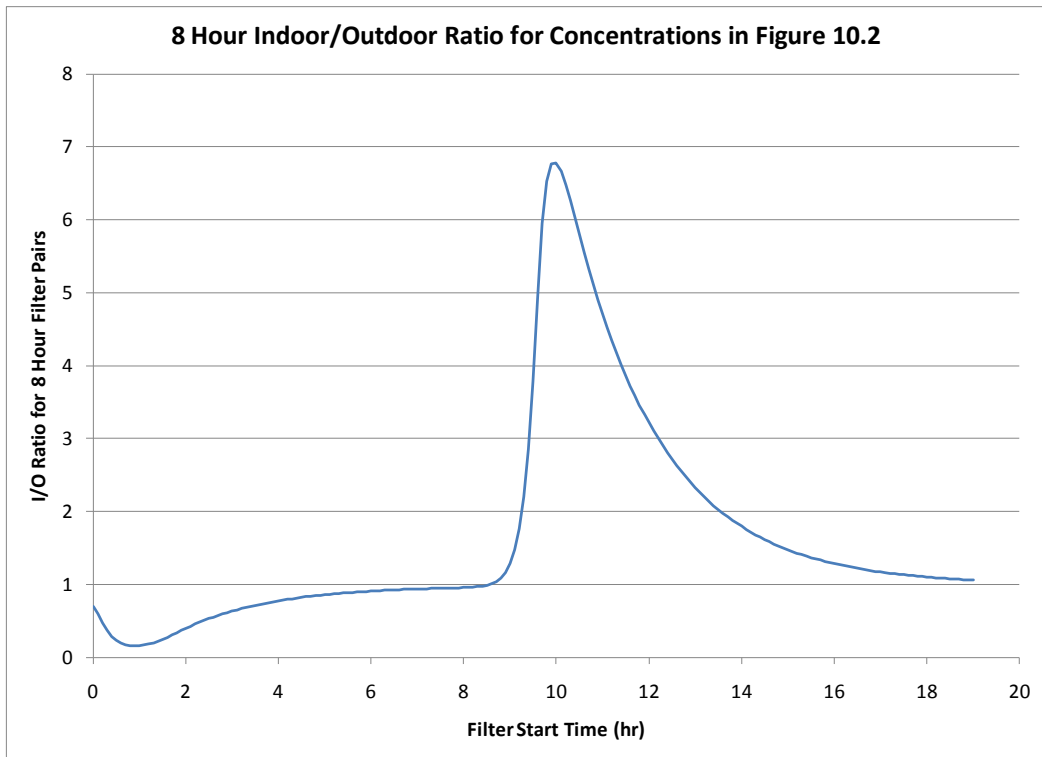


**Figure 11.3** Indoor/outdoor ratios that would be obtained from the data in Figure 11.2 for 8 hour integrated filters started at different times

$$\frac{C_{indoor}}{C_{outdoor}} = \frac{P\lambda_v}{k_{dep} + \lambda_v} \quad (11.5)$$

Equation 11.5 shows that the average indoor/outdoor ratio is a function of three factors: the air exchange rate, which depends on meteorology and home construction, the deposition rate, which depends primarily on particle characteristics, and the penetration rate, which depends primarily on particle characteristics but is also influenced by infiltration rate. Therefore, a given indoor/outdoor ratio is most accurate when it is applied to homes with similar infiltration characteristics and under similar meteorological conditions. This means that not only can two homes in the same region have different indoor/outdoor ratios for the same time period, but also that the ratio for the same home will typically vary with meteorology. Nevertheless, indoor/outdoor ratios are a useful construct to provide a basic understanding of indoor contaminant levels.

For this study, 12 hour integrated filter samples were taken simultaneously indoors and directly outdoors at a residence and analyzed for black carbon using optical absorbance. Samples were collected to coincide with an IOP. Since outdoor black carbon concentrations typically peaked in the early evening and decreased around midnight, this timing had a higher probability of capturing an entire peak event. A total of 14 pairs of filter samples were collected, however 4 of the pairs had at least one filter below the detection limit and 2 filters had sampling errors. By supplementing the filter data with aethalometer data, 13 indoor/outdoor pairs were complete as shown in Table 11.1.

**Table 11.1 Indoor/outdoor ratios for 12 hour integrated black carbon concentrations by residence and intensive operation period (IOP)**

| IOP                       | Residence | I/O Ratio               |
|---------------------------|-----------|-------------------------|
| 1a                        | E         | 0.99 <sup>a</sup>       |
| 2a                        | E         | 0.86 <sup>a</sup>       |
| 3a                        | E         | 0.42 <sup>a</sup>       |
| 4a                        | E         | 0.87                    |
| 7a                        | E         | 1.06 <sup>a</sup>       |
| 8a                        | E         | 0.87 <sup>a</sup>       |
| 1a                        | G         | 0.69                    |
| 3a                        | G         | 2.97 <sup>b</sup>       |
| 4a                        | J         | 1.96                    |
| 3a                        | M         | 0.86                    |
| 4a                        | M         | 0.69                    |
| 7a                        | M         | 0.45                    |
| 8a                        | M         | 2.25 <sup>b</sup>       |
| <b>Average</b>            |           | <b>0.88<sup>c</sup></b> |
| <b>Standard Deviation</b> |           | <b>0.41</b>             |

<sup>a</sup> ratio includes concentrations integrated from an aethalometer, <sup>b</sup> resident operated fireplace during test, <sup>c</sup> ratio from 3G and 8M were excluded from the average due to fireplace usage

Although there is a large amount of variability in the indoor/outdoor ratios, the average indicates that the indoor environment is not highly effective at reducing exposures to black

carbon from residential wood smoke generated in the near-field. As can be seen in Equation 11.5, a value for I/O close to one can result either from high air exchange rates, low loss rates, or a combination of these factors. If the relatively high ratio resulted from a higher than normal air exchange rate then these conclusions would be expected to have limited applicability to other residences. However, if the high I/O ratio is due to low loss rates then a similar ratio would be expected in other residences. Abnormally high air exchange rates would not be expected for this study, since wind speeds were low, indoor/outdoor temperature differences were moderate, windows were closed, and homes were of standard construction and well maintained. On the other hand, relatively fresh wood smoke particles would be expected to be small, trending toward the accumulation mode. Particles in this size range don't settle or diffuse quickly, leading to low loss rates.

To help confirm the findings of the filter based measurements, additional tests were performed at residence E. A total of 16 burning events were recorded between November 30, 2008 and March 20, 2009, defined as a substantial increasing in outdoor black carbon concentration followed by a return to concentrations pre-event. These events usually began around 6 to 8 PM and the time period for the outdoor concentration increase ranged from a few hours to less than an hour. Figure 11.4 shows the indoor and outdoor BC concentrations for a single burning event. The length of the time lag between the start of elevated outdoor concentrations and the indoor response is an indication of a relatively low air exchange rate.

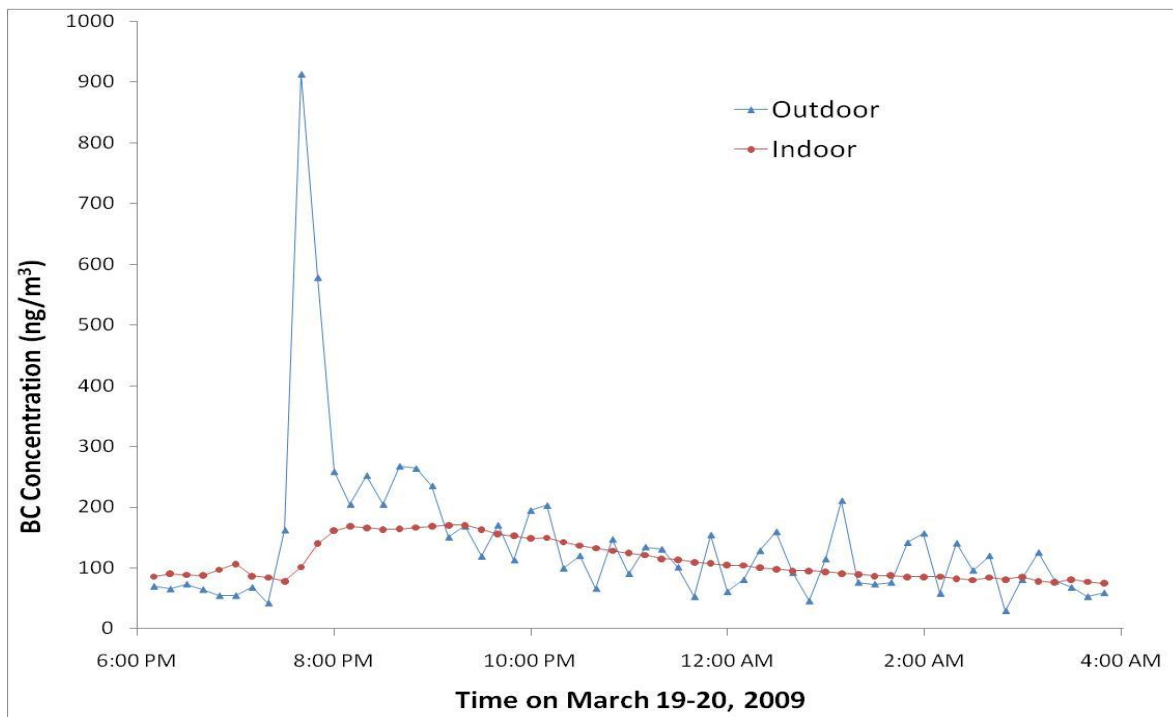


**Figure 11.4 Indoor and outdoor aethalometer black carbon concentrations (10 minute averages) for home E in Cambria, CA**

Measured indoor concentrations were compared with modeled indoor concentrations to estimate air exchange rate, penetration factor, and deposition rate. A mass balance model was developed and parameters were fit using a minimization of the sum of squared differences between the modeled and measured indoor concentrations. The model assumed re-suspension, chemical reactions, and source generation inside the home were negligible. Minimal foot traffic

during the night hours allowed the dismissal of re-suspension. Because black carbon is relatively non-reactive, chemical reactions were assumed to be insignificant. Finally, the home was chosen such that the residents did not burn firewood, eliminating source generation. Cooking is a possible generation source of black carbon, however no anomalous increases in black carbon concentrations were observed indoors. Based on these assumptions, the following time dependant mass balance equation was used to model indoor concentrations.

$$C_{I,t} = C_{I,t-1} + [C_{o,t-1}P\lambda_{v,t} - C_{I,t-1}(\lambda_{v,t} + k_{dep})] \Delta t \quad (11.6)$$

It was assumed that infiltration and deposition loss rates were constant throughout the event. The infiltration rate, however, is unlikely to remain constant throughout the burning evening, since it is dependent on meteorological conditions and indoor/outdoor temperature difference. Consequently, the value for infiltration rate was allowed to vary every 2 hours. For minimization, the Solver program for Microsoft Excel, developed by Frontline Systems was used. This program calculates optimal solutions to models within Excel, when the objective is to find maximum or minimum values based upon inputs and constraints, if needed. The infiltration model used the minimization of the sum of squared differences between the measured and modeled indoor concentrations normalized by dividing the difference term by the measured concentration. Normalization deemphasizes high concentrations, which may otherwise shift the parameters to minimize small regions of high concentrations.

$$SSD = \sum \left( \frac{C_{measured} - C_{modeled}}{C_{measured}} \right)^2 \quad (11.7)$$

where  $C_{measured}(\text{ng}/\text{m}^3)$  = indoor concentration of black carbon determined by the aethalometer ,  
 $C_{modeled}(\text{ng}/\text{m}^3)$  = concentration of black carbon determined from the indoor infiltration model

One issue that arises when using this method is that the equation is over parameterized, that is, there can be more than one value for each parameter that minimizes the sum of squared differences. Depending on the starting values for each parameter, Solver may find different solutions for minimization. To provide a more robust solution, deposition rates and penetration factors were calculated based on periods of relative dominance for each term. The deposition rate has a greater influence on the concentration of indoor BC when indoor concentrations are larger than outdoor concentrations (decreasing indoor concentrations) while the penetration factor has a greater influence when outdoor concentrations are higher than indoor concentrations (increasing indoor concentrations). Consequently, the penetration factor was fit only during periods when indoor concentrations were increasing and the deposition rate was fit only during periods when indoor concentrations were decreasing. This method is based on the analytical method developed by Thatcher et al. (2003). Figure 11.5 compares the modeled indoor concentrations with measured concentrations for the burning event on March 16-17, 2009. Although the fit is generally good, the slight difference in the lag at the beginning of the burning event indicates that the air exchange rate may be slightly higher than the model predicts. Figure 11.6 compares modeled and measured concentrations over the same burning event. Across all 16 burning events, the slope of the model fitting line varied between 0.88 and 1.02 with an average of 0.98. The lowest  $R^2$  for the model fit was 0.93 and the average for all events was 0.97.

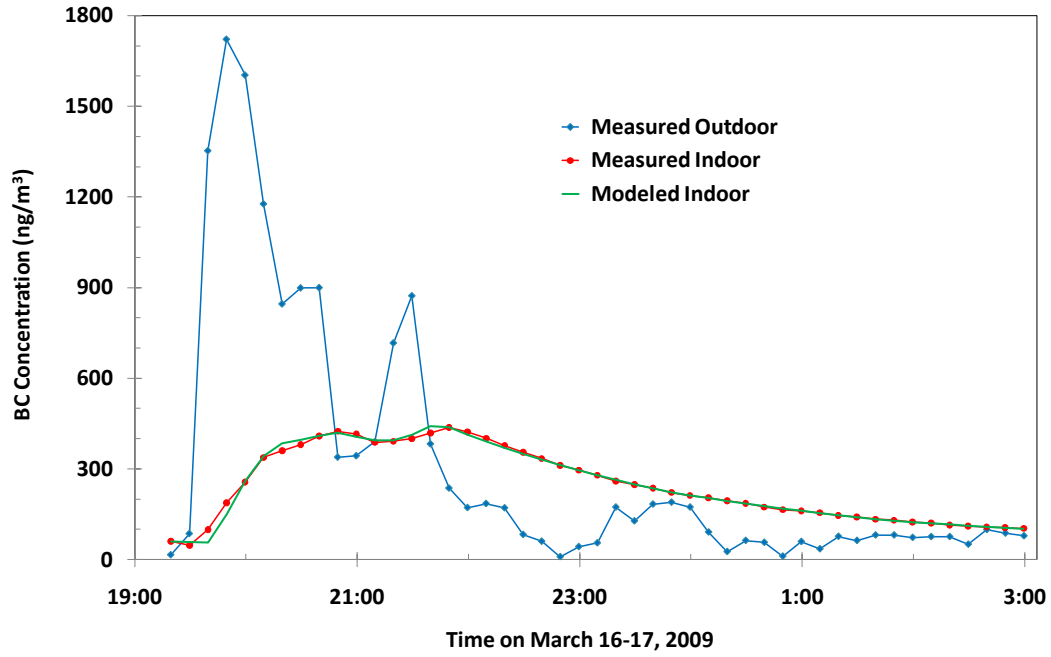


Figure 11.5 Modeled versus measured indoor black carbon aethalometer concentrations for Home E on March 16-17, 2009

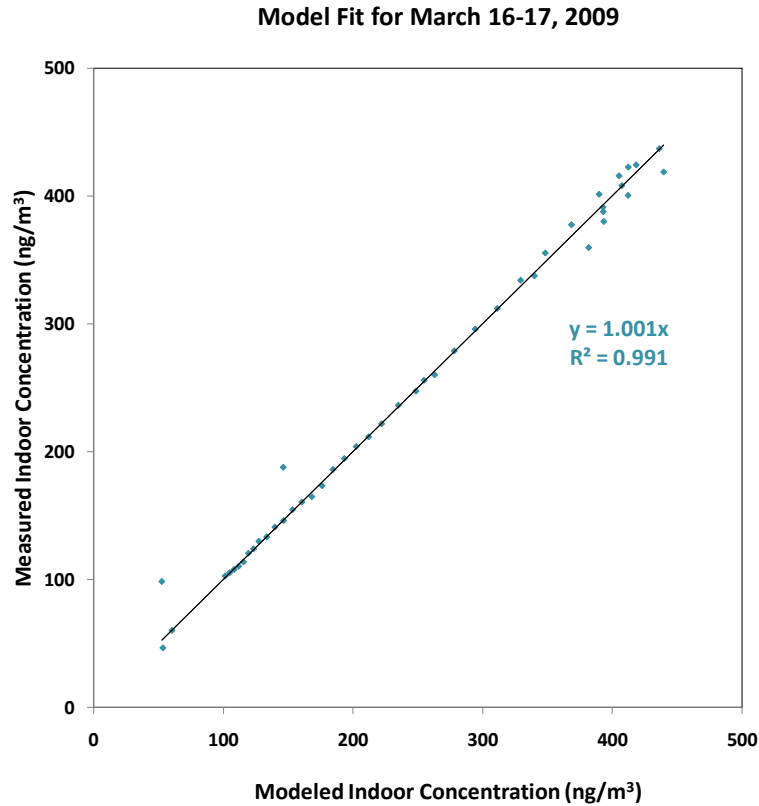


Figure 11.6 Model fit for the burning event on March 16-17, 2009 shown in Figure 11.5

For the 16 burning periods, the average air exchange rate for the home was  $0.26/\text{hr} \pm 0.08/\text{hr}$ . This value is lower than the wintertime average residential air exchange rate of  $0.55/\text{hr}$  reported in the review by Thatcher, et al. (2001). However, wind speeds were low during most of the study and average outdoor temperatures, while cool, are not as cold as winters in many regions. Consequently, the lower driving forces would be expected to lead to lower air exchange rates.

The air exchange rates determined by the mass balance model were compared to those calculated using the LBNL infiltration model in Equation 11.4. For use in the model, regional temperature and wind speed was gathered at a weather station located 1.7 miles southwest from the residence using wunderground.com. Indoor temperature was recorded using a HOBO environmental data logger. The house was assumed to have equal distribution of air infiltration giving a value of  $X=0$  and  $R=0.67$ . Because the home was one story, the height was assumed to be 2.5m giving a value of  $f_s = 0.13 \text{ m}\cdot\text{s}^{-1}\cdot\text{K}^{-1/2}$ . Since Cambria is located in a heavily forested area, it was classified as terrain class 4. The shielding factor was classified as a class 4 because of the heavy shielding provided by the trees. The resultant wind factor,  $f_w$ , was calculated at 0.062. The leakage area was calculated using an average normalized leakage area for California determined by Sherman & Dickerhoff, (1998). Using a building height of 2.5m,  $A_{Leak}/A_{Floor} = 0.00073$ . Using these model parameters, the average air exchange rate over the 16 burning periods was  $0.44/\text{hr} \pm 0.02/\text{hr}$ . This value is higher than the exchange rate calculated using the mass balance model. This may indicate either that the model under predicts air exchange or that the residence used in our study is more tightly constructed than the average California home. However, either value of air exchange rate,  $0.26/\text{hr}$  or  $0.44/\text{hr}$ , indicates that the home used in this study was not unusually leaky and therefore minimal protection from near-field wood smoke is afforded by an average home.

Based on the mass balance model, the average deposition rate was  $0.08/\text{hr} \pm 0.03/\text{hr}$  and the average penetration factor was  $0.97 \pm 0.02$ . These values are consistent with the expectation that many recently generated BC particles will be accumulation mode or smaller. Although most studies investigate penetration factors and deposition rates based on particle size and not aerosol source, similar findings have been suggested by various authors. For wood smoke, particle size distributions have been reported between 30-100 nm in diameter (Davy et al., 2007),  $38 \pm 11$  nm in diameter (Kocbach et al., 2005) and 100-200 nm in diameter (Kleeman et al., 1999). Some coagulation could be expected as these studies examined particles from freshly burned sources. Differences in burning conditions, type of wood, and time since combustion have the most predominate effects on the size distribution. Thatcher, et al. (2001) reported a wide range of deposition rate values in their review, with a general trend showing a decrease in deposition rate as particle size decreased down to around  $0.4 \mu\text{m}$  and then a leveling off of the rate. Wallace (1996) reviewed indoor particles studies for a large number of homes and reported an average deposition loss rate for ambient particles of  $0.39 \pm 0.16 \text{ h}^{-1}$  for PM<sub>2.5</sub>, which is expected to be larger than the median wood smoke particle in this study. For median optical diameter particles less  $0.225 \mu\text{m}$ , Thatcher et al., (2003) reported average deposition rates ranged from  $0.12 - 0.3 \text{ hr}^{-1}$ , while penetration factors ranged from 0.8 - 1. These previous results are consistent with our findings that deposition and penetration losses have only a slight mitigating effect on indoor concentrations.

Using the air exchange rate, deposition rate, and penetration factor from the mass balance model in the steady state indoor/outdoor equation (Equation 11.5) yields an estimated indoor/outdoor ratio of 0.74, which is 16% lower than the average ratio for the filter samples

(0.88). If the air exchange rate from the LBNL infiltration model yields an I/O ratio of 0.82. Due to the high penetration factors and low deposition rates, simple indoor/outdoor models can adequately represent indoor conditions in most cases. Although indoor concentrations are reduced relative to adjacent outdoor concentrations, the variation between different locations outdoors is more significant than the variation between indoor and outdoor concentrations.

## 12 Intake Fraction

One way to approach the analysis of the impact of near source concentration variability is using the fraction of the emissions that are inhaled by individuals (Lai, et al 2000). Intake fraction methodology can be used to quantify the relationship between pollutants that are emitted and their intake by populations (Bennett, et al. 2002). The concept is especially useful when comparing the potential impact on populations between two different sources or mitigation measures. A recent ARB report (Marshall and Nazaroff, 2004) built upon this concept, discussing the implications of the intake fraction on the relative impact of emission sources. They describe intake fraction as “ a metric that summarizes the emission-to-inhalation relationship, (that) may be useful in policy decisions because it facilitates comparisons among sources in terms of their exposure potential.” For a primary pollutant, like wood smoke, the intake fraction is defined as the mass of the pollutant inhaled (by all exposed individuals) divided by the emissions of that pollutant. For a pollutant that is equally distributed throughout an air basin, the intake fraction is calculated using the average concentration for the air basin and the total population. However, for a pollutant that has receptors within the localized plume area, intake fraction can be significantly increased. In addition, if elevated concentrations and concentration peaks occur within neighborhoods, they will lead to elevated risks for those individuals. The primary concern for our intake fraction analysis is whether near field concentration variability has a significant impact on overall intake fractions. Previous studies, as summarized by Marshall and Nazaroff (2004), have shown that emissions sources that are farther from the people who are impacted (such as taller stacks or rural emissions) can have significantly lower intake fractions (up to an order of magnitude) than those that are closer.

Intake fraction (iF) is defined as the mass intake of a pollutant by an individual or group of individuals divided by mass released into the environment. The intake fraction for a particular source depends on a variety of factors such as emission location relative to receptors, meteorology and transport, loss mechanisms, and population distributions. Consequently, intake fractions for a particular type of source will vary from day-to-day and location-to-location. When comparing intake fractions for different source types, it is important to consider all of the factors which can influence the results.

### 12.1 Methods

Intake fraction (iF) is defined as the ratio of pollutant intake over pollutant emissions. It can be calculated as:

$$iF = \frac{\sum_i Q_B D_E P_i C_i}{E} \quad (12.1)$$

where  $Q_B$  is the average breathing rate for the population ( $m^3$ /person hour),  $D_E$  is the duration of exposure (hour),  $P_i$  is the population in area  $i$ ,  $C_i$  is the concentration in area  $i$  (g), and  $E$  is the mass of emissions (g) which lead to the concentrations  $C_i$ . This approach has been used by Ries,

et al. (2009) for wood smoke intake for a large metropolitan region. Using regional data for Vancouver, Canada during 2004-2005, they estimated an  $iF$  of  $13 \times 10^{-6}$  for  $PM_{2.5}$  from urban wood combustion.

An important question in this study was whether intake fraction calculations would be significantly impacted if near-field effects were taken into account. Comparing the impact fractions impact requires that we compare intake fractions with and without taking into account near field exposures. Calculating intake fractions requires an accurate estimation of emissions, exposure concentrations, and the population affected. However, for a single neighborhood many of the relevant parameters will be the same for both the near field and non-near-field calculations. Consequently, it is possible to reduce the data required for the calculation by considering the relationship between the two  $iF$ . A measure of this impact is the ratio of the intake fraction determined from locally specific data ( $iF_{Local}$ ) to the  $iF$  determined using the average concentration for the area ( $iF_{ave}$ ), such as would be obtained from a regional monitoring site. In this instance, the duration ( $D_E$ ) and the mass of emissions ( $E$ ) would be the same for both  $iF_{Local}$  and  $iF_{ave}$ . If there are no known differences between the populations in the local areas, then it is also reasonable to assume that the breathing rate ( $Q_B$ ) and average number of people per home would be the same. Therefore, based on Equation 12.1, the ratio of  $iF$ s would be:

$$iF_{ratio} = \frac{iF_{Local}}{iF_{ave}} = \frac{\sum_i H_i C_i}{H C_{ave}} \quad (12.2)$$

where  $H_i$  and  $H$  are the number of homes in area  $i$  and the number of homes in all areas, respectively. Since dispersion modeling results did not provide an adequate description of measured concentrations, for these calculations average concentrations were based on PEM BC measurements. The study area was divided into seven sections, as shown in Figure 12.1. For each IOP, the average concentration for all PEMs within that section was used to represent the concentration in that region ( $C_i$ ). The average concentration for the overall study area was determined using an area weighted average of the  $C_i$

$$C_{ave} = \sum_i F_i C_i \quad (12.3)$$

where  $F_i$  represents the fraction of the total study area represented by region  $i$ . If there were no PEMs in an area for a particular IOP, then the concentration from the adjacent area with the most similar characteristics was used. Table 12.1 shows the fractional area and number of houses for each of the regions in Figure 12.1. Information for this table was based on satellite imagery of the area.

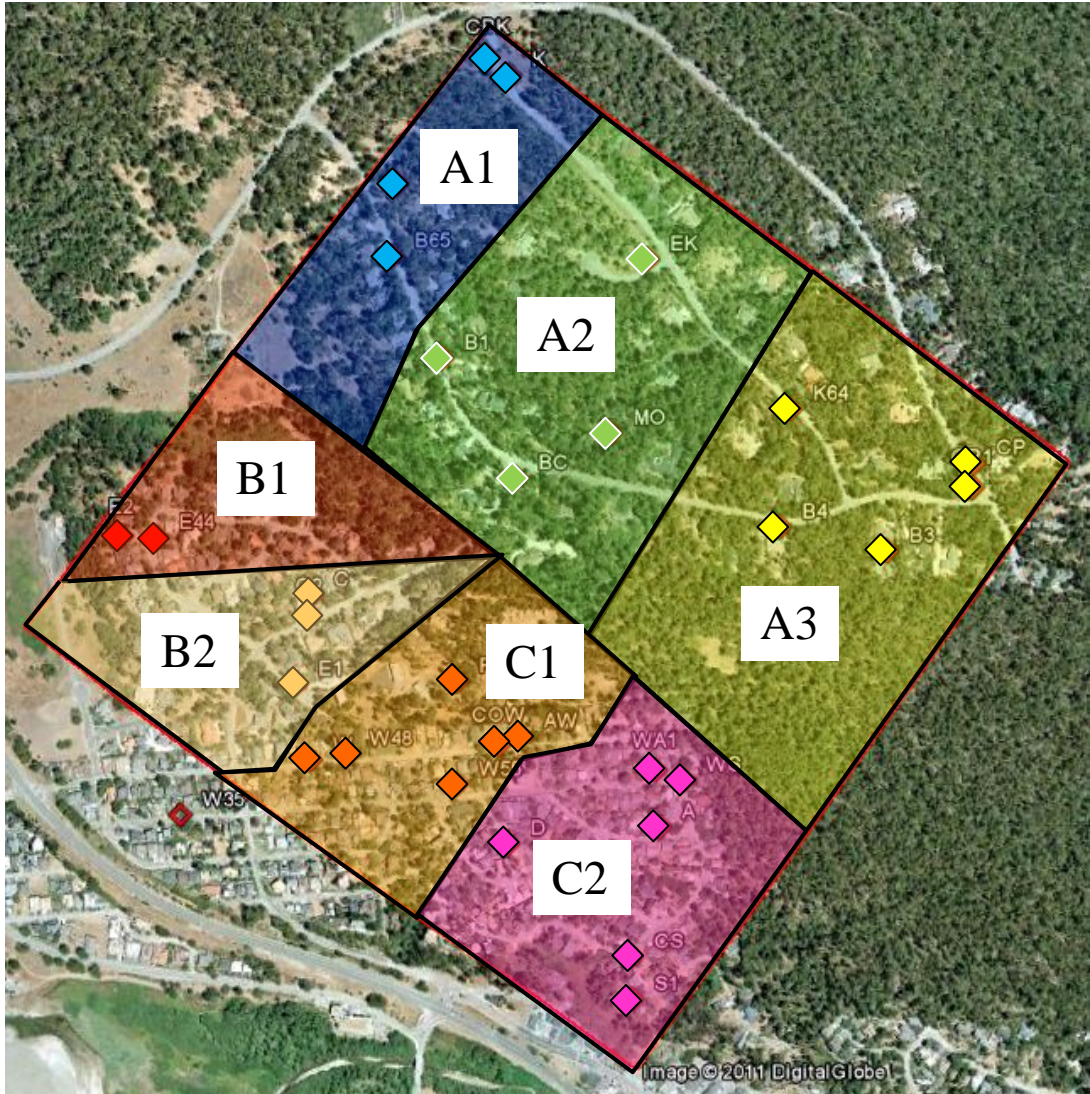


Figure 12.1 Study area divisions used for intake fraction calculations

Table 12.1 Fractional area and number of houses in each division shown in Figure 12.1

| Area | Fraction of Total Area | Number of Houses |
|------|------------------------|------------------|
| A1   | 0.11                   | 9                |
| A2   | 0.23                   | 35               |
| A3   | 0.24                   | 22               |
| B1   | 0.08                   | 30               |
| B2   | 0.09                   | 52               |
| C1   | 0.12                   | 63               |
| C2   | 0.13                   | 122              |

## 12.2 Near-field Effects on Intake Fraction

The intake fraction ratio ( $iF_{\text{ratio}}$ ) is shown for the various IOPs in Table 12.2. The minimum  $iF_{\text{ratio}}$  was 0.95, the maximum was 1.77, and the average was 1.26. Note that IOPs 7a and 8a both have a significant fraction of samples below the detection limit, which may make these  $iF_{\text{ratio}}$  appear to be closer to one than they actually are. The fact that the  $iF_{\text{ratio}}$  was larger than 1 for all but 2 IOPs is consistent with the observation that concentrations tended to be higher in the regions with higher home density. Although this tendency may not hold true for all other locations, areas with higher home density will generally also have a higher density of sources. This can be expected to typically lead to higher intake fractions, as seen in this study.

In addition to the impact that near-field effects have on intake fractions on the neighborhood level, the impact on exposures to individuals can be substantial. In this study, concentrations varied in a somewhat consistent manner between sampling locations. This means that individuals in some locations were generally exposed to a higher level of wood smoke than other individuals who live within the same 1 km<sup>2</sup> neighborhood. For instance, over all IOPs, a person living by sampler D would be exposed to over 3 times the concentration seen by a person near sampler B2. An added concern is the very high concentrations seen by some of the samplers, apparently due to impingement from nearby source. The highest 12 hour PEM concentration was seen at sampler E1 during IOP 5b. The concentration at E1 was more than 10 times higher than average of all of the other PEM concentrations during this IOP, and 6.7 times higher than the next highest PEM. This means that even during periods of relatively good air quality, individuals located near a local source of wood smoke can receive substantial exposures. For sensitive individuals this could lead to health effects even when air quality measurements indicate no risk.

**Table 12.2 Intake fraction ratio by IOP based on concentrations and housing densities by division as shown in Table 12.1**

| IOP | iF ratio |
|-----|----------|
| 1a  | 0.98     |
| 2a  | 1.34     |
| 3a  | 1.28     |
| 4a  | 1.13     |
| 7a  | 1.03     |
| 8a  | 0.95     |
| 2b  | 1.77     |
| 3b  | 1.51     |
| 4b  | 1.17     |
| 5b  | 1.27     |
| 6b  | 1.30     |
| 7b  | 1.55     |
| 8b  | 1.30     |
| 9b  | 1.10     |
| 10b | 1.29     |

The intake fraction ratio calculated here is not affected by the impact of sheltering indoors, since the calculation is based on the assumption that individuals spend an equal amount of times indoors for both the  $iF_{\text{Local}}$  and  $iF_{\text{ave}}$  scenarios. However, the  $iF$  for an individual will be impacted by the amount of time spent indoors. In Section 11.2, average indoor/outdoor ratios between 0.74 and 0.88 were estimated, depending on which method was used. This means that, based on the relative efficiency with which wood smoke enters the indoor environment, sheltering indoors will reduce an individual's risk by about 15 to 25% over the risk to an individual spending the entire time outdoors.

### 13 Summary and Conclusions

The purpose of this project was to improve our understanding of the impact of near-field effects on wood smoke exposures to individuals within a residential area. To accomplish this, field experiments were performed within a residential neighborhood of Cambria, CA. Cambria was chosen due to the favorable meteorology, prevalence of wood burning, and lack of prominent non-wood smoke PM sources. Fifteen, 12 hour Intensive Operational Periods (IOPs) were conducted during the winters of 2008-09 and 2009-10 when forecasts predicted favorable weather for the study (low wind speeds, inversions, low temperatures, and no precipitation). During each IOP, 8 to 16 outdoor filter samplers (PEMs) and 1 to 4 aethalometers (measuring time resolved black carbon concentrations) were deployed at sample locations distributed throughout the study area. In addition, for some IOPs, samplers and/or aethalometers were placed indoors in up to four residences within the study area. Black carbon, a significant component of soot, was used as an indicator compound for wood smoke. The absorption Ångström exponent, a metric of how the light absorption of particulate matter varies with wavelength and an indicator of wood smoke, was determined by measuring samples using a spectrometer. The study was designed to answer four main research questions:

1. What is the concentration variability associated with wood burning within a residential neighborhood?
2. Can near-source contributions be properly estimated based on information on burning patterns, meteorology, and regional monitoring site data?
3. Does indoor exposure to outdoor wood smoke sources correlate with expected values based on simple indoor-outdoor models?
4. How does the near-source contribution affect intake fraction calculations for wood smoke exposures?

In response to the first research question, the variability of wood smoke within a 1 km<sup>2</sup> residential neighborhood was found to be significant. Filter based measurements of 12 hour average concentrations illustrated that the highest concentration was typically several times the average concentration of all locations each evening and often nearly an order of magnitude higher than the lowest concentration. The standard deviation of concentrations for all of the sites measured during a single IOP ranged between 20% and 150% of the average concentration for that IOP. Aethalometer black carbon measurements also showed substantial temporal variability. Concentrations typically rose in the early evening (between 5 and 7 pm) and peaked before midnight. Over a single sampling period, peak black carbon concentrations were 2 to 100 times higher than the average concentration and up to 2500 times larger than the minimum recorded concentrations. The timing and strength of these peaks varied between aethalometer sites. Although the relative concentration between sampling sites was not always consistent,

general trends indicated that the regions with higher home density in the southwestern portion of the study area generally had higher concentrations. Filter black carbon concentrations averaged across all IOPs were 2 to 10 times higher at sites with elevated concentrations than they were at the sites with the lowest average concentrations.

The second research question, “Can near-source contributions be properly estimated based on information on burning patterns, meteorology, and regional monitoring site data?”, was investigated using both statistically-based multiple linear regression models and physically-based dispersion models. Regression models suggest that meteorology, time, and site characteristics can potentially account for between 47 and 81 percent of variability in BC concentration and deviation. However, these models detected curvature and interactions that could not be accounted for in models. The correlations between BC concentration and deviation and explanatory variables determined to be significant were often visually unclear with high variability in BC concentration for the same values of explanatory variables. There was little consistency between average BC and BC deviation analyses using aethalometer data to indicate the more representative weather station for the study area. The analyses suggest a stochastic relationship between meteorological representations of an area that may be difficult to resolve in the absence of an intensive grid of weather stations within the area of interest.

Regression analyses of PEM and aethalometer data collected during this study suggest that BC is significantly correlated with sampling day, time of day, BC concentrations occurring 30 minutes apart, location of BC sampling, wind speed, humidity, and potentially wind direction and number of burning sources. The relationship between average BC concentration and sampling day and time of day was expected due to variations in residential wood burning patterns. Residential wood burning often occurs during periods of cold weather and wood burning often begins in the evening when residents return home, with fireplaces allowed to burn out as the evening progresses. Likewise, the high correlation of black carbon concentrations occurring 30 minutes apart was expected because of relationships between wind speed, direction, and burning sources over this time scale. Other expected associations include the number of wood burning sources and wind direction. The more wood burning sources present during an IOP, the more wood smoke emitted. Still, no 95 percent significance was found for average BC concentration and number of sources. This may indicate that number of burning sources has a larger impact on BC variability than on average BC concentrations themselves in the near-field. Correlations between average BC concentration and wind direction were also expected and were demonstrated for PEM BC. Wind directions directing wood smoke toward receptors are expected to result in higher BC concentrations. This relationship was only detected for PEMs, likely due to the higher fluctuation of high time resolution aethalometer data. The results of the physical modeling provide some insight into the difficulties encountered during the statistical modeling process. Physical modeling showed complex concentration contour lines that varied substantially over short distances and often had multiple “peaks” and “valleys” within the study area. These sort of complex inter-relationships are difficult to capture using basic statistical parameters such as wind speed and source location.

Two dispersion models were used to predict BC concentrations within the study area: ISC-PRIME and ISCST3. Both models under-predicted BC concentrations with modeled-to-measured ratios averaging 0.25 and 0.15 for ISC-PRIME and ISCST3, respectively. When modeled concentration contour patterns were compared to measured concentrations, ISC-PRIME typically performed better than ISCST3, especially when modeling the location of the highest measured PEM BC concentration. Still, while ISC-PRIME was sometimes able to model the

location of the highest measured PEM BC concentrations and the general direction of decreasing BC concentration, there were also many instances where there was no observable correlation between measured and modeled concentration patterns. Contours indicated that ISC-PRIME and ISCST3 could not consistently model BC variability within the study area.

The third research question, “Does indoor exposure to outdoor wood smoke sources correlate with expected values based on simple indoor-outdoor models”, showed that a simple indoor mass balance model could adequately represent the average protection provided by the indoor environment. Aethalometer data was collected during 16 nights in a single residence which did not burn wood during the testing. This data was used to estimate wood smoke model parameters: penetration factor, deposition loss rate, and air exchange rate. A time dependent mass balance model of the aethalometer data yielded an average air exchange rate of  $0.26/\text{hr} \pm 0.08$ , a deposition loss rate of  $0.08/\text{hr} \pm 0.03$ , and a penetration factor of  $0.97 \pm 0.02$ . The values for penetration factor and deposition loss rate are consistent with expectations, based on the anticipated size of wood smoke particles in the near-field. The air exchange rate was lower than expected. The LBNL infiltration model estimated an average air exchange rate of  $0.44/\text{hr}$  for the same periods. Using these average values in a steady state mass balance model predicted an average indoor/outdoor concentration ratio of 0.74 using the air exchange from the time dependent model and 0.84 using the air exchange rate from the LBNL infiltration model. These values compare favorably with the measured indoor/outdoor ratio of  $0.88 \pm 0.41$  derived from 13 PEM measurement pairs at 4 different residences.

The final research question, “How does the near-source contribution affect intake fraction calculations for wood smoke exposures”, was investigated by comparing the intake fraction derived using specific concentrations within the neighborhood to those derived using the average concentration. The intake ratio was defined as the intake fraction calculated when concentration variations within the region were included divided by the intake fraction calculated using the average concentration for the region. For the 15 sampling periods in this study, the average intake ratio was  $1.26 \pm 0.22$ . The intake ratio ranged between 0.95 and 1.8, with all but two of the values being greater than 1, meaning that, in general, including local effects increased the intake fraction. The increased intake fraction seen in this study is due to the fact that higher concentrations were observed in areas with higher home density. Further study is needed to determine whether it is the home density or the nature of the specific geography of the area that led to this intake fraction increase.

An additional topic investigated in this study was a comparison of analytical methods for detecting wood smoke in ambient air. Cambria, CA offered a fairly unique opportunity to study ambient wood smoke in the near absence of confounding particulate matter from other sources. Black and elemental carbon concentrations estimated using four techniques (aethalometer, two methods of thermal-optical analysis, and light transmission) showed significant differences, illustrating the degree of measurement uncertainty, but followed similar trends. Although general trends were apparent, there was some variability between levoglucosan and the organic particle fraction. This variability was even more significant when comparing levoglucosan with elemental and black particle fraction. Comparison of  $\text{PM}_{2.5}$  concentrations with levoglucosan, EC, BC (TOA), and BC (ATN) concentrations showed variability in the fraction of  $\text{PM}_{2.5}$  represented for all measurements. No one metric appeared to be better suited than the others for representing the  $\text{PM}_{2.5}$  concentration from wood smoke generated in the near-field.

## 14 Recommendations

Near-field wood smoke concentration variations have been shown to have a significant impact on exposures for residents in a neighborhood where wood burning is prevalent. The results show that near-field exposure variations are potentially important and deserve additional research to be better quantified. There are still many research questions to be answered. Although the implications of this study are significant, extrapolating the data from one neighborhood to the entire state of California is difficult. Intake fraction was shown to increase in areas with higher home densities. If this increase is caused by the increase in source density, as opposed to geographic causes, then this would increase general intake fraction as well as lead to higher concentrations in the most populous regions, which are also typically of lower income. Additional field studies to quantify the concentration variation and intake fraction effect would increase certainty in exposure calculations. In addition, no single metric was found to adequately represent  $PM_{2.5}$  from wood smoke. Although this was not a significant issue for this study, since wood smoke was nearly the only source of  $PM_{2.5}$ , the ability to quantify the wood smoke contribution to  $PM_{2.5}$  amidst a complex aerosol mixture is needed if field studies are to be conducted in large urban and suburban areas. Ideally this methodology would be simple and inexpensive enough to allow for large sample numbers within a study area. Finally, the failure of dispersion models to adequately represent near-field concentrations within a complex residential terrain suggests that additional work is required in this area. In particular, further work is needed to determine the data requirements for obtaining an adequate concentration representation in terms of meteorology, source description, and geographic representation.

## 15 References

- Andreae, M. O., & Gelencser, A. (2006). Black carbon or brown carbon? The nature of light absorbing carbonaceous aerosols. *Atmospheric Chemistry and Physics*, 6(10), 3131–3148.
- Bennett, D. H., McKone, T. E., Evans, J. S., Nazaroff, W. W., Margni, M. D., Jolliet, O., & Smith, K. R. (2002). Defining intake fraction. *Environmental Science & Technology*, 36(9), 207A-211A.
- Birch, M. E., & Cary, R. A. (1996). Elemental carbon-based method for monitoring occupational exposures to particulate diesel exhaust. *Aerosol Science and Technology*, 25(3), 221–241.
- Branis, M., Koznarová, J., & Domasová, M. (2000). Coal and wood burning as main cause of particulate pollution in a rural area: Case study from the Czech Republic. *Journal of Aerosol Science*, 31(Supplement 1), 889-890. doi:10.1016/S0021-8502(00)90899-1
- California Air Resources Board (CA ARB). (2006, September 8). CEPAM: 2009 Almanac – Top 25 Tool. Retrieved January 31, 2010, from [http://www.arb.ca.gov/app/emsmv/t25cat/cat\\_top25.php](http://www.arb.ca.gov/app/emsmv/t25cat/cat_top25.php)
- Cambria Chamber of Commerce. (2010). *Facts About Cambria*. Retrieved May 1, 2009, from <http://www.cambriachamber.org/info.php>
- Chen, Y., & Bond, T.C. (2010) Light absorption by organic carbon from wood combustion. *Atmospheric Chemistry & Physics*, 10, 1773–1787.
- Chow, J. C., Watson, J. G., Pritchett, L. C., Pierson, W. R., Frazier, C. A., & Purcell, R. G. (1993). The DRI thermal/optical reflectance carbon analysis system: Description, evaluation and applications in U. S. air quality studies. *Atmospheric Environment; Part 71 A, General Topics*, 27(8), 1185–1201.
- Chow, J. C., Watson, J. G., Crow, D., Lowenthal, D. H., & Merrifield, T. (2001). Comparison of IMPROVE - and NIOSH - Carbon Measurements. *Aerosol Science and Technology*, 34(1), 23. doi:10.1080/02786820119073
- Citizen Weather Observer Program (CWOP). (2010, December 30). CWOP Information for CW8373. *Weather Quality Reporter*. Retrieved February 2, 2011, from <http://weather.gladstonefamily.net/site/C8373>
- Dasch, J. M. (1982). Particulate and gaseous emissions from wood-burning fireplaces. *Environmental Science & Technology*, 16(10), 639-645. doi:10.1021/es00104a003
- Davy, P. K., Markwitz, A., & Watherburn, D. C. (2007). Composition, size and Morphological Comparison of Wood Smoke Particles from Source Emissions and in Urban Air by SEMEDS. In *International Union of Air Pollution Prevention and Environmental Protection Associations*. Presented at the 14th IUAPPA World Congress clean air partnerships, Brisbane.
- Demuzere, M., Trigo, R. M., Vila-Guerau de Arellano, J., & van Lipzig, N. P. M. (2009). The impact of weather and atmospheric circulation on O<sub>3</sub> and PM<sub>10</sub> levels at a rural mid-latitude site. *Atmospheric Chemistry and Physics*, 9(8), 2695-2714. doi:10.5194/acp-9-2695-2009
- Demuzere, M., & van Lipzig, N. P. (2010). A new method to estimate air-quality levels using a synoptic-regression approach. Part I: Present-day O<sub>3</sub> and PM<sub>10</sub> analysis. *Atmospheric Environment*, 44(10), 1341-1355. doi:10.1016/j.atmosenv.2009.06.029
- Durbin, J., & Watson, G. S. (1951). Testing for Serial Correlation in Least Squares Regression. II. *Biometrika*, 38(1-2), 159 -178. doi:10.1093/biomet/38.1-2.159

- Electric Power Research Institute (EPRI). (1997, November). *Results of the Independent Evaluation of ISCST3 and ISC-PRIME*. Retrieved June 2, 2011, from: <http://www.epa.gov/scram001/7thconf/iscprime/evalrpt.pdf>
- Fine, P. M., Cass, G. R., & Simoneit, B. R. (2002). Chemical characterization of fine particle emissions from the fireplace combustion of woods grown in the southern United States. *Environmental Science & Technology*, 36(7), 1442–1451.
- Fine, P. M., Cass, G. R., & Simoneit, B. R. (2004a). Chemical characterization of fine particle emissions from the wood stove combustion of prevalent United States tree species. *Environmental Engineering Science*, 21(6), 705–721.
- Fine, P. M., Cass, G. R., & Simoneit, B. R. (2004b). Chemical characterization of fine particle emissions from the fireplace combustion of wood types grown in the Midwestern and Western United States. *Environmental Engineering Science*, 21(3), 387–409.
- Fraser, M. P., & Lakshmanan, K. (2000). Using Levoglucosan as a Molecular Marker for the Long-Range Transport of Biomass Combustion Aerosols. *Environmental Science & Technology*, 34(21), 4560–4564. doi: 10.1021/es991229l
- Glasius M., Ketzela M., Wahlina P., Jensen B., Mønster J., Berkowicz R., and Palmgren F. (2006) Impact of wood combustion on particle levels in a residential area in Denmark, *Atmospheric Environment* 40, 7115–7124.
- Gorin, C. A., Collett, J. L., Jr, & Herckes, P. (2006). Wood smoke contribution to winter aerosol in Fresno, CA. *Journal of the Air & Waste Management Association* (1995), 56(11), 1584–1590.
- Goswami, E., Larson, T., Lumley, T., & Liu, L. J. S. (2002). Spatial characteristics of fine particulate matter: identifying representative monitoring locations in Seattle, Washington. *Journal of the Air & Waste Management Association* (1995), 52(3), 324–333.
- Gulliver, J., & Briggs, D. J. (2004). Personal exposure to particulate air pollution in transport microenvironments. *Atmospheric Environment*, 38(1), 1–8. doi:10.1016/j.atmosenv.2003.09.036
- Hadley, O.L., Corrigan, C.E., & Kirchstetter, T.W. (2008). Modified thermo-optical analysis using spectral absorption selectivity to distinguish black carbon from pyrolyzed organic carbon. *Environmental Science & Technology*, 42, 8459–8464.
- Hansen, A. D. A. (2005). *The Aethalometer, manual*. Magee Scientific Company. Berkeley, California, USA.
- Hering, S. V., Lunden, M. M., Thatcher, T. L., Kirchstetter, T. W., & Brown, N. J. (2007). Using regional data and building leakage to assess indoor concentrations of particles of outdoor origin. *Aerosol Science and Technology*, 41(7), 639–654.
- Hoffer, A., Gelencser, A., Guyon, P., Kiss, G., Schmid, O., Frank, G. P., et al. (2006). Optical properties of humic-like substances (HULIS) in biomass-burning aerosols. *Atmospheric Chemistry and Physics*, 6(11), 3563–3570.
- Jenkins, P. L., Phillips, T. J., Mulberg, E. J., & Hui, S. P. (1992). Activity patterns of Californians. Use of and proximity to indoor pollutant sources. *Atmospheric Environment*, 26(12), 2141–2148.
- Jeong, C. H., Hopke, P. K., Kim, E., & Lee, D. W. (2004). The comparison between thermal-optical transmittance elemental carbon and Aethalometer black carbon measured at multiple monitoring sites. *Atmospheric Environment*, 38(31), 5193–5204.

- Kirchstetter, T. W., Corrigan, C. E., & Novakov, T. (2001). Laboratory and field investigation of the adsorption of gaseous organic compounds onto quartz filters. *Atmospheric Environment*, 35(9), 1663-1671. doi: 10.1016/S1352-2310(00)00448-9
- Kirchstetter, T. W., Novakov, T., & Hobbs, P. V. (2004). Evidence that the spectral dependence of light absorption by aerosols is affected by organic carbon. *Journal of Geophysical Research-Atmospheres*, 109(D21), D21208.
- Kleeman, M. J., Schauer, J. J., & Cass, G. R. (1999). Size and composition distribution of fine particulate matter emitted from wood burning, meat charbroiling, and cigarettes. *Environmental Science & Technology*, 33(20), 3516-3523.
- Kobach, A., Johansen, B. V., Schwarze, P. E., & Namork, E. (2005). Analytical electron microscopy of combustion particles: a comparison of vehicle exhaust and residential wood smoke. *Science of the Total Environment*, 346(1-3), 231-243.
- Lai, A.C.K., Thatcher, T.L., and Nazaroff, W. W. (2000) Inhalation Transfer Factors for Air Pollution Health-Risk Assessment, *Journal of the Air & Waste Management Association*. **50**, 1688-1699. LBNL-43712
- Locker, H. B. (1988). *The use of levoglucosan to assess the environmental impact of residential wood-burning on air quality*.
- Marshall J.D. and Nazaroff W.W. (2004) Using Intake Fraction To Guide ARB Policy Choices: The Case of Particulate Matter, unpublished ARB Report.
- McMeeking, G. R., Kreidenweis, S.M., Baker, S., Carrico, C.M., Chow, J.C., Collett, J.L. Jr., Hao, W.M., Holden, A.S., Kirchstetter, T.W., Malm, W.C., Moosmüller, H., Sullivan, A.P., & Wold, C.E. (2009). Emissions of trace gases and aerosols during the open combustion of biomass in the laboratory. Lawrence Berkeley National Laboratory. LBNL Paper LBNL-2081E. Retrieved from: <http://escholarship.org/uc/item/2g98h6bk>
- Met One Instruments, Inc. (2001). EBAM Operation Manual. Rowlett, Texas, USA.
- Nerriere, É., Zmirou-Navier, D., Blanchard, O., Momas, I., Ladner, J., Le Moullec, Y., Personnaz, M., et al. (2005). Can we use fixed ambient air monitors to estimate population long-term exposure to air pollutants? The case of spatial variability in the Genotox ER study. *Environmental Research*, 97(1), 32-42. doi:10.1016/j.envres.2004.07.009
- NIOSH. (2003). Method 5040 Elemental Carbon (Diesel Exhaust), Issue 3. In *Manual of Analytical Methods*. Cincinnati, OH: National Institute of Occupational Safety and Health.
- Novakov, T., & Corrigan, C. E. (1995). Thermal characterization of biomass smoke particles. *Microchimica Acta*, 119(1), 157-166.
- Ott, L., & Longnecker, M. (2010). *An introduction to statistical methods and data analysis*. Cengage Learning.
- Patterson, E. M. and C. K. McMahon, (1984) Absorption characteristics of forest fire particulate matter, *Atmospheric Environment*, 18, 2541-2551.
- Pérez, P., Trier, A., & Reyes, J. (2000). Prediction of PM<sub>2.5</sub> concentrations several hours in advance using neural networks in Santiago, Chile. *Atmospheric Environment*, 34(8), 1189-1196. doi:10.1016/S1352-2310(99)00316-7
- Perry, S. G., Cimorelli, A. J., Paine, R. J., Brode, R. W., Weil, J. C., Venkatram, A., Wilson, R. B., et al. (2005). AERMOD: A Dispersion Model for Industrial Source Applications. Part II: Model Performance against 17 Field Study Databases. *Journal of Applied Meteorology*, 44(5), 694-708. doi:doi: 10.1175/JAM2228.1

- Pires, J.C.M., Martins, F.G., Sousa, S.I.V., Alvim-Ferraz, M.C.M., Pereira, M.C., (2008). Prediction of the daily mean PM10 concentrations using linear models. *American Journal of Environmental Sciences*, 4(5), 445-453.
- Purvis, C. R., McCrillis, R. C., & Kariher, P. H. (2000). Fine Particulate Matter (PM) and Organic Speciation of Fireplace Emissions. *Environmental Science & Technology*, 34(9), 1653-1658. doi:10.1021/es981006f
- Rau, J. A. (1989). Composition and size distribution of residential wood smoke particles. *Aerosol Science and Technology*, 10(1), 181-192.
- Ries, F.J., Marshall, J.D., & Brauer, M. (2009). Intake Fraction of Urban Wood Smoke. *Environmental Science & Technology*, 43(13), 4701-4706.
- Robinson, D., Monro, J., & Campbell, E. (2007). Spatial variability and population exposure to PM2.5 pollution from woodsmoke in a New South Wales country town. *Atmospheric Environment*, 41(26), 5464-5478. doi:10.1016/j.atmosenv.2007.01.059
- Sandradewi, J., Prévôt, A. S. H., Weingartner, E., Schmidhauser, R., Gysel, M., & Baltensperger, U. (2008a). A study of wood burning and traffic aerosols in an Alpine valley using a multi-wavelength Aethalometer. *Atmospheric Environment*, 42(1), 101-112.
- Sandradewi, J., Prévôt, A. S., Szidat, S., et al. (2008b). Using aerosol light absorption measurements for the quantitative determination of wood burning and traffic emission contributions to particulate matter. *Environmental Science & Technology*, 42(9), 3316-3323.
- Savin, N. E., & White, K. J. (1977). The Durbin-Watson Test for Serial Correlation with Extreme Sample Sizes or Many Regressors. *Econometrica*, 45(8), 1989-1996.
- Schnaiter, M., Horvath, H., Möhler, O., Naumann, K. -, Saathoff, H., & Schöck, O. W. (2003). UV-VIS-NIR spectral optical properties of soot and soot-containing aerosols. *Journal of Aerosol Science*, 34(10), 1421-1444. doi: 10.1016/S0021-8502(03)00361-6
- Sherman, M. H., & Grimsrud, D. T. (1980). Infiltration-Pressurization Correlations: Simplified Physical Modeling. In *Conference of the American Society of Heating, Refrigeration and Air Conditioning Engineers* (Vol. 22).
- Sherman, M. H., and Dickerhoff, D. J. (1998). Air Tightness of US Dwellings, *ASHRAE Transactions*, 104(2), 1359-1367.
- Simoneit, B. R., Schauer, J. J., Nolte, C. G., Oros, D. R., Elias, V. O., Fraser, M. P., et al. (1999). Levoglucosan, a tracer for cellulose in biomass burning and atmospheric particles. *Atmospheric Environment*, 33(2), 173-182.
- Slini, T., Kaprara, A., Karatzas, K., & Moussiopoulos, N. (2006). PM10 forecasting for Thessaloniki, Greece. *Environmental Modelling & Software*, 21(4), 559-565. doi:10.1016/j.envsoft.2004.06.011
- Stadlober, E., Hörmann, S., & Pfeiler, B. (2008). Quality and performance of a PM10 daily forecasting model. *Atmospheric Environment*, 42(6), 1098-1109. doi:10.1016/j.atmosenv.2007.10.073
- Tai, A. P., Mickley, L. J., & Jacob, D. J. (2010). Correlations between fine particulate matter (PM2.5) and meteorological variables in the United States: Implications for the sensitivity of PM2.5 to climate change. *Atmospheric Environment*, 44(32), 3976-3984. doi:10.1016/j.atmosenv.2010.06.060
- Thatcher, T. L., McKone, T. E., Fisk, W. J., Sohn, M. D., Delp, W. W., Riley, W. J., et al. (2001). *Factors affecting the concentration of outdoor particles indoors (COPI)*:

- Identification of data needs and existing data.* Retrieved from <http://www.osti.gov/energycitations/servlets/purl/820780-8m21pL/native/>
- Thatcher, T. L., Lunden, M. M., Revzan, K. L., Sextro, R. G., & Brown, N. J. (2003). A concentration rebound method for measuring particle penetration and deposition in the indoor environment. *Aerosol Science and Technology*, 37(11), 847–864.
- Trinity Consultants. (2001, December 1). *Understanding and Adapting to New Dispersion Models*. Retrieved from Trinity Consultants website: <http://trinityconsultants.com/WorkArea/DownloadAsset.aspx?id=1251>
- Turpin, B. J., Weisel, C. P., Morandi, M., Colome, S., Stock, T., Eisenreich, S., & Buckley, B. (2007). Relationships of Indoor, Outdoor, and Personal Air (RIOPA): part II. Analyses of concentrations of particulate matter species. *Research Report (Health Effects Institute)*, (130 Pt 2), 1-77; discussion 79-92.
- US Census Bureau (2000). Census Bureau Home Page. Retrieved November 1, 2010, from <http://www.census.gov/>
- US Environmental Protection Agency (EPA) (1995, September). User's guide for the Industrial source complex (ISC3) dispersion models: Volume I - User Instructions. Retrieved May 31, 2011, from <http://www.epa.gov/scram001/userg/regmod/isc3v1.pdf>
- US EPA (2003, June). Comparison of regulatory design concentrations: AERMOD vs ISCST3, CTDMPLUS, ISC-PRIME. Retrieved May 31, 2011, from <http://www.epa.gov/scram001/7thconf/aermod/compar.pdf>
- US EPA (2008, August 13). “Clarification of Regulatory Status of CALPUFF for Near-Field Applications.” Retrieved January 7, 2011, from <http://www.epa.gov/scram001/clarification%20of%20regulatory%20status%20of%20calpuff.pdf>
- Valari, M., & Menut, L. (2010). Transferring the heterogeneity of surface emissions to variability in pollutant concentrations over urban areas through a chemistry-transport model. *Atmospheric Environment*, 44(27), 3229-3238. doi:10.1016/j.atmosenv.2010.06.001
- Vukovich, F. M., & Sherwell, J. (2002). Comparison of fine particles and the relationship between particle variations and meteorology at an urban site and a remote site in the Eastern United States. *Journal of the Air & Waste Management Association (1995)*, 52(5), 573-584.
- Wallace, L. (1996). Indoor particles: a review. *Journal of the Air & Waste Management Association (1995)*, 46(2), 98-126.
- Watson, J.G., Chow, J.C., Antony Chen, L.W. (2005). Summary of organic and elemental carbon/black carbon analysis methods and intercomparisons. *Aerosol and Air Quality Research*, 5, 65–102.
- Weijers, E. P., Khlystov, A. Y., Kos, G. P. A., & Erisman, J. W. (2004). Variability of particulate matter concentrations along roads and motorways determined by a moving measurement unit. *Atmospheric Environment*, 38(19), 2993-3002. doi:10.1016/j.atmosenv.2004.02.045
- Wilson, W. E., Mage, D. T., & Grant, L. D. (2000). Estimating separately personal exposure to ambient and nonambient particulate matter for epidemiology and risk assessment: why and how. *Journal of the Air & Waste Management Association (1995)*, 50(7), 1167-1183.
- Yan, B., Zheng, M., Hu, Y. T., Lee, S., Kim, H. K., & Russell, A. G. (2007). Organic composition of carbonaceous aerosols in an aged prescribed fire plume. *Atmospheric Chemistry and Physics Discussions*, 7(6), 18015–18042.

Zeger, S. L., Thomas, D., Dominici, F., Samet, J. M., Schwartz, J., Dockery, D., & Cohen, A. (2000). Exposure measurement error in time-series studies of air pollution: concepts and consequences. *Environmental Health Perspectives*, *108*(5), 419–426.

## 16 Glossary of Terms

| Term                 | Definition  |
|----------------------|---|
| $y$                  | Response variable ( $BC_{ave}$ or $BC_{dev}$ ) used for multiple regression                       |
| $\beta_0$            | Constant  |
| $\beta_i$            | Partial slope for independent variable $i$  |
| $x_i$                | Independent variable used for multiple regression (i.e. wind speed, humidity, etc.)               |
| $\epsilon$           | Random error  |
| $BC_{ave}$           | Average BC concentration (over 30 minutes for aethalometers and over 12 hours for PEMS)           |
| $BC_{dev}$           | Weighted deviation  |
| std dev <sub>t</sub> | Standard deviation of all operating aethalometers at time $t$                                     |
| $BC_{t,ave}$         | Average BC concentration of BC measurements from all operating aethalometers at time $t$          |
| $dC_{in}/dt$         | Change in incoming concentration over time  |
| $C_{in(I)}$          | Indoor concentration ( $\mu\text{g}/\text{m}^3$ )   |
| $C_{out(O)}$         | Outdoor concentration ( $\mu\text{g}/\text{m}^3$ )  |
| $t$                  | Time (hr)   |
| $\lambda_v$          | Air exchange rate ( $\text{h}^{-1}$ )   |
| $P$                  | Dimensionless penetration factor  |
| $k_{dep}$            | Deposition loss rate ( $\text{h}^{-1}$ )  |
| $G$                  | Generation of particles from indoor sources ( $\mu\text{g}/\text{m}^3 \cdot \text{h}$ )           |
| $S$                  | Particle formation through gas/particle exchange ( $\mu\text{g}/\text{m}^3 \cdot \text{h}$ )      |
| $F$                  | Particle formation due to reaction ( $\mu\text{g}/\text{m}^3 \cdot \text{h}$ )                    |
| $K$                  | Particle size change through coagulation ( $\mu\text{g}/\text{m}^3 \cdot \text{h}$ )              |
| $H$                  | Particle size change through hygroscopic growth ( $\mu\text{g}/\text{m}^3 \cdot \text{h}$ )       |
| $R$                  | Generation of indoor particles from resuspension ( $\mu\text{g}/\text{m}^3 \cdot \text{h}$ )      |
| $\lambda$            | Infiltration rate ( $\text{hr}^{-1}$ )  |
| $A_{leak}$           | The total leakage area of the building ( $\text{m}^2$ )   |
| $A_{floor}$          | Floor area of the building ( $\text{m}^2$ )   |
| $H$                  | Building height (m)   |
| $f_s$                | The stack parameter determined by the geometry of the building ( $\text{ms}^{-1}\text{K}^{1/2}$ ) |
| $\Delta T$           | Absolute temperature difference (K)   |
| $f_w$                | The wind factor determined environmental shielding (unitless)                                     |
| $W$                  | Wind speed (m/s)  |
| $iF$                 | Intake fraction   |
| $Q_B$                | Average breathing rate for the population ( $\text{m}^3/\text{person hour}$ )                     |
| $D_E$                | Duration of exposure (hour)   |
| $P_i$                | Population in area $i$  |
| $C_i$                | Concentration in area $i$ (g)   |
| $E$                  | Mass of emissions (g) which lead to the concentrations $C_i$                                      |